DISCLAIMER

This report was prepared as an account of work sponsored by an agency of the United States Government. Neither the United States Government nor any agency thereof, nor any of their employees, makes any warranty, express or implied, or assumes any legal liability or responsibility for the accuracy, completeness, or usefulness of any information, apparatus, product, or process disclosed, or represents that its use would not infringe privately owned rights. Reference herein to any specific commercial product, process, or service by trade name, trademark, manufacturer, or otherwise does not necessarily constitute or imply its endorsement, recommendation, or favoring by the United States Government or any agency thereof. The views and opinions of authors expressed herein do not necessarily state or reflect those of the United States Government or any agency thereof. Reference herein to any social initiative (including but not limited to Diversity, Equity, and Inclusion (DEI); Community Benefits Plans (CBP); Justice 40; etc.) is made by the Author independent of any current requirement by the United States Government and does not constitute or imply endorsement, recommendation, or support by the United States Government or any agency thereof.

SANDIA REPORT
SAND2026-19311
Printed April 2026

Sandia National Laboratories

Model Validation Database for Fires Involving Fuels at Liquefied Natural Gas Facilities (Version 2)

Anay Luketa

Prepared by
Sandia National Laboratories
Albuquerque, New Mexico
87185 and Livermore,
California 94550

Issued by Sandia National Laboratories, operated for the United States Department of Energy by National Technology & Engineering Solutions of Sandia, LLC.

Available to DOE and DOE contractors from
U.S. Department of Energy
Office of Scientific and Technical Information
P.O. Box 62
Oak Ridge, TN 37831

Telephone: (865) 576-8401
Facsimile: (865) 576-5728
E-Mail: reports@osti.gov
Online ordering: http://www.osti.gov/scitech

Available to the public from
U.S. Department of Commerce
National Technical Information Service
5301 Shawnee Rd
Alexandria, VA 22312

Telephone: (800) 553-6847
Facsimile: (703) 605-6900
E-Mail: orders@ntis.gov
Online order: https://classic.ntis.gov/help/order-methods/

ABSTRACT

This document provides a description of the model evaluation protocol (MEP) database for fires involving liquefied natural gas (LNG) and processing fuels at LNG facilities. The purpose of the MEP is to provide procedures regarding the assessment of a model's suitability to predict thermal exclusion zones resulting from a fire. The database includes measurements from pool fire, jet fire, and fireball experiments which are provided in a spreadsheet. Users are to enter model results into the spreadsheet which automatically generates statistical performance measures and graphical comparisons with the experimental data. The intent of this document is to provide a description of the experiments and of the procedure required to carry out the validation portion of the MEP. In addition, the statistical performance measures, measurements for comparisons, and parameter variation are provided.

ACKNOWLEDGEMENTS

The author would like to thank the technical advisory panel for their valuable input, discussion, and review of this protocol. The members include:

Thach Nguyen – DOT PHMSA

Scott Davis, Ph.D., P.E., GexCon

Bjorn Erling Vembe, Ph.D., DNV

Jason Floyd, Ph.D., Underwriters Laboratory Fire Safety Research Institute

Bryant Hendrickson, P.E., Jensen Hughes

Andrew Kohout, P.E., FERC

Kevin McGrattan, Ph.D., National Institute for Standards and Technology

James Stewart, Health and Safety Executive

The author would also like to thank Douglas Michael Johnson from DNV and Steven Betteridge from Shell for their permission to provide data from the Montoir test reports. With respect to the Montoir data the following disclaimer applies:

The content of the reports is intended only to provide data and analysis of experimental studies and is not intended to be any substitute for professional advice. DNV Group of companies, including GL Industrial Services UK Ltd, and any other person or company, including, but not limited to, Shell Research Ltd., concerned with furnishing information or data used therein, excludes to the maximum extent permissible by law any legal liability in contract and tort (including negligence) for the up-to-date nature, accuracy, completeness, quality, or usefulness of any information, apparatus, product, or process disclosed or demonstrated.

The author would also like to thank Douglas Michael Johnson from DNV for providing the full British Gas test report on propane and butane fireballs and granting permission to include the data in the database. With respect to the data the following disclaimer applies:

The content of the reports is intended only to provide data and analysis of experimental studies and is not intended to be any substitute for professional advice. DNV Group of companies, including GL Industrial Services UK Ltd, and any other person or company, concerned with furnishing information or data used therein, excludes to the maximum extent permissible by law any legal liability in contract and tort (including negligence) for the up-to-date nature, accuracy, completeness, quality, or usefulness of any information, apparatus, product, or process disclosed or demonstrated.

CONTENTS

LIST OF FIGURES

LIST OF TABLES

This page left blank

ACRONYMS AND DEFINITIONS

Abbreviation	Definition
A-S	Advantica and Shell
BGC	British Gas Corporation
C5+	Pentanes and heavier hydrocarbon gas content
CEC	Council of the European Communities
CERTEC	Centre for Studies on Technological Risk
CFD	Computational Fluid Dynamics
DFT	Directional Flame Thermometer
DNV	Det Norske Veritas
DOE	Department of Energy
FLAME	Fire Laboratory for Accreditation of Models and Experiments
HSL	Health and Safety Laboratory
IR	Infrared Radiation
LNG	Liquefied Natural Gas
LU	Loughborough University
MEP	Model Evaluation Protocol
NRCC	National Research Council of Canada
NWC	Naval Weapons Center
SEP	Surface Emissive Power
SNL	Sandia National Labs
TAMU	Texas A&M University
TTC	Thermal Test Complex
USN	United States Navy

This page left blank

1. INTRODUCTION

This document provides a description of the experiments included in the model evaluation protocol (MEP) database spreadsheet for fires involving liquefied natural gas (LNG) and fuels at facilities involved in the processing of LNG. In addition to LNG, the processing fuels that may be present at a facility include:

- Refrigerants: Ethane/Ethylene, Propane, Butane, and Iso-pentane as single or mixture release.
- Stabilized condensate or C5+: mixture of butane, pentane, and hexane.
- Diesel fuel
- Anhydrous ammonia
- Hydrogen sulfide

The MEP database does not include anhydrous ammonia and hydrogen sulfide since relevant experimental data is not available. Past researchers have found that ammonia cannot maintain a stable flame due to its high ignition temperature (1100 K), relatively high lower flammability limit (LFL=16.6%), low flame propagation speed, low heating value, and low flame temperature [1] [2] [3]. Data for hydrogen sulfide does not exist because of its inhalation toxicity hazards, not only from hydrogen sulfide but also from sulfur dioxide, one of its combustion products. Note that for diesel fuel, the most likely combustion event is a pool fire at LNG facilities, thus the database does not include a comparison to jet fires and fireballs for this fuel. Further note that comparison to condensate fuel is provided by experiments using crude oil due to similar combustion behavior as discussed in references [2] [4].

The database is provided in the form of a spreadsheet that includes experimental data for comparison to model predictions allowing for the assessment of a model's performance for siting purposes. The prediction of heat flux from the flame to an external target is the primary objective in the use of these models since it allows for thermal exclusion zones to be determined.

The experiments included in the MEP and listed in Table 1-1 include pool fires, jet fires, and fireballs. A pool fire is defined as a horizontally oriented fuel burning upwardly in free convection. They can occur whenever liquid fuel is spilled, and an ignition source is present. Jet fires are high velocity combusting jets that can arise when a pressurized tank is ruptured thereby releasing its contents which could be either in single phase such as liquid, gas or two- phase with a combination of liquid and gas. Jet fires can result in very high heat fluxes to engulfed objects as well as very high velocities, as found experimentally. Fireballs are partially pre-mixed diffusion flames which rapidly combust on the order of seconds to tens of seconds due to enhanced turbulent mixing and atomization. Fireballs can arise when a tank containing liquid fuel is heated sufficiently to a thermodynamic state that will result in rapid phase change, causing the tank to rupture through thermal (or mechanical) damage. The evaluation is based on comparison of model predictions to experimental data for each of these types of fires.

In addition to the fire experiments, data on the thermal response of concrete walls that could serve as thermal barriers is included. The motivation to include the data is due to the potential for current LNG facilities requiring the installation of radiant thermal barriers to satisfy the factor of uncertainty criteria within the MEP. These facilities were built before the MEP for fires was developed, hence the potential need for thermal barriers.

Table 1-1: Summary of experimental series

Test Series	Fuel	Fire Type	Number of tests	Pool diameter or length (m)	Flame length or height (m)	Land/ water	Engulfed object?
Sandia gas burner [5]	LNG	pool (circular)	28	3	1.1-6.9	land	no
Phoenix [5]	LNG	pool (circular)	2	27, 56	70, 146	water	no
Montoir [6]	LNG	pool (circular)	3	35	70-85	land	no
BGC trench [7] [8]	LNG	pool (rectangular)	13	4.4-52	1.5-7.7	land	no
LU [9]	LNG	jet	3	na	20- 50	land	yes
Shell [10]	LNG	fireball	3	na	42-56*	land	no
USN [11]	propane	pool	4	14.9-16.9	51.9-54.9	water	no
SNL-indoor [4]	crude oil	pool	1	2	4.4	land	no
SNL-outdoor [2]	crude oil	pool	1	5	4.5	land	yes
CERTEC [12] [13]	diesel	pool	5	1.5-6	~3-12	land	no
Sandia pool fire [14]	ethane, ethylene, propane, isopentane	pool	4	5	~10-25	land	no
TAMU [15] [16] [17]	propane	jet fire	4	na	2-4	na	no
A-S [18]	crude oil	jet fire	2	na	22-23	na	yes
Sandia jet fire [14]	ethane, ethylene, isopentane	jet fire	3	na	~12-17	na	no
HSL-BG [19]	propane	fireball	4	na	54-72*	na	no
BG propane [20] [21]	propane	fireball	1	na	65*	na	no
BG butane [20] [21]	butane	fireball	4	na	60-76*	na	no
SNL-fireball [2]	crude oil	fireball	3	na	60-69*	na	no
Sandia fireball [14]	ethane, ethylene, isopentane	fireball	3	na	72-84*	na	no

Test Series	Fuel	Fire Type	Number of tests	Pool diameter or length (m)	Flame length or height (m)	Land/ water	Engulfed object?
SNL concrete wall [14]	Insulated formed concrete	na	1	na	na	na	na
SNL masonry wall [14]	Masonry brick wall	na	1	na	na	na	na

*Maximum fireball diameter

The experiments in the MEP were selected based on the following criteria:

- public availability
- completeness of information regarding the experimental setup and results
- pertinence of measured parameters for hazard analysis
- fire size, that is, at a scale sufficient to reflect several if not all physical features of accident-scale fires.

The following sections provide a description of measurement quantities, quantification of the comparison, thermal exclusion zones based on model performance, and organization of the accompanying MEP database spreadsheet. This is followed by a description of the experimental datasets with details regarding the measurements for comparison, model inputs, and experimental uncertainties for performance evaluation.

1.1. Version changes

The following items are the main changes from Version 1 to Version 2 of the MEP Database. Note that future versions may be released if corrections are necessary and/or improvements are recommended by users.

1. The addition of 10 non-LNG fire experiments and 2 concrete wall thermal experiments. The experiments include:

    a. 3 jet fires (ethane, ethylene, and isopentane)
    b. 4 pool fires (ethane, ethylene, propane, and isopentane)
    c. 3 fireballs (ethane, ethylene, and isopentane)
    d. 2 concrete walls (formed and masonry)

2. The recently added Sandia pool fire test series provides data for a propane (99+%) pool fire and has replaced the 'USN' test series. Since it's uncertain whether the 'USN' test series used LPG with propane as the main constituent, it has been removed from the MEP. LPG is commonly comprised of either mostly butane or propane and will contain other components such as propene, methane, and ethane.

3. In the comparison plot in the 'Montoir_T1' worksheet, the line for 'model' was corrected since it was not showing on the graph of 'predicted vs. measured' for the period of 130-170 sec. Also, the radiant fraction has been removed from the worksheets for the Montoir test series since it was derived by the MEP Database author and not provided in the experimental reports.

4. Worksheet 'CERTEC summary' indicated an error internal to Excel where the data was not linked. The worksheet now functions correctly after a new worksheet with the same data and formulas was created and replaced the non-functioning worksheet.

5. The data for comparison in the worksheets for the 'HSL-BG' experiments has been simplified and is now commensurate with the data provided for other fireball test series.

6. The radiative fraction for the experiment 'Phoenix T2' has been corrected from 0.3 to 0.24.

7. In the MEP Database spreadsheet, the listing of cells where data is entered in the Master List sheet has been removed due to the high number of worksheets now in the database spreadsheet, however a list of the worksheets remains.

8. Section 2.2 has been revised to improve clarity in describing the equations used to determine performance in the Database spreadsheet.

9. In section 2.3, the probability criteria used to determine the uncertainty factor has been changed from 0.01 to 0.025 to reflect a 95% confidence interval.

2. COMPARISON METRICS

The following sections provide discussion of various measurements of pool fires, jet fires, and fireballs. A description of the method to quantify the scatter and bias of a model's performance is also provided, along with thermal exclusion zones based on the model's performance. These statistical measures are automatically calculated in the accompanying spreadsheet after model results are entered by the user. Description of the format of the spreadsheet is also provided.

2.1. Measurement Comparison

For pool fires, experimental measurements used for comparison include incident heat flux, thermocouple temperatures, burn rate, flame length, flame tilt, and flame drag. For jet fires, measurement comparison includes incident heat flux, jet length, and lift-off. For fireballs, measurement comparison includes incident heat flux and geometric and temporal measurements such as the diameter, rise height, and duration of the fireball. All fire test series include incident heat flux measurements by instruments placed external to the fire. For the concrete wall experiments, measurements for model comparison are temperatures within the walls after 30 minutes of heating from radiant ceramic heaters.

The average surface emissive power of the flame is of interest for all these types of fires but is typically not measured directly. For most of the experiments in this database the average surface emissive power is derived using integral models wherein radiometer measurements of incident heat flux are used in conjunction with video footage. Thus, this quantity is not considered as robust as comparing directly to radiometer data. Modern measurement techniques typically use infrared cameras which take temperature measurements and derive the surface emissive power using an assumed flame emissivity.

The burn rate is a quantity often measured for pool fires but is commonly used directly as an input for models due to the complexity of the burning of multi-component fuels and due to the computational costs of resolving pool dynamics in conjunction with the gas phase of the fire. This is especially true for the Phoenix water-based pool fire experiments discussed in Section 3.1.3 where ice formation occurred. If a code can feasibly calculate the multiphase behavior, then this approach should be taken, otherwise it is reasonable to specify the burn rate using experimental measurement.

The instruments used to measure incident heat flux are usually radiometers or heat flux gauges which will have different viewing angle ranges. They are typically classified as 'wide-angle' for viewing angles of 120 to 180 degrees and 'narrow-angle' for viewing angles typically around 5 to 10 degrees. Most computational codes do not have models reflecting a narrow-angle radiometer response, but rather will have a model more applicable for wide-angle gauges since the code usually assumes a viewing angle of 180 degrees. Thus, it is important to take note of the instrument type used experimentally together with the heat flux gauge model used computationally to have a fair comparison. Additionally, the measurements provided in the database have not been corrected for atmospheric attenuation. Thus, a model for atmospheric attenuation is required to have a fair comparison to the radiometer data provided in the MEP database. The transmissivity, τ, ranging from values of 0 to 1 characterizes the degree of atmospheric attenuation due, principally, to the presence of H_2O and CO_2. When radiometer measurements are corrected for atmospheric attenuation by dividing by the transmissivity, the measurement will increase if the transmissivity value is below 1.

Other instruments used to determine incident heat flux are directional flame thermometers (DFT) in which two steel plates separated by insulation have thermocouples mounted on the inner faces of the plates. The heat flux is calculated from these thermocouple measurements using inverse heat conduction methods which involve several assumptions. This method is also used to determine the

heat flux to engulfed objects using a calorimeter. The computational cost of resolving the structure of the DFT while adequately capturing the much larger scale of the simulation domain is impractical with regards to run time. Thus, DFT measurements are not included in the spreadsheet.

With regards to thermocouple measurements, when used to measure temperature within the fire plume, the measurement will be significantly lower than the true gas temperature due to factors that affect heat transfer in the thermocouple device [22]. Thus, when using a CFD model, a thermocouple model is required for fair comparison to measurements.

The criteria to determine flame height, drag, and tilt are based on the luminous portion of the flame. Flame tilt occurs when pool fires are subject to wind influence which can cause the flame to tilt in the downwind direction. The degree of flame tilt is typically defined as the angle of the flame from vertical. Flame drag is the distance that the flame extends along the ground outside the pool due to wind. It is normalized by adding the pool diameter to the extension length, then dividing by the pool diameter.

Time-averaged flame height is usually defined as the height at which the intermittency reaches a value of 0.5, while maximum height is usually defined at an intermittency level of 0.05. Intermittency is defined as the fraction of time the flame is at a certain height. The geometric aspects of fires, such as flame height, tilt, and drag are typically derived from video footage from the experiments, which requires a criterion to define the bounds of the luminous portion of the flame. The criterion used is often not reported. The lack of standard criteria is, in part, responsible for the variation in reported measurements for equivalent fire conditions among different research groups. Thus, among the measurements for comparison considered in this report, these parameters are not as robust for the purposes of a model validation exercise.

If provided for a test series, the criterion used to identify flame geometry should be used for model evaluation. For test series not providing a criterion, it is reasonable to use a flame temperature of 580°C for estimating flame height since this corresponds to a blackbody surface emissive power of about 30 kW/m^2, which is the mid-range (20-40 kW/m^2) of what has been measured for black smoke, the non-luminous portion of the flame. Thus, temperatures around 580°C would approximately indicate the transition zone between luminous and non-luminous regions. In performing evaluation of a model for the MEP, the criteria used to define the luminous portion of the flame should be reported.

Note that for most hydrocarbons it is difficult to accurately identify the luminous portion of the flame due to smoke shrouding the flame itself. Significant smoke production occurs for heavier hydrocarbons, but it has been found that for LNG pool fires the smoke production is significantly less, allowing for most of the flame height to be identified. The largest LNG test conducted on land (35 m) indicated an average visible flame length-to-diameter ratio up to 2.4, which is much higher than for other hydrocarbons at equivalent scales, and the 21-m and 56-m diameter Phoenix pool fire tests on water resulted in negligible smoke production. Heavier hydrocarbons at these pool sizes would produce sufficient smoke to cover nearly the entire flame except for a portion near to the flame base and in the downwind direction where large vortices develop which tend to clear the smoke. This has significant implications for exclusion zones since smoke serves as a radiant barrier, reducing the radiant heat flux at a distance relative to non-shrouded flames, thereby resulting in smaller exclusion zones.

2.2. Quantification of Comparison

The approach taken to quantify the accuracy of model predictions of experimental results follows the recommendation provided in [23] [24]. The approach presented in [23] [24] addresses how to identify model uncertainty and provides performance measures for the degree of under or over-prediction and scatter. The degree of a model's under- or over-prediction is measured by the bias factor, δ, and the degree of scatter is measured by the relative standard deviation, $\tilde{\sigma}_M$. It is assumed that model predictions are normally distributed about true values multiplied by the bias factor. This method considers three sources of uncertainty, namely, from experimental measurement, model parameter inputs from experimental measurement, and those arising directly from the model. Assessing those arising directly from the model can be impractical for CFD codes due to the numerous parameters to evaluate. Thus, this method was developed to allow for model uncertainty to be evaluated indirectly by assessing the experimental uncertainty and model input uncertainty. Model input uncertainties are based on experimental measurement which include quantities such as wind conditions, fuel characterization or burn rate, for example. In the following, the term 'propagated input uncertainty' represents the model input uncertainty. The measurement uncertainty and propagated unput uncertainty are then combined to provide an uncertainty termed, 'combined uncertainty'.

The measurement uncertainty pertains to measurements used for model comparison. In reference [23], measurement uncertainty has been determined for certain measured quantities of interest (e.g. flame temperature, heat flux, gas concentrations, velocity etc.) from a range of experiments that have measured these quantities. Pertinent values from reference [23] are provided in Table 2-1 and are used in the spreadsheet for those test series where measurement uncertainty is not reported, otherwise the reported measurement uncertainties are used. Measurement uncertainties for burn rate and heat flux measurements engulfed in a fire are provided in Table 2-2 and are used in the MEP spreadsheet. A Schmidt-Boelter type gauge listed in Table 2-2 is a non-optical heat flux gauge that measures convective and radiative heat flux versus an optical gauge which is a photon detector that responds to incident radiative heat flux only.

The combined uncertainty in Table 2-1 is $\tilde{\sigma}_E$ and is determined by taking the square root of the sum of the squares of the measurement uncertainty and the propagated uncertainty of the model input parameters obtained from experiments. Note that both the measurement and propagated measurement uncertainties are in the form of relative standard deviations. In [23], the effect of parameter input uncertainty on model predictions is determined by using empirical correlations to identify functional relationships between model inputs and outputs. In this MEP, the propagated input uncertainty is determined by the user performing cases that span the range of measurement uncertainty for an applicable input parameter.

Table 2-1. Measurement uncertainty estimates.

Quantity	Measurement Uncertainty	Propagated input uncertainty	Combined uncertainty, $\tilde{\sigma}_E$
Gas temperatures	0.05	0.05	0.07
Heat flux (external to fire)	0.05	0.10	0.11

Table 2-2: Measurement uncertainty estimates for incident radiative flux of various measurement instruments internal to the fire

Quantity	Measurement Uncertainty
Burn rate [25]	0.6% (differential pressure gauge, mm/min) 4.3% (thermocouple rake within pool, mm/min) 4.1% (uncertainty in converting regression rate (mm/min) to a mass flux (kg/m^{2}s) using pool area and fuel density)
Incident radiative heat flux (kW/m^2, engulfed) measured by a Schmidt-Boelter Type Gauge [26]	±39% (low wind, <10 m/s) ±23% (high wind, >10 m/s)

In the MEP spreadsheet there is a worksheet for each test series that provides the measured input parameters and their associated uncertainty for evaluating the propagated input uncertainty. The variation of these parameters using a model is to be carried out using a single experiment within a test series. The specific test to be used for this purpose is provided in the respective worksheets and in the following sections of this report describing each test series. The set of results from the input parameter variations is then used to determine an average relative standard deviation to characterize the propagated input uncertainty, which is automatically calculated in the worksheet. This allows for the combined uncertainty, $\tilde{\sigma}_E$, to be determined which is also calculated automatically in the worksheet.

The bias factor, δ, and relative standard deviation, $\tilde{\sigma}_M$, are evaluated using equations (1)-(3) where E_i are experimental measurements and M_i are model predictions at all measurement locations, 'i' for each test. Equations (1) and (2) allow for $\tilde{\sigma}_M$ to be determined once the combined uncertainty, $\tilde{\sigma}_E$, is evaluated as described above. Once $\tilde{\sigma}_M$ and $\tilde{\sigma}_E$ are determined, the bias factor, δ, can then be evaluated using Equation (3).

$$\tilde{\sigma}_M^2 + \tilde{\sigma}_E^2 \approx \frac{1}{n-1}\sum_{i=1}^{n}\left[ln\,(M_i/E_i) - \overline{ln\,(M/E)}\right]^2 \quad (1)$$

where the last term on the right of Equation (1) is defined as

$$\overline{ln\,(M/E)} = \frac{1}{n}\sum_{i=1}^{n} ln\,(M_i/E_i) \quad (2)$$

$$\delta \approx \exp\left(\overline{\ln\,(M/E)} + \frac{\tilde{\sigma}_M^2}{2} - \frac{\tilde{\sigma}_E^2}{2}\right) \quad (3)$$

Once $\tilde{\sigma}_M$ and δ are evaluated, graphical representations of the results, as shown in Figure 2-1, are automatically generated in the spreadsheet for each test. If a test has an insufficient number of measurements for a particular quantity, then measurements from all tests within a series are combined to generate graphical comparison on a separate spreadsheet. The predicted values in Figure 2-1 (red circles) is an example where radiometer measurements from all tests within a test series have been combined.

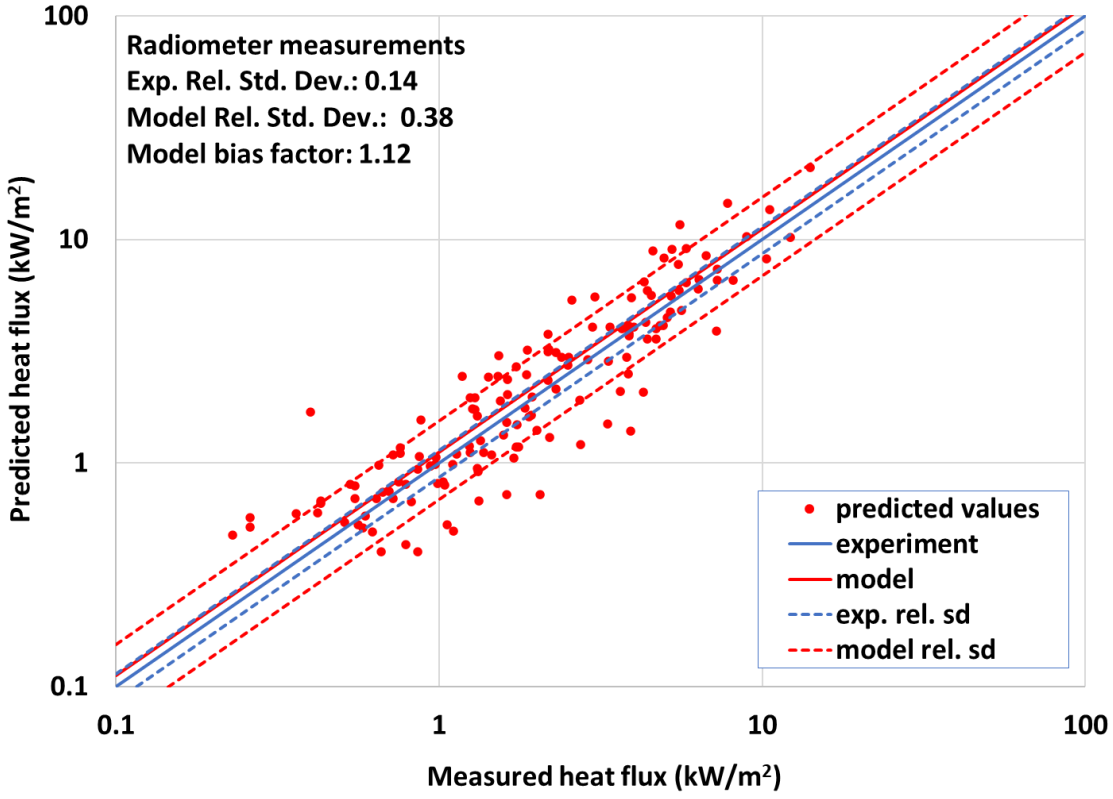

Figure 2-1. Comparison of predicted to measured values use statistical measures of relative standard deviation and bias factor

2.3. Thermal exclusion zones based on model performance

There are several performance measures that can be used to characterize the scatter and bias of a set of model predictions. These measures are ascribed a value to determine acceptable performance and are based on expert judgement, which can be subject to debate among experts. In practice, a model will often meet the criteria set out by some measures but not others, which creates difficulty when assessing overall model performance, particularly if the number of 'pass/fails' are balanced. Due to variations in model performance a safety factor of two is often recommended. The approach taken in this model evaluation database is not to specify a specific value to determine the acceptability of a model, rather to assess the probability that a model prediction will exceed a critical value of interest.

As an example, the model relative standard deviation and bias factor are applied in the following way. Assume that the critical heat flux of interest is 5 kW/m^2 and a model is used to predict heat flux versus distance. A normal distribution curve can be calculated using the mean and standard deviation, that is, $\mu = \mathrm{M}/\delta$ and $\sigma = \widetilde{\sigma_M}\mu$, where M is the heat flux predicted using the model, δ is the bias factor, and $\widetilde{\sigma_M}$ is the model relative standard deviation. Assuming a normal distribution based on assessment of the ln(M/E) histograms, the probability that the "true" heat flux exceeds the critical heat flux at the predicted distance can be determined by

$$\mathrm{P}(\dot{q}'' > \dot{q}''_c) = \frac{1}{2}\mathrm{erfc}\left(\frac{\dot{q}''_c - \mu}{\sigma\sqrt{2}}\right) \qquad (4)$$

where $\dot{q}''_c$ is the critical value of interest, which in this case is 5 kW/m^2. Using Equation (4), the probability of the model exceeding 5 kW/m^2 as a function of distance can then be generated from predictions of heat flux as a function of distance from the center of a fire.

An example curve of a hypothetical pool fire is shown Figure 2-2 using a model relative standard deviation of 0.38 and bias factor of 1.12. The model predicts a heat flux of about 5 kW/m^2 at 190 m. The curve indicates that the probability of exceeding 5 kW/m^2 at 190 m is about 38%.

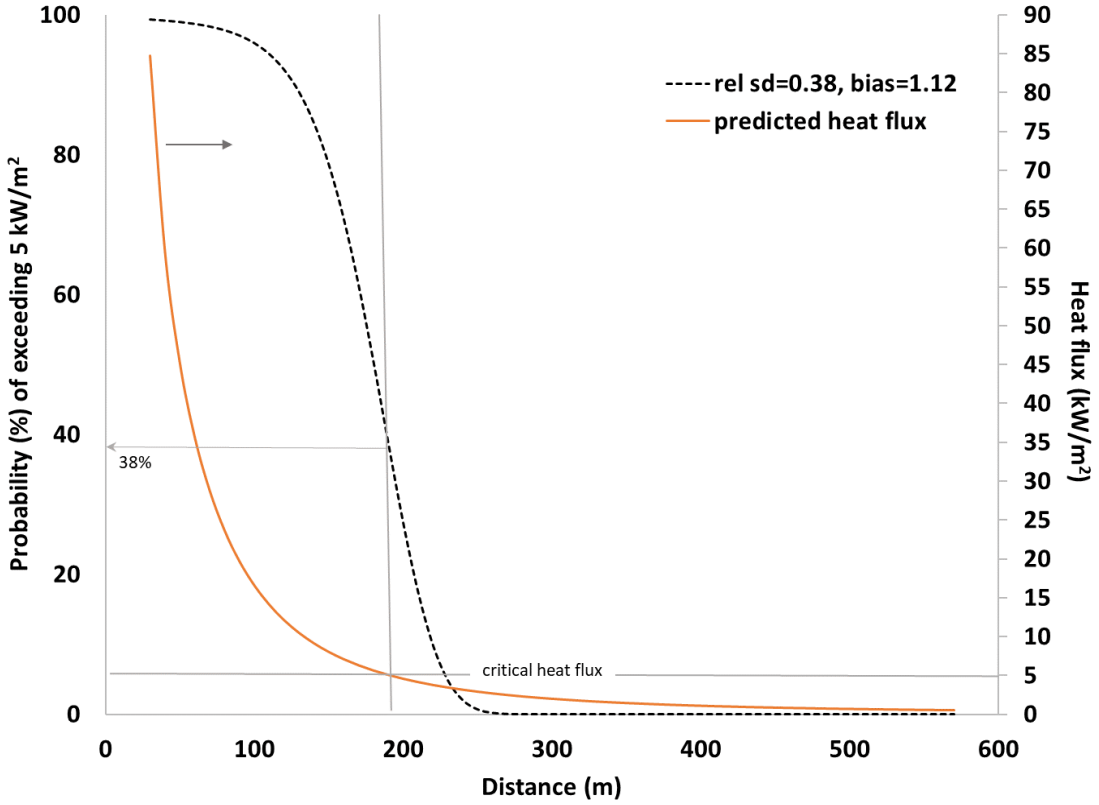

Figure 2-2: Probability of exceeding 5 kW/m^2 at various distances for a hypothetical pool fire (rel. sd=0.38, bias=1.12).

For contrast, an under-predictive model is shown in Figure 2-3 with a bias factor of 0.38 and a model relative standard deviation of 1.4. For this model there is a 66% probability of exceeding 5 kW/m^2 at 190 m. A 38% probability occurs at distances of 360 m and heat fluxes of 1.35 kW/m^2 which is almost a factor of two greater in distance to achieve the same level of probability as the better performing model.

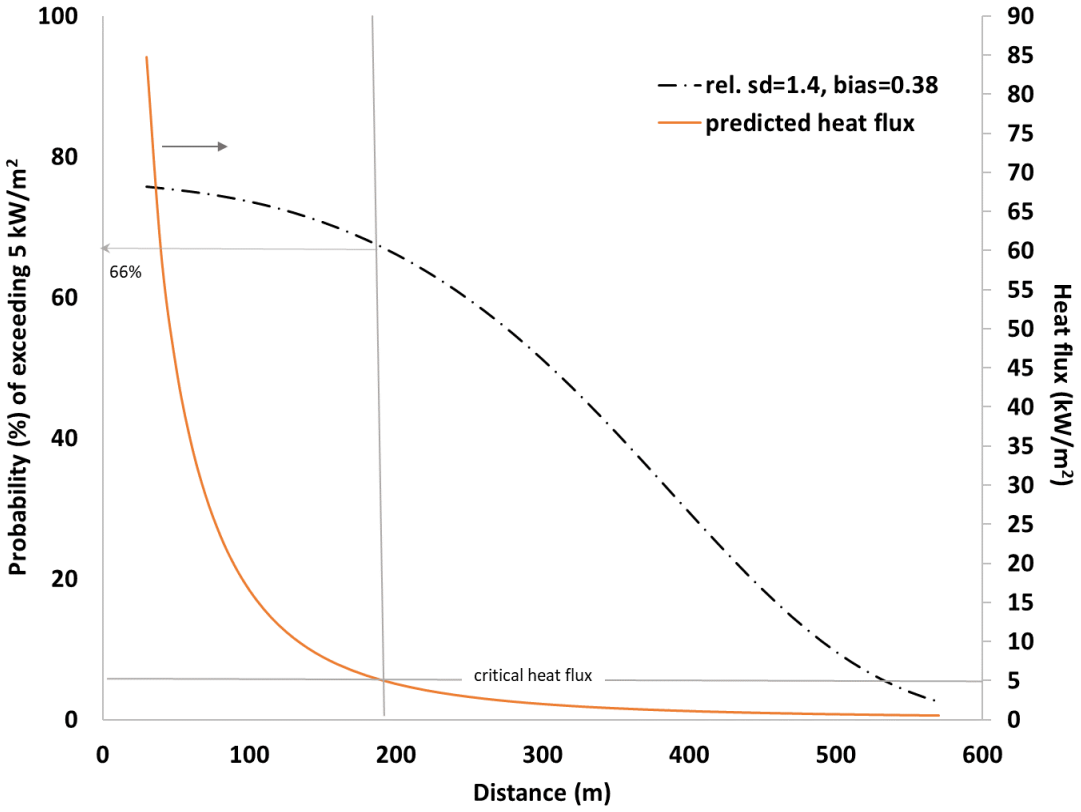

Figure 2-3: Probability of exceeding 5 kW/m^2 at various distances for a hypothetical pool fire (rel. sd=1.4, bias=0.38).

Conversely, a highly over-predictive model with a model relative standard deviation of 0.38 and bias factor of 2 will reduce the probability at the critical value of interest as shown in Figure 2-4. In this example, the probability of exceeding 5 kW/m^2 at 190 m is 0.5% since most likely it is over predicted. If a probability of 38% is desired, then the distance reduces to about 140 m vs. 190 m compared to the model having a model standard deviation of 0.38 and bias factor of 1.12.

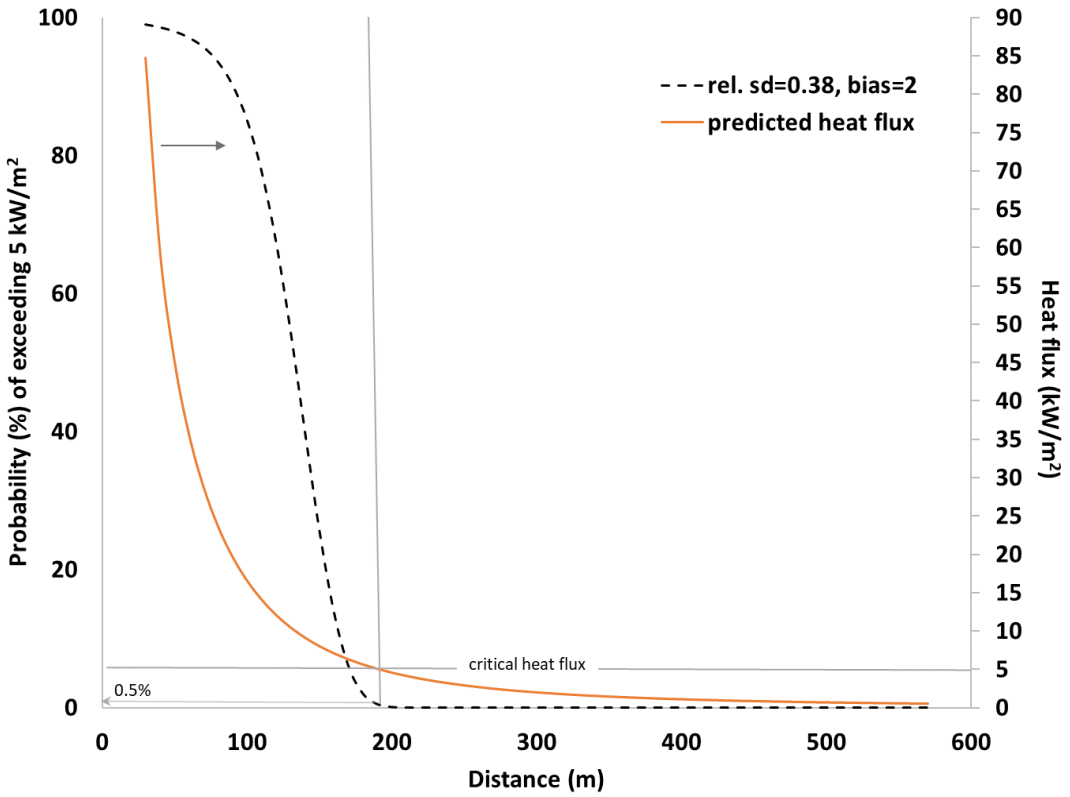

Figure 2-4: Probability of exceeding 5 kW/m² at various distances for a hypothetical pool fire (rel. sd=0.38, bias=2).

A highly accurate model which has a bias equal to unity and a model relative standard deviation approaching zero will display behavior where locations below and above the predicted distance at which 5 kW/m² occurs will approach a 100% and 0% probability of exceeding 5 kW/m², respectively. An over-predictive model will have a probability of exceeding 5 kW/m² below 50%, whereas an under-predictive model will have a probability above 50%.

To determine a thermal exclusion zone based on model performance, a model uncertainty factor is identified based on the ratio of the critical heat flux to the heat flux at which the probability drops to 0.025 or within a 95% confidence interval. For over predictive models which have a heat flux greater than the critical heat flux at a probability of 0.025, the heat flux is to be set equal to the critical heat flux to provide a model uncertainty factor of one.

The model uncertainty factor pertains to a factor reduction of the critical heat flux level and does not pertain to a factor increase in the predicted distance to the critical heat flux. In the first, second, and third examples above, the heat flux levels at which a probability of 0.025 occurs are 3.2 kW/m², 0.51 kW/m², and 5.7 kW/m² and thus provide model uncertainty factors of 1.6, 9.8, and 1.0, respectively. The distances for these model uncertainty factors are 238 m, 570 m, and 178 m which provides distance ratios of 1.3, 3.0, and 0.94, respectively. Distance ratios are not used to determine the model uncertainty factor because distances at which specific heat flux values occur change with changes in the parameters characterizing the specific application such as wind speed, pool size, etc. Whereas for a given value of scatter and bias based on model results, the heat flux value at which a probability of 0.025 occurs remains the same regardless of how distances may shift for a particular application. It is

also invariant to the critical heat flux of interest so that the same model uncertainty factor applies whether a critical heat flux of 31.5 kW/m^2 or 5 kW/m^2 is evaluated.

2.4. Organization of the database spreadsheet

The MEP database spreadsheet provides individual worksheets for each experiment. The left-hand section of each of these worksheets provides the inputs required for models such as geometric descriptions, atmospheric conditions, and instrument placement. On the right-hand section of each of these sheets, cells highlighted in yellow are where model results are to be entered. Once the model results are entered, the relative standard deviation and bias factor are automatically calculated in respective titled cells for the individual tests. Graphical results comparing model predictions to the experimental data are also automatically generated. For each test series there is a worksheet that combines all tests within the series to provide an overall relative standard deviation and bias factor. Note that the relative standard deviation and bias factor are not calculated for quantities with few measurements within an experimental series. The comparison of model predictions to experimental results is to be provided in tabular form in the MEP report for these test series.

There are also worksheets that provide further grouping of data in which model results for all LNG experiments are combined into worksheets for each fire type, as well as worksheets combining non-LNG experiments for each fire type. Worksheets that combine model results for both LNG and non-LNG experiments for each fire type is also provided. The final worksheet provides uncertainty factors based on model predictions of incident heat flux for LNG and non-LNG experiments, as well as both combined for each fire type. Data from insulated concrete wall experiments is also included in the MEP spreadsheet.

A key input to determine the model relative standard deviation and bias factor is the propagated input uncertainty mentioned in Section 2.2. This is determined by performing simulations involving the variation of model inputs based on possible ranges for experimental parameters. The experimental parameters to vary are provided in Section 3 as well as in the MEP database spreadsheet for each test series where respective worksheets are titled "s*eries name* prop. uncert.". Results for each variational case pertaining to experimental uncertainties is to be entered for each measurement location in this worksheet for each experimental series.

A worksheet for entering results from a sensitivity study is also included for each experimental series. The sensitivity analysis is to be performed on at least one test within a series, the individual test is to be chosen by the user of the MEP, though more than one may be chosen if desired. If more than one test is chosen, then the sheet may be copied to allow entry of results for another test. There is a table in the spreadsheet where descriptions of the parameters being varied are to be entered. The parameters encompass those that apply to features discussed in Sections 5.1.1 through 5.1.5 in the MEP document, *Model Evaluation Protocol for Fire Models Involving Fuels at Liquefied Natural Gas Facilities (Version 2)*. [27].

This page left blank

3. DESCRIPTION OF LNG DATABASE

The following sections pertain to LNG fire experiments and are categorized according to fire type that includes pool fire, jet fire, and fireball. The information provided for each test series is a general description, specification of instrumentation, measured quantities for comparison, and experimental input parameters to vary to determine the propagated input uncertainty for the model.

3.1. Pool Fires Experiments

There are four test series included under this fire type, one conducted indoors and the other three outdoors, two of which are on land and the other is on water. Although the indoor test series is not reflective of the typical scale of an industrial accident, it has the advantage of having relatively well-defined boundary conditions. In contrast, the outdoor tests do not have boundary conditions that are as well-defined (e.g. atmospheric conditions and burn rate) but the tests are at a scale pertinent to accident scenarios.

3.1.1. Sandia methane gas burner tests

A series of 3-m diameter methane gas burner tests were conducted in a controlled environment in the Fire Laboratory for Accreditation of Models and Experiments (FLAME) test cell in the Thermal Test Complex at Sandia National Laboratories [5]. Table 3-1 provides a general description of the Sandia methane gas burner tests.

Table 3-1: General description of Sandia methane gas burner tests

General description	
Test location	Thermal Test Complex (indoor), Albuquerque, NM
Test performed by	Sandia National Laboratories
Pool diameter	3-m gas burner
Number of tests	28
Fuel composition	99.9% (vol) methane
Engulfed object	No
Data confidentiality	Open, publicly available
References	Blanchat, T., et al. [5]

Figure 3-1 shows a cut-away of the cylindrical FLAME test chamber which has an inner diameter of 18.3 m (60 ft) and height of 13.1 m (43 ft) around the perimeter. The ceiling slopes upwards (~18º) from the perimeter walls to a height of 15.2 m (50 ft) over the center of the facility. A round hole at the top of the facility 5.5 m (18 ft) in diameter transitions to a 3.0 m by 3.7 m (10 ft by 12 ft) chimney duct. The outer walls are made of steel channel sections, filled with water for cooling during tests. The gas burner is surrounded by a 12.7 m (42 ft) diameter steel spill plate. Beyond the spill plate is steel grating which air can flow through from the basement of the facility.

Air is supplied from a forced draft (FD) fan in a central utility building (not shown) through a large underground pipe (3.7-m (12 ft) diameter) to a plenum that feeds 18 radial pipes 0.91-m (3 ft) diameter) to a 1.22-m by 1.22-m (4 ft by 4 ft) annular ring in the FLAME basement. The air ring is 3.7 m (12 ft) below the ground level gas burner. For these tests the flow through the annular ring was reduced to a

width of 0.61-m (2 ft) by placing steel plates on its outer perimeter to equalize the flow. Air exits the grated top of the annular ring and enters the ground level steel grating. An induced draft (ID) fan just before the exhaust stack automatically adjusts speed to maintain the differential pressure (to ambient) across the FLAME wall near zero. The facility was designed to replicate quiescent outdoor conditions in that no excess pressure or re-radiation from the walls impacts the fire. Thus, it is considered acceptable to perform simulations without including the geometry of the FLAME facility. The overall objective of the experiments was to develop a flame height correlation for methane. A total of 28 tests were performed for various methane flow rates. The measurements and instrumentation used for the experiments are provided in Table 3-2.

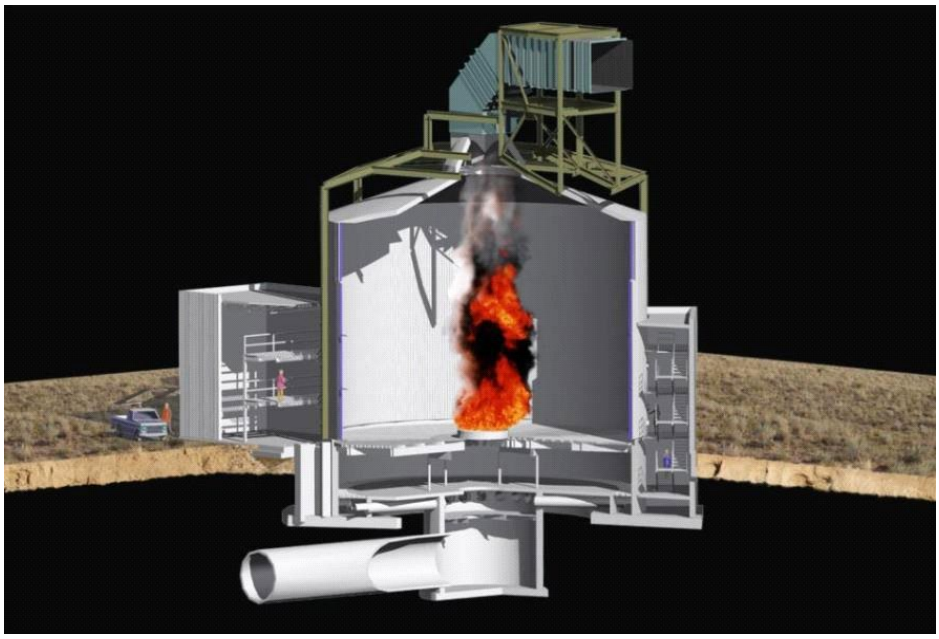

Figure 3-1. A cutaway view of the Sandia FLAME facility.

Table 3-2. Measurements and instrumentation for methane gas burner experiments

Measurement	Instrument
Total heat flux	Wide-angle total heat flux gauges
Spot surface emissive power	Narrow-angle radiometers
Flame height	Cameras
Test cell conditions	Incoming fuel and air temperature

Eight narrow-angle radiometers and eight total heat flux gauges measured the radiation intensity as a function of height. Pairs of Medtherm gauges, a narrow-angle radiometer (5º view angle) and a total heat flux gauge (180º view angle) were mounted together at approximately 9 m from the center of the fire at heights of ~0.5 m to 4.0 m with a spacing of 0.5 m. The spot diameter for the narrow-angle gauges (at 9 m) is about 0.8 m. The gauge pairs were at heights of ~0.5 m to 4.0 m with a spacing of 0.5 m between gauges. The line of sight for each gauge passed through the centerline of the fire at the height of the gauge. All heat flux gauges were water cooled. Table 3-3 provides the inlet conditions for the 28 tests.

Table 3-3. Inlet conditions for methane gas burner experiments

Test #	Ambient press (Pa)	Ambient RH (%)	Incoming gas temp (ºC)	Incoming air temp (ºC)	mass flux of injected methane (kg/m^{2}s)
1	82,970	6	29	23	0.0164
2	82,970	6	29	24	0.0091
3	82,970	6	29	24	0.0072
4	83,480	12	17	18	0.0077
5	83,480	12	18	18	0.0096
6	83,480	12	19	18	0.0160
7	83,480	12	20	18	0.0077
8	83,240	7	30	23	0.0165
9	83,150	7	31	24	0.0178
10	83,150	7	31	24	0.0246
11	83,150	7	28	24	0.0269
12	83,150	7	27	24	0.0308
13	82,380	9	27	25	0.0352
14	82,380	9	26	25	0.0287
15	82,380	9	26	25	0.0241
16	82,380	9	27	25	0.0105
17	82,380	9	29	25	0.0030
18	82,380	9	29	25	0.0050
19	82,380	9	30	25	0.0022
20	82,380	9	31	25	0.0034
21	82,510	17	18	17	0.0273
22	82,510	17	18	17	0.0190
23	82,510	17	19	17	0.0124
24	82,510	17	20	17	0.0088
25	82,510	17	20	17	0.0067
26	82,510	17	21	17	0.0054
27	82,510	17	21	17	0.0032
28	82,510	17	22	18	0.0024

3.1.1.1. Sandia gas burner tests: experimental comparisons and parameter variation

The experimental measurements for model comparison included in the MEP spreadsheet are provided in Table 3-4. If a code includes a model for a narrow-view radiometer, then this can be used for

comparison to spot surface emissive power measurements. The total heat flux gauge values are a combined measurement of incident and convective heat flux. For similar comparison to the thermocouple measurements within the fire plume a code also requires a model that captures the features of a thermocouple since measured flame temperatures are much lower than actual flame temperatures as discussed in [22].

Table 3-4. Sandia gas burner tests: measurements for validation

Parameter	Instrument	Measurement Uncertainty
Average total heat flux	Wide-angle total heat flux gauges	5%
Spot surface emissive power	Narrow-angle radiometers	5%
Average fire plume temperature	MIMS, 40 mil, Type K, thermocouples	3%
Average flame height	Reduction method from video coverage	2%

To determine the propagated input uncertainty, experimental parameter variations are provided in Table 3-5. Test 1 was chosen since it falls in the mid-range among the tests with regards to mass flux and flame height. The inlet fuel mass flux had a reported uncertainty of ± 8%. The inlet temperatures have an uncertainty of ± 3°C which is not a significant variation so are excluded from the parameter variation exercise. Uncertainty in the environmental conditions of pressure and relative humidity were not reported. For most codes, the anticipated uncertainty of these parameters (<2%) will not cause significant differences in the results.

Table 3-5. Sandia gas burner Test 1: Experimental input parameters to vary

Test 1	
Parameter	**Variation**
Inlet fuel mass flux	0.0151 kg/m^{2}s (low) 0.0164 kg/m^{2}s (base) 0.0177 kg/m^{2}s (high)

3.1.2. Montoir pool fire tests

The Montoir tests were a collaboration among many sponsoring companies: British Gas, British Petroleum, Shell, Elf Aquitaine, Total CFP, and Gaz de France with tests performed by British Gas Midlands Research Station and Shell Research Ltd. at a facility near the Montoir de Bretagne methane terminal [6]. A total of three 35-m diameter LNG pool fire experiments were performed over a wind speed range of 2.7 to 10.1 m/s. Flame geometry, incident thermal radiation at various ground level positions, spot surface emissive power, gas composition and heat flux above the pool surface, fuel mass burning rate, and flame emission spectra in both the visible and infra-red regions were measured. Table 3-6 provides a general description of the Montoir pool fire tests.

Table 3-6 . General description of the Montoir pool fire tests

General description	
Test location	Montoir, France
Test performed by	British Gas Midlands Research Station and Shell Research Ltd.
Pool diameter	35-m
Number of tests	3
Fuel composition	methane (>99 vol% during measurements)
Engulfed object	No
Data confidentiality	Partial data available in conference publication. Permission granted by DNV and Shell to provide data for MEP from test reports on condition of inclusion of disclaimer[1].
References	Nedelka, et al. [6] (publicly available publication) Test reports from British Gas and Shell

Since LNG was used and not pure liquefied methane, the gas concentrations were monitored at the surface of the fuel to determine durations of nearly pure methane burning. The reported measurements pertain to durations over which the vapors above the pool were measured to have at least a 99-mole% methane content.

To measure incident heat flux, up to 45 wide-angle radiometers were placed along eight spokes surrounding the pool at an elevation of 1 m and aimed horizontally towards a point 1 m above the bund center. Both slow-response and fast-response wide-angle radiometer measurements were obtained. The slow-response wide-angle total heat flux gauges were Land and Medtherm Schmidt-Boelter sensors, with viewing angles ranging from 50º to 150º and the five fast-response (time constant <20 ms) wide-angle total heat flux gauges included a Barnes thermistor-type and an IRD pyroelectric type with viewing angles of 40º by 70º and 55º, respectively. The fast-response wide-angle gauges were aligned with video cameras to determine the average surface emissive power of the flame.

Three steerable, fast response (time constant <30 ms) narrow-angle radiometers with a view angle of 1º were used to measure spot surface emissive power of the flame. To determine the point of aim of the narrow-angle radiometers a video camera was aligned with the detectors. One narrow-angle radiometer used narrow-band filters for wavelengths of 0.62 μm, 2.25 μm, and 4.02 μm to provide information regarding the radiative characteristics of soot.

Although atmospheric attenuation was determined, the data provided in the database spreadsheet is uncorrected radiometer data. Thus, a model for atmospheric attenuation should be included in the

[1] *The content of the reports is intended only to provide data and analysis of experimental studies and is not intended to be any substitute for professional advice. DNV Group of companies, including GL Industrial Services UK Ltd, and any other person or company, including, but not limited to, Shell Research Ltd., concerned with furnishing information or data used therein, excludes to the maximum extent permissible by law any legal liability in contract and tort (including negligence) for the up-to-date nature, accuracy, completeness, quality, or usefulness of any information, apparatus, product, or process disclosed or demonstrated.*

simulations. Table 3-7 provides the measurements and instrumentation used for the Montoir pool fire tests.

Table 3-7. Measurements and instrumentation for Montoir pool fire tests

Measurement	Instrument	Measurement Uncertainty
Spot surface emissive power	Narrow-angle radiometers (fast-response, steerable)	±10%
Incident radiative heat flux	Wide-angle radiometers (fast-response and slow-response	±10% (fast response) ±3% (fast response)
Total heat flux to pool	Calorimeters (total heat flux gauge, water cooled, 180^{o} view angle)	±23% [26]
Flame geometry (flame height, flame drag, flame tilt)	Cameras (video, cine, and SLR)	Not reported ±10%*
Mass burning rate	Diptube Thermocouple rake within pool	4.1% [25] (diptube; thermocouples proved not to be reliable)
Composition above pool	Gas chromatography	Not reported
Spectral radiation	Spectrometers (visible, near-infrared, and infrared)	Not reported
Weather conditions	Wind speed: Anemometer Wind direction: Wind vane Pressure: barometer Air temperature and humidity: thermometer and RH meter	Wind speed: greater of ±2.5% or ±0.25 m/s Wind direction: ±5^{o} Pressure: ±1% Thermometer and RH meter: ±5%

*approximate value provided by subject matter experts at Sandia. Main contributing factor is error correction regarding the lens.

Table 3-8 provides measurements of wind speed and direction taken at two different locations separated by several hundred meters. One measurement was made by British Gas and the other by Shell. Shell collected wind speed and direction measurements at a single elevation of 8.4 m above ground with standard deviations not reported. Note that the wind speed was not reported at a height of 4.5 m for Test 1 from the British Gas tower. The wind direction is based on an average among the British Gas and Shell measurements and the inferred direction based on contours of incident heat flux from the wide-angle radiometers. Note that the wind direction is relative to magnetic north. Table 3-9 provides atmospheric conditions for each experiment.

Table 3-8. Wind speed and direction for Montoir pool fire tests

Experiment	Duration (sec)	Height (m)	Wind speed (m/s)	Wind direction (degrees)
Test 1	60-100	1	1.9 ± 0.5	59
		8.4	2.3	
		9	2.5 ± 0.7	
	130-170	1	3.1 ± 1.0	70
		8.4	5.5	
		9	4.8 ± 0.7	
Test 2	35-50	1	5.4 ± 0.4	268
		4.5	6.1 ± 1.0	
		8.4	7.1	
		9	6.8 ± 1.0	
	65-85	1	5.3 ± 0.9	263
		4.5	8.9 ± 1.2	
		8.4	10.4	
		9	9.8 ± 0.7	
	100-130	1	6.6 ± 1.3	260
		4.5	9.7 ± 1.6	
		8.4	8.9	
		9	10.3 ± 1.1	
	165-185	1	5.8 ± 1.6	257
		4.5	8.6 ± 1.3	
		8.4	11.1	
		9	9.1 ± 1.0	
Test 3	57-70	1	1.1 ± 0.3	87
		4.5	2.1 ± 0.3	
		8.4	3.7	
		9	1.9 ± 0.5	
	90-120	1	2.4 ± 0.6	79
		4.5	3.1 ± 0.7	
		8.4	4.1	
		9	3.5 ± 0.5	
	130-160	1	2.8 ± 0.5	82
		4.5	3.3 ± 0.9	
		8.4	4.7	
		9	4.2 ± 0.6	

Table 3-9. Atmospheric conditions for Montoir pool fire experiments

Experiment	Ambient temperature (^{O}C)	Atmospheric Pressure (Pa)	Relative humidity (%)
Test 1	25	102,200	53
Test 2	21	101,500	54
Test 3	14	100,900	85

Table 3-10 provides the burn rate averaged over durations which were selected jointly by British Gas and Shell by evaluating periods of steady-state fire conditions in conjunction with examining changes in wind conditions and incident heat flux measurements. The burn rates are based on two diptubes placed 5 cm from the bottom of the pan that measured the head of the fuel over time. For this MEP, measurements of mass per unit area over time from the two diptubes were digitized using the open-source code WebPlotDigitizer [28], in order to evaluate the gradient or burn rate over these durations. The test reports only provide the burn rate averaged over the entire duration during which methane was burning. Obtaining the burn rate over the specific durations of interest is important due to differences in wind speed that occurred which affect the burn rate.

Table 3-10. Average burn rate and radiative fraction for Montoir pool fire tests

Experiment	Duration (sec)	Average burn rate (kg/m^{2}s)
Test 1	60-100	0.12
	130-170	0.13
Test 2	35-50	0.14
	65-85	0.15
	100-130	0.16
	165-185	0.15
Test 3	57-70	0.11
	90-120	0.13
	130-160	0.13

For Test 1, the burn rate is based on readings from diptube 1 because diptube 2 had nearly constant readings of mass per unit area over the first period of 60-100 seconds and partially into the 130-170 second duration. The readings are suspect during these times since the mass should be decreasing over time and should not provide a constant reading due to burning. For Test 2, the burn rate for the first two durations, namely 35-50 seconds and 65-85 seconds, could not be determined from the diptube measurements since readings were either nearly constant or spurious up until about 100 seconds. Thus, for these durations the burn rate was estimated by examining the wind speed with identifiable burn rates. For the 35-50 second duration of Test 2, its wind speed was unique but fell between wind speeds for period 2 of Test 1 and period 4 of Test 2. Thus, a burn rate value is estimated based on interpolation of the burn rates for these two periods. For the 65-85 duration of Test 2, its wind speed is similar to period 4 of Test 2, thus the burn rate from this period is used.

3.1.2.1. Montoir pool fire tests: experimental comparisons and parameter variation

The experimental measurements for model comparison included in the MEP spreadsheet are provided in Table 3-11. The heat flux gauges above the pool surface are not included in the MEP spreadsheet since they are total heat flux gauges and adequately capturing the convective heat transfer would be computationally infeasible due to meshing requirements given their size as noted previously in section 2.1. Note that there were also two radiometers used to measure radiative heat flux above the pool, but soot deposited on their windows due to water cooling providing unreliable results. The steerable narrow-angle radiometer data are not included in the spreadsheet because they were aimed at a small portion of the flame for a short time (<10 s). Most likely there would be poor agreement between model and experimental results because the spot surface emissive power will fluctuate significantly from one 10 second span to the next. One fixed narrow-angle gauge was used in the experiments but is not included in the spreadsheet because it was aimed at a single location with a small spot area. Any deviation from the true atmospheric condition can greatly affect the comparison. The data for narrow-angle and wide-angle radiometer measurement surrounding the pool, and the heat flux gauges above the pool surface, are provided in Appendix A.

The flame length is defined as the distance from the center of the pool to the tip of the flame. Flame tilt is the angle with respect to the vertical axis and flame drag ratio is defined as the sum of the pool diameter and the extent that the flame extends beyond the pool, divided by the pool diameter.

Table 3-11. Montoir pool fire tests: measurements for validation

Parameter	Instrument
Average incident heat flux during steady state	Wide-angle heat flux gauges
Average flame height during steady state	Cameras
Average flame tilt during steady state	Cameras
Average flame drag ratio during steady state	Cameras

To determine the propagated input uncertainty, experimental parameter variations are provided in Table 3-12. The wind speed is not included as a parameter because a 2.5% uncertainty does not provide significant variation. Test 2 over the period of 100-130 seconds was chosen since it had the highest average windspeed which reflects the 49 CFR 193 criteria regarding evaluation of exclusion zones. In a hazard evaluation for siting purposes, a wind speed resulting in the maximum exclusion distance is to be used with exception of wind speeds that occur less than 5 percent of the time.

Table 3-12. Montoir Test 2: Experimental input parameters to vary

Test 2 (100-130 sec)	
Parameter	**Variation**
Burn rate	0.14 kg/m^{2}s (low) 0.16 kg/m^{2}s (base) 0.18 kg/m^{2}s (high)
Wind direction	255^o (low) 260^o (base) 265^o (high)

3.1.3. Phoenix pool fire tests

Two large scale pool fire tests were conducted at Sandia National Laboratories involving spills of liquid methane (>99.5 vol%, density 420 kg/m^3) as a surrogate for LNG [5]. The spills were onto a water pool resulting in effective pool diameters of 21 m and 56 m (Figure 3-2). This is considered a surrogate because, as found from the Montoir tests, methane boils off first before other hydrocarbons and will provide the highest heat flux compared to later times when the heavier hydrocarbons are burning.

The liquid methane was contained in a reservoir and approximately 58 m^3 and 198.5 m^3 were spilled for Test 1 and Test 2, respectively. The reservoir consisted of an above-ground dome-covered, truncated cone structure constructed with compacted soil. The liquid methane in the reservoir was gravity driven through a pipe that delivered the fuel to the center of a 120-m diameter water pool. A diffuser was constructed at the end of the pipe for uniform dispersal. Table 3-13 provides a general description of the Sandia Phoenix tests.

(a) **(b)**

Figure 3-2: Sandia Phoenix 21-m pool fire Test 1 (a) and 56-m pool fire Test 2 (b).

Table 3-13 : General description of the Sandia Phoenix pool fire tests

General description	
Test location	Sandia (outdoor), Albuquerque, NM
Test performed by	Sandia National Laboratories
Pool diameter	21-m and 56-m
Number of tests	2
Fuel composition	methane (>99.5 vol%)
Engulfed object	No
Data confidentiality	Open, publicly available
References	Blanchat, T., et al. [5]

The experimental measurements and instrumentation used in the tests are provided in Table 3-14. Measurement locations were along North, West, East and South spokes, where the North spoke (also called the 0 spoke) has a magnetic heading of 340 degrees. Three heat flux instrument towers on each spoke were located approximately 110 m (tower 1), 160 m (tower 2), and 210 m (tower 3) from the

center of the water pool. Cameras located on the end of each spoke (~226 m) focused on the vertical centerline of the water pool.

Table 3-14: Phoenix tests: Measurements and instrumentation

Measurement	Instrument	Measurement Uncertainty
Fuel regression	Inferred from reservoir liquid height over time and overhead video	±20%
Pool diameter	Cameras	±10%
Incident radiative heat flux	Wide-angle heat flux gauges (150º view angle)	±5%
Spot surface emissive power	Narrow-angle radiometers (5.5º view angle)	±5%
Inferred heat flux to pool	Directional flame thermometers	±9%
Spectral radiation	Spectrometers (mid-infrared and long-range infrared)	±6%-50% for maximum and minimum intensities, respectively (mid-infrared) ±21% (long-range infrared)
Flame geometry	Cameras (real time and IR)	±5%
Weather conditions	Wind speed: Anemometer Wind direction: Anemometer Pressure: barometer Air temperature and humidity Temperature and RH probe with an integral radiation shield	±1%

Some spokes contained additional instrumentation, such as IR cameras, spectrometers, and meteorological instrumentation. The heat flux instruments were water-cooled and the towers, approximately 1.5 m tall, were thermally insulated.

Twenty-eight (28) narrow-angle radiometers measured the spot surface emissive power at various heights of the flame plume surface (5.5º view angle). The relative angle of the narrow-angle gauges (to the ground plane) was adjusted to measure the flame plume heat flux at different heights (approximately equal spacing) with the line of sight for each gauge passing through the vertical centerline of the pool. Twelve (12) wide-angle heat flux gauges measured the total heat flux, where each tower had one gauge. The wide-angle gauges were water-cooled, Medtherm Schmidt-Boelter sensors, with a view angle of 150º. Although atmospheric attenuation was determined, the data provided in the database spreadsheet is uncorrected heat flux data. Thus, a sub-model for atmospheric attenuation should be included for these tests.

Tower 1 of each quadrant was the primary tower, supporting five narrow-angle radiometers for spot intensity measurements and one-wide angle heat flux gauge. Towers 2 and 3 each supported one narrow-angle radiometer and one-wide angle heat flux gauge used to determine heat flux variation with distance. Based on using a point-source model and the wide-angle heat flux gauge measurements,

the radiative fraction averaged among all instruments is 0.21 ± 0.03 for Test 1 and 0.24 ± 0.08 for Test 2.

The fuel regression rate was inferred from changes to the liquid level in the reservoir over time and overhead video to determine the real-time extent of the spreading pool fire. Note that the center location of the pool for both tests was not at the center of the water pool, instead offset to some extent due to the wind. The offset of the pool was measured and the distances from the fire's center to the radiometers in the database spreadsheet have been adjusted accordingly.

Wind direction and velocity, temperature, relative humidity, and barometric pressure were measured and recorded with near-field instruments. Wind speed and direction were measured at 2 m, 5 m, and 10 m heights on the North tower and at 10 m on the East tower (Table 3-15). The environmental conditions for each experiment are provided in Table 3-16.

Table 3-15 : Wind speed and direction for Phoenix Test 1 and Test 2

	Test 1		Test 2	
Height (m)	Wind speed (m/s)	Wind direction* (degrees)	Wind speed (m/s)	Wind direction* (degrees)
2	4.27 ± 0.67	319 ± 25	1.5 ± 0.3	309 ± 8.5
5	4.69 ± 0.67	321 ± 22	1.6 ± 0.2	313 ± 5.9
10	4.77 ± 0.69	321 ± 11	1.6 ± 0.2	319 ± 5.7

*Clockwise from North

Table 3-16 . Environmental Conditions for Phoenix Test 1 and Test 2

Experiment	Ambient Pressure (Pa)	Relative humidity (%)	Ambient Temperature (ºC)	Water temperature (ºC)
Test 1	84943	32	4	4
Test 2	84047	59	-2	1

The discharge rate, steady-state intervals, equivalent diameters, and mass flux are provided in Table 3-17. During Test 2 a portion of the spreading pool did not ignite primarily due to entrainment of water vapor into the base of the fire which formed a thermally protective layer above the non-burning portion of the pool in conjunction with formation of an ice sheet that encapsulated the methane [29]. The mass regression rate could not be accurately determined for Test 2 since the reservoir emptied before the steady-state pool area was reached. Dividing the measured release rate of 802 kg/s by the mass flux of 0.147 kg/m^{2}s determined in Test 1 provides an equivalent circular diameter of 83.3 m, very close to the measured 82.8 m. Thus, the MEP assumes that the mass flux from Test 1 can be used for Test 2. Note that the range of values provided in Table 3-17 reflect measurement uncertainties and not measurement standard deviations. Thus, this range differs from the summary tables presented in reference [5] which reflects the standard deviation of the collected data from average values and not measurement uncertainty.

Table 3-17: Effective pool diameter and mass regression rate for Phoenix Test 1 and Test 2

Test	Average mass discharge rate at diffuser (kg/s)	steady-state interval (s)	equivalent circular diameter (m)	mass flux (kg/m^2s)
1	49.4 ± 4.9	390-510	20.7 ± 3.6	0.147 ± 0.03
2	802 ± 80.2	250-300	82.8 ± 8.3 (total pool) 56.1 ± 9.8 (burning region)	0.147 ± 0.03*

*Assumed regression rate based on Test 1

3.1.3.1. Phoenix tests: experimental comparisons and parameter variation

The experimental measurements for model comparison included in the MEP spreadsheet are provided in Table 3-18. If a code includes a model for a narrow-view radiometer, then this can be used for comparison to spot surface emissive power. The flame length is defined as the distance from the center of the pool to the tip of the flame and flame tilt is the angle with respect to the vertical axis. To determine the propagated input uncertainty, experimental parameter variations are provided in Table 3-19. Test 1 was chosen since it has the feature of being a wind-driven fire.

Table 3-18: Phoenix tests: measurements for validation

Parameter	Instrument
Average spot emissive power	Narrow-angle radiometers
Average incident radiative heat flux during steady state	Wide-angle heat flux gauges
Average flame tilt during steady state	Cameras
Average flame length during steady state	Cameras

Table 3-19: Phoenix Test 1: Experimental input parameters to vary

Test 1	
Parameter	**Variation**
Effective pool diameter	18.8 m (low) 20.7 m (base) 22.4 m (high)
Mass flux	0.117 kg/m^2s (low) 0.147 kg/m^2s (base) 0.177 kg/m^2s (high)

3.1.4. BGC Trench fire tests

A series of LNG trench fire experiments of various sizes were performed by the British Gas Corporation with management oversight by Arthur D. Little, Inc. Table 3-20 provides a general description of the test series. Trench fires are a class of rectangular pool fires that have a high aspect ratio, typically above four. Thus, one dimension of the pool will be significantly longer than the other. Trench fires can occur when an accidental release of fuel spills into facility impoundments which are typically elongated dikes or trenches. Some distinguishing features of trench fires are that the flame

height scales, and surface emissive power increases, according to the shortest dimension. Thus, they will have a lower flame height and emitted radiation than a circular pool of equivalent area. They also have a flame structure that is not coherent, but that is broken up into lengthwise distinct peaks and valleys that vary over time. Detailed information regarding the test series can be found in the publicly available reports [7] [8]. In this experimental series 13 tests were performed for various trench dimensions and aspect ratios as provided in Table 3-21.

Table 3-20: General description of BGC trench fire tests

General description	
Test location	British Gas Spadeadam Test Facility, Cumbria, England
Test performed by	British Gas Corporation (BGC)
Trench dimensions	Listed in Table 3-21
Number of tests	13
Fuel composition	>98% (vol) methane during which data was collected
Engulfed object	No
Data confidentiality	Open, publicly available
References	Croce, et al. [7] [8]

Table 3-21. Experimental matrix for BGC trench fires

Test No.	Trench length (m)	Trench width (m)	Aspect Ratio
1	23.53	1.81	13.00
2	15.52	1.81	8.57
3	9.23	1.83	5.04
4	23.50	1.83	12.84
5	9.05	1.82	4.97
6	23.45	3.94	5.95
7	23.45	0.82	28.60
8	11.82	0.82	14.41
9	9.10	0.82	11.10
10	52.05	3.89	13.38
11	4.37	0.81	5.40
12	52.15	1.82	23.65
13	23.10	0.77	30.00

Measurements and instrumentation used for the tests are provided in Table 3-22. The experimental uncertainties were not reported for any of the measurements thus values are used from Table 2-1 and other sources as referenced. The atmospheric conditions for each test are provided in Table 3-23. The measured burn rate and density for each test is provided in Table 3-24. Models can use a burn rate

that is an average of the three values, each determined using a different method, provided in Table 3-24. Note that the wind angle is relative to the short axis of the pool where the positive and negative directions are as indicated in Figure 3-3.

Table 3-22. Measurements and instrumentation for BGC trench fire experiments

Measurement	Instrument	Measurement Uncertainty
fuel regression	Three methods: Thermocouple rake within fuel Diptube with pressure transducer Initial fuel depth divided by test duration	Not reported
Incident radiative heat flux	Wide-angle radiometers (slow-response wide-angle, 45o; fast-response, 20o x 70o)	Not reported ±5% (Table 2-1)
Spot surface emissive power (points on flame)	Narrow-angle radiometers	Not reported ±5% (Table 2-1)
Temperature external to flame	Metal plate thermometers	±9% (based on [30])
Flame geometry (length, tilt, and drag)	Cameras (upwind, downwind, and crosswind)	Not reported 10%*

*Approximate value provided by subject matter experts at Sandia. Main contributing factor is error correction regarding the lens.

Table 3-23. Atmospheric conditions for BGC trench fires

Test No.	Ave. Wind Speed (m/s)	Ave. Wind Direction (degrees)	Ambient Temperature (ºC)	Atmospheric Pressure (kPa)	Relative Humidity (%)
1	3.8	-3.6	4.5	95.7	94
2	1.5	12.9	2.0	95.9	92
3	~1.0	47 ± 8	2.1	95.9	91
4	8.36 ± 1.4	3.0 ± 4	6.6	99.7	90
5*	9.31± 2.0*	-5*	6.6	99.7	90
6	4.98 ± 0.95	-177.0 ± 11.0	15.8	98.6	68
7	3.80 ± 1.10	1.0 ± 13.0	21.8	98.3	69
8	2.05 ± 0.70	9.0 ± 9.0	20	98.2	85
9	5.40 ± 1.14	157.7 ± 9.2	13.0	98.1	83
10	7.05 ± 1.64	5.6 ± 6.0	16.1	99.53	88
11	5.90 ± 1.15	173 ± 4.9	17.9	98.95	73
12	8.60 ± 1.4	-10.5 ± 4.7	13.9	97.95	72

Test No.	Ave. Wind Speed (m/s)	Ave. Wind Direction (degrees)	Ambient Temperature (°C)	Atmospheric Pressure (kPa)	Relative Humidity (%)
13	3.69 ± 0.48	-14.5 ± 2.7	14.5	98.74	85

*Data not readable in report. Wind speed and direction estimated from graphical output. Ambient temperature, atmospheric pressure, and relative humidity taken from test 4 performed the previous day.

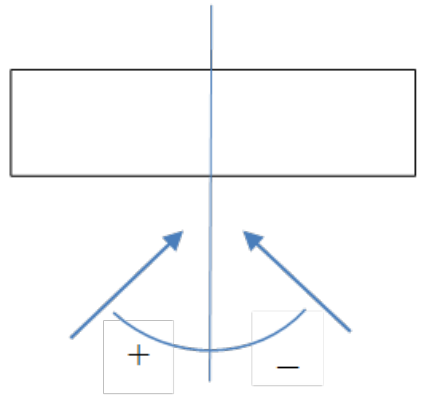

Figure 3-3. Reference for wind direction angle (trench fires).

Table 3-24. Burn rates and densities for BGC trench fires

	Burn rate (kg/m^{2}s)			
Test no.*	Dipstick	Diptube	Thermocouples	Density (kg/m^3)
1	0.057	0.063	0.068	450
2	0.066	0.063	0.078	475**
3	0.088	-	0.107	475**
4	0.054	0.058	0.053	475**
5	-	0.060	0.063	475**
6	0.083	-	0.080	463
7	0.042	0.049	0.059	461
8	0.054	0.053	0.067	472
9	0.041	0.054	0.057	485
10	0.052	-	0.068	477
11	0.044	0.054	0.059	479
12	0.049	0.037, 0.045	0.054	520
13	0.046	0.040, 0.043	0.043	471

*If no value entered, then data was not successfully collected
**Not measured, but estimated

Flame geometry parameters were determined by camera recordings in the upwind, crosswind, and downwind locations and based on evaluating flame luminosity by 'eye'. The flame length had to be corrected for the angles of wind-induced flame tilt away from the normal planes of the video coverage. In the upwind and crosswind directions it was observed that the flame tended to breakup into 'flamelets' (individual flames) that varied with time and distance. From the crosswind direction the camera captured a superimposition of these flamelets. To correct the two-dimensional images for three dimensional effects, the reported values for length, tilt, and drag are based on idealizing the flame as a skewed rectangular prism. The average and maximum flame lengths are based on assessing the height through the centerline of the flame.

3.1.4.1. BGC trench fires: experimental comparisons and parameter variation

The experimental measurements for model comparison included in the MEP spreadsheet are provided in Table 3-25. To determine the propagated input uncertainty, experimental parameter variations are provided in Table 3-26. Test 6 was chosen since it falls in the midrange among the tests with regards to wind speed and trench dimensions.

The measurements from the narrow-angle radiometer used in four tests are not included since only hand-drawn contour plots of the heat flux are provided in the test reports. As previously mentioned regarding the difficulties of including DFTs in simulations, the metal plates used in the trench fire tests are not included since they are similar in size to the DFTs.

Table 3-25. Measurements for validation for BGC trench fires

Parameter	Instrument
Average incident radiative heat flux during steady state	Radiometers (Land and Barnes)
Average flame geometry (length, tilt, and drag) during steady state	Cameras

Table 3-26. BGC trench fire Test 6: Experimental input parameters to vary

Test 6	
Parameter	**Variation**
Burn rate	Variation in measurement method (Table 3-24)

3.2. LU Jet fire experiments

Lowesmith and Hankinson from Loughborough University (LU) performed six jet fire experiments as part of the European Commission funded NaturalHy project using natural gas and natural gas/hydrogen (24% vol. hydrogen) mixtures. Flow rates ranging from 2.9 – 19.5 kg/s were used with nozzle diameters of 20, 35, and 50 mm, which provided heat outputs ranging from 137 – 939 MW [9]. Table 3-27 provides a general description of the test series. The heat flux to a 0.9 m diameter pipe target placed at distances of 9.45, 15.45, and 21.61 m from the nozzle was measured. The target pipe was constructed from steel and was 16 m long with a 12.7 mm wall thickness. The pipe was located at an elevation of 3.25 m above the ground, the same height as the release point. Twelve wide-angled radiometers were used to measure heat flux away from the flame. Total heat load to the pipe was measured using 40 calorimeters and 4 radiometers. The instrumentation and release conditions are

provided in Table 3-28 and Table 3-29, respectively. The mass flow rate as measured from the orifice plate can be used as a model boundary condition. The measurement uncertainty of the calorimeters and radiometers on the pipe is not reported, thus the uncertainty is based on values provided in Table 2-2. The atmospheric conditions provided in Table 3-30 were measured at an elevation of 10.85 m. Wind direction was reported relative to the jet which can be considered at zero degrees.

Table 3-27. General description of the LU jet fire experiments

General description	
Test location	GL Noble Denton Spadeadam Test Facility, Cumbria, England
Test performed by	Loughborough University (LU)
Mass release rates	Listed in Table 3-29
Number of tests	3
Fuel composition	Approximately 93% methane, 5% ethane, 0.3% propane, 1.7% nitrogen
Engulfed object	Yes
Data confidentiality	Open, publicly available only through journal publication thus complete dataset not available
References	Lowesmith and Hankinson [9] Bradley, I. [31] (provides additional heat flux measurements to engulfed pipe, p. 32)

Table 3-28. Measurements and instrumentation for LU jet fire experiments

Measurement	Instrument	Measurement Uncertainty
Mass flow rate	Pressure transmitters	±0.15%
Incident radiative heat flux	Wide-angle radiometers (150° view angle)	±5%
Total heat flux to pipe	Calorimeters	±20%
Radiative heat flux to pipe	Radiometers	±23%
Flame length and lift-off	Camera (crosswind)	Not reported ±10%*
Weather conditions	Wind speed and direction: Anemometers	Not reported

*Approximate value provided by subject matter experts at Sandia. Main contributing factor is error correction regarding the lens.

Table 3-29. Release conditions for LU jet fires experiments

Test No.	Release diameter (mm)	Gauge pressure of release (bar) (psi)	Distance to Pipe target* (m)	Mass flowrate by orifice plate (kg/s)**	Mass flowrate from exit conditions*** (kg/s)	Mean net power (MW)	Radiant fraction
1	20	59.4 (862)	9.45	2.9 ± 0.2	2.9	140	0.137
2	35	61.5 (892)	15.45	9.6 ± 0.4	9.4	462	0.179
3	50	58.8 (853)	21.61	19.5 ± 0.2	18.4	939	0.202

*From release point to pipe centerline
**Based on 0.15% uncertainty
***Discharge coefficient assumed to be 0.9

Table 3-30. Atmospheric conditions for LU jet fire experiments

Test No.	Wind direction (degrees)*	Wind speed (m/s)
1	1 ± 11 (S)	6.3 ± 1.5
2	27 ± 5 (S)	6.2 ± 0.5
3	3 ± 13 (N)	3.6 ± 0.5

*Release direction of jet was nominally to the east. Wind direction predominately from west to east. S and N denote south and north of release direction, respectively.

3.2.1. LU jet fires: experimental comparisons and parameter variation

The experimental measurements for model comparison are provided in Table 3-31. The locations corresponding to the reported measurements from the radiometers embedded in the pipe were not provided. Thus, the radiative heat flux averaged among all radiometers is used for comparison. Flame length is defined as the horizontal distance from the release point to the edge of the visible flame. The propagated input uncertainty for the model should be assessed using the experimental parameter variations included in Table 3-32. Test 2 was chosen for this purpose since it is the mid-range with regards to release conditions among the tests. The upper value for the mass flow rate is based on adding the reported uncertainty of 0.15% to the average value from the orifice plate measurement, while the lower value is based on subtracting 0.15% from the reported mass flow rate at the exit.

Table 3-31. Measurements for validation for LU jet fires

Parameter	Instrument
Average total heat load to pipe during steady state	Calorimeters
Average radiative load to pipe during steady state	Radiometers
Average incident radiation	Wide-angle radiometers
Average flame length	Real-time video

Table 3-32. LU jet fire Test 2: Experimental input parameters to vary

Test 2	
Parameter	**Variation**
Mass flowrate	8.0 kg/s (low) 9.5 kg/s (base) 11.0 kg/s (high)

3.3. Shell fireball experiments

A series of four LNG fireball experiments were performed by Betteridge and Phillips [10] using two different tank capacities (0.935 and 5.055 m^3), fill ratios, release pressures and temperatures. Table 3-33 provides a general description of the test series. The tanks were ruptured with a copper-based explosive cutting charge which was sized to allow for the rupture to propagate to the end caps of the vessel. Measurements taken and instrumentation used for the tests are provided in Table 3-34.

Table 3-33. General description of the Shell fireball experiments

General description	
Test location	DNV GL Spadeadam Test Facility, Cumbria, England
Test performed by	Shell
Mass released	Listed in Table 3-35
Number of tests	3 (4 performed for test series)
Fuel composition	Approximately 96.7 mol% methane, 3 mol% ethane, <0.2 mol% nitrogen and <0.1 mol% propane.
Engulfed object	No
Data confidentiality	Open, publicly available only through journal publication thus complete dataset not available
References	Betteridge and Phillips [10]

The vessel dimensions were not provided, but the length to width ratios for the large and small test vessels were reported as 6.5:1 and 5.5:1, respectively. Thus, for purposes of the MEP a length of 6.5 m and diameter of 1 m can be assumed. In Test 1, using a vessel capacity of 0.935 m^3, the fuel was not ignited until 3 seconds after the release and did not provide for a complete dataset, thus the results are not included here. Tests 2 and 4 resulted in complete fracturing of the vessel, whereas in Test 3 a 4 m^2 orifice resulted due to the lower tank pressure. In Tests 2 through 4, the release had a preferential direction in the West-East plane, which was perpendicular to the vessel, oriented along the North-South plane.

Table 3-34. Measurements and instrumentation for Shell fireball experiments

Measurement	Instrument	Measurement Uncertainty
Incident radiative heat flux	Wide-angle radiometers (150° view angle); Narrow-angle radiometers (0.055° view angle)	±5%

Measurement	Instrument	Measurement Uncertainty
Fireball diameter, height, rise time, and extinction	Camera (crosswind)	±10%
Weather conditions	Wind speed and direction: Anemometers	Not reported

A total of twelve Schmidt-Boelter wide-angle radiometers with a 150° field of view and response time <1 s were used together with one narrow-angle radiometer with a field of view of 0.055°. The wide-angle radiometers were placed at an elevation of 1.5 m and spaced 10 m apart, with nine in the East direction, two in the South direction, and two in the south-east direction, i.e. at 45 degrees. The narrow-view radiometer was placed 20 m from the tank along the east line.

Diameter, fireball rise height, and duration were measured using real-time cameras at the north-west and east locations and high-speed cameras (2000 fps) at the north and east locations. High frequency pressure transducers were collocated with the wide-angle radiometers to measure over-pressure.

In reference [10] a limited number of radiometer measurements were provided. The radiometer measurements reported include east locations of 40 m, 70, and 100 m for Test 4, and at 100 m for all the tests. The narrow-angle radiometer measurement was not reported. The fireball diameter over time was reported only for Test 4. For all tests the maximum diameter, time at maximum diameter, height at maximum diameter, time at lift-off, and time of extinction were provided. The time at lift off is the point at which the fireball separated from any remaining LNG burning near the ground. The time of extinction is taken as the point when the fireball breaks up. The height of the fireball is defined as the distance from the center of an equivalent spherical fireball to the ground. Due to the uncertainty in the initial release conditions of the LNG, that is, its velocity and thermodynamic state, time of lift-off is not included in the MEP.

Wind speed and direction were measured using anemometers located 100 m to the east of the test tank. Relative humidity was taken from the Spadeadam weather station located 500 m from the test site. Although the atmospheric conditions were measured, they were not reported. The release conditions are provided in Table 3-35.

Table 3-35. Release conditions for LNG fireball experiments

Test No.	Vessel capacity (m^3)	Vessel pressure (bar) (psi)	Vessel temperature (°C)	Fill ratio (%)	Density (kg/m^3)	Calculated release mass (kg)
2	5.055	13.01 (189)	-115	37	364.1	681
3	5.055	6.07 (88)	-131	67	385.6	1306
4	5.055	13.62 (198)	-115	69	358.7	1251

3.3.1. Shell fireballs: experimental comparisons and parameter variation

The experimental measurements for model comparison are provided in Table 3-36. Although the surface emissive power is reported it was not directly measured, instead being calculated using the

radiometer measurements and video coverage. Thus, it is not considered to be a principal parameter for comparison since it is a derived quantity, as mentioned previously in Section 2.1.

Table 3-36. Measurements for validation for LNG fireball experiments

Parameter	Instrument
Incident radiation	Wide-angle radiometers (150° view angle)
Fireball geometry and duration	Real-time and high-speed video

The diameter data is an average between the northwest and east cameras for Test 4. The peak heat flux from radiometer measurements at 40 m, 70 m, and 100 m from the test tank for Test 4, and at 100 m for Tests 2, 3, and 4 are included in the spreadsheet. Fireball rise height, diameter, and extinction time consist of only three measurements, one for each test, thus no relative standard deviation or bias factor are calculated for these measurements. Nonetheless, entries for these quantities are included in the MEP spreadsheet to allow for comparison. Also, due to the limited data regarding radiometer heat flux measurements, graphical comparison is not provided for individual tests, rather a spreadsheet is provided where data from all tests are combined to provide graphical comparison as well as a relative standard deviation and bias factor.

Table 3-37 provides the experimental input parameter to vary to determine the propagated input uncertainty, namely the mass of release whose range is based on the three tri-cock valves used to determine the liquid level where the upper and lower valves were set at percent volume fill heights of +2% and -2%, respectively.

Table 3-37. Shell fireballs Test 4: Experimental input parameters to vary

Test 4	
Parameter	**Variation**
Mass of release	1226 kg (low) 1251 kg (base) 1276 kg (high)

4. DESCRIPTION OF NON-LNG FUELS DATABASE

The following sections pertain to experiments involving non-LNG fuels present at LNG facilities and are categorized according to fire type that include pool fire, jet fire, and fireball. The information provided for each test series include a general description, specification of instrumentation, measured quantities for comparison, and experimental input parameters to vary to determine the propagated input uncertainty for the model.

4.1. Pool Fires Experiments

The experimental series for pool fires includes two datasets for propane, two for crude oil, one for diesel, and one each for ethane, ethylene, and isopentane. One propane pool fire test series was conducted on water while the remaining datasets were conducted on land. The crude oil datasets encompass both indoor and outdoor experiments and are an adequate surrogate for a condensate fuel with regards to combustion behavior affecting thermal exclusion zones due to the findings in [4] [2]. The 2-m diameter indoor crude oil experiment is not reflective of the typical scale of an industrial accident, but as mentioned previously has the advantage of having relatively well-defined boundary conditions.

4.1.1. U.S. Navy (USN) liquefied propane gas pool fire experiments

The Department of Energy (DOE) funded a series of pool and vapor cloud fire experiments conducted by U.S. Navy personnel at the Naval Weapons Center (NWC) in China Lake, California [11]. The tests included five liquefied petroleum gas (LPG) pool fires, four liquefied propane vapor cloud fires, and one gasoline pool fire. The LPG was spilled onto a 50 m x 50 m water pond approximately 1 m deep and immediately ignited for the pool fire experiments. One pool fire test did not provide complete data and was not reported in the experimental report. Of the reported data, Test 4 is excluded from the MEP due to incomplete data for flame height and pool diameter. A general description of the NWC propane pool fire experiments is provided in Table 4-1.

Table 4-1: General description of USN LPG pool fire experiments

General description	
Test location	China Lake, California
Test performed by	U.S. Navy
Pool diameter	Up to 16.9 m
Number of tests	3 (5 performed for test series)
Fuel composition	Liquefied petroleum gas; propane (>90 vol%)
Engulfed object	No
Data confidentiality	Open, publicly available
References	Mudan, K.S. [11]

The measurements include flame length, flame tilt, incident heat flux from wide- and narrow- angle radiometers, video recordings, and meteorological conditions. The heat flux measurements include four wide-angle radiometers with a view angle of 150° and two narrow-angle radiometers with a view angle of 7°. Three of the wide-angle radiometers were placed crosswind to the fire at distances of 40 m, 60 m, and 80 m, and one upwind at 55 m from the spill point. One narrow-angle radiometer was

used in Test 1 and was place crosswind to the fire at 60 m from the spill point. It was aimed at a height about 4 m above the spill point and had a spot diameter of 7 m, thus the entire view was covered by flame. The remaining tests had two narrow-angle radiometers also placed crosswind to the fire at 60 m from the spill point with one aimed similar to that of Test 1 and the other aimed towards the spill point allowing for one-half of its view to be filled by the flame. The height of the radiometers above the ground was not provided. For purposes of the MEP a reasonable height to assumed is 1 m since radiometers are often mounted on a stand of this approximate height in experiments. Also, radiometers were place along orthogonal directions designated as crosswind and upwind. The crosswind and upwind directions were rotated 45 degrees counterclockwise from the north. In the spreadsheet the wind is parallel to the west-east direction and the radiometer (x, y) locations are determined by considering the wind direction and the radiometer's rotational shift of 45 degrees.

Table 4-2 provides the type of measurements taken and instruments used in the experiments. The test conditions for each test are provided in Table 4-3. Wind speed and direction was measured at two stations, one located 1 m upwind from edge of the pond and another on top of the instrument bunker. The elevation of the upwind location was 2 m, and the elevation of the bunker location was not reported.

Table 4-2. Measurements and instrumentation for the USN LPG pool fire experiments

Measurement	Instrument
Incident radiative heat flux	Wide-angle radiometers
Spot surface emissive power	Narrow-angle radiometers
Flame length and tilt	Video cameras
Pool dimensions	Video cameras

Table 4-3. Test conditions for the USN LPG pool fire experiments

Test #	Quantity spilled (m^3)	Spill Duration (s)	Spill rate (m^3/s)	Air Temperature (K)	Relative humidity (%)	Wind Speed (m/s)	Wind direction (degrees from north clockwise)
1	5.3	65	0.082	312	23	calm	-
3	4.8	82	0.059	309	30	1.0	45
5	5.5	57	0.096	306	38	2.5	120

The pool fires were reported to have the flame's upper portion covered in a layer of black smoke which periodically opened in regions exposing visible flame. The flame height definition includes the continuous luminous lower portion of the flame as well as the uppermost portion where the smoke layer periodically opened exposing visible flame. The pool fire dimensions were determined by using crosswind, upwind, and overhead video footage. The pool dimensions were assumed to be the same as the boundary of the white vapor cloud at the water level. Since the shape of the pools were closer to an ellipse, the average pool diameter was determined to be the diameter of a circle of equivalent area. The average burn rate provided in the report was estimated by dividing the total volume of fuel spilled by the duration of burning. The average pool width, diameter, burn rate, and mass flux for each

test is provided in Table 4-4. The mass flux was not provided in the report but was calculated for the MEP by assuming that during steady state the fuel entering the pool is balanced by the fuel burning. The burn rate was divided by the pool area and then multiplied by the density of liquid propane. The average flame height and tilt are provided in Table 4-5.

Table 4-4. Average pool diameter and burn rate for USN LPG pool fire experiments.

	Average Pool Width (m)					
Test #	Crosswind camera	Overhead camera	Upwind camera	Average pool diameter (m)	Burn rate (m^3/s)	Mass flux** (kg/m^2s)
1	17.1	NA	16.6	16.9	0.082	0.21
3	15.3	11.2	12.1	12.9	0.059	0.26
5	12.6	19.1	13.0	14.9	0.096	0.32

*NA – not available

**Calculated using the reported spill rate, pool area, and density of liquid propane (581 kg/m^3)

Table 4-5: Average flame height and tilt for USN LPG pool fire experiments.

Test #	Average flame height (m)	Flame tilt from vertical (degrees)
1	54.4	0
3	54.9	15
5	51.9	30

*NA – not available

4.1.1.1. USN LPG pool fire tests: experimental comparisons and parameter variation

The experimental measurements for model comparison included in the MEP spreadsheet are provided in Table 4-6. The measurements uncertainty for the radiometers was not reported, thus the values provided in Table 2-1 are used. If a model includes a sub-model for a narrow-view radiometer, then this can be used for comparison to the spot surface emissive power.

Table 4-6. USN LPG pool fire tests: measurements for validation

Parameter	Instrument	Measurement Uncertainty
Average radiative heat flux	Wide-angle radiometers	5%
Spot surface emissive power	Narrow-angle radiometers	5%
Average flame/pool geometry	Reduction method from video coverage	10%*

*Approximate value provided by subject matter experts at Sandia. Main contributing factor is error correction regarding the lens.

To determine the propagated input uncertainty, the parameter for variation is the mass flux whose range is provided in Table 4-7. Test 5 was chosen since it was conducted in the highest wind speed among the tests. As mentioned previously, for purposes of the MEP the mass flux was calculated by using the reported burn rate divided by the pool area and then multiplied by the density of liquid propane. Since the pool area is used in the calculation, the mass flux uncertainty is based on using the uncertainty of 10% regarding video analysis of the pool diameter provided in Table 4-6.

Table 4-7. USN LPG pool fire Test 5: Experimental input parameter to vary

Test 5	
Parameter	**Variation**
mass flux	0.26 kg/m^{2}s (low) 0.32 kg/m^{2}s (base) 0.39 kg/m^{2}s (high)

4.1.2. Sandia National Laboratories indoor (SNL-Indoor) crude oil pool fire experiments

A series of 2-m pool fire tests were conducted at Sandia National Laboratories' (SNL) Thermal Test Complex (TTC) sponsored by the National Research Council of Canada (NRCC) [4]. The experiments include three test series each involving different fuels. The first series included three heptane tests, the second six Bakken crude oil tests, and the third six diluted bitumen (dilbit) crude oil tests. The effect of the following parameters was investigated: the presence and placement of a calorimeter engulfed in the fire, fuel feed temperature, allowing the fuel to burn down, and oil composition. A companion report regarding the sampling, analysis, and characterization of the fuels and post-test residue is provided in [32]. A general description of the Sandia indoor crude oil pool fire experiments is provided in Table 4-8.

Table 4-8: General description of Sandia outdoor crude oil pool fire experiments

General description	
Test location	Sandia Thermal Text Complex, Albuquerque, NM, USA
Test performed by	Sandia National Laboratories
Pool diameter	2 m
Number of tests	1 (15 experiments performed for tests series)
Fuel composition	heptane and two types of crude oil (full composition provide in MEP spreadsheet)
Engulfed object	No for case in MEP (Yes for test series)
Data confidentiality	Publicly available
References	Luketa, et al. [4]

Measurements include burn rate, surface emissive power, flame height, heat flux to an engulfed calorimeter, heat flux to external instruments, thermocouple temperatures within the fuel and fire plume, and heat release rate.

The fuels relevant to the MEP are the two crude oil test series since they are considered an adequate surrogate for a condensate fuel due to similarities of combustion behavior. Between the crude oil test series, Bakken crude oil is included for comparison since the burn rate was nearly constant compared to the dilbit crude oil experiments. The dilbit experiments resulted in the burn rate varying during the tests due to preferential burning between its components, that is, a mixture of a condensate and bitumen. However, for both durations of burning of the different components, the average surface emissive power did not significantly change. Also, the average surface emissive power for the dilbit crude oil was similar to that measured for the Bakken crude oil experiments, though the average flame height for the Bakken crude oil was higher overall by about 30% than the dilbit. Further, it was found from experiments described in section 4.1.3 involving 5-m diameter pools using the same Bakken crude oil that the average surface emissive power was similar to that of a 2-m diameter pool. Also, for the test series in section 4.1.3 the average surface emissive power was similar among the three oils tested even though they varied significantly with regards to composition and vapor pressure. [2].

Of the six experiments performed for the Bakken crude oil only one is included in the MEP database because it did not have a calorimeter placed in the fire and a constant fuel level was maintained, that is, the fuel was not allowed to burn down. The pipe calorimeter used in four of the experiments had an outer diameter of 0.33 m and was 1.8 m in length, thus was sizable compared to the 2-m diameter fire. To capture its affect on the fire due to its thermal mass and alteration of flow dynamics, modeling its complex geometry requires detailed drawings. Thus, the single experiment included in the MEP, Bakken Test 2.1, does not have the calorimeter present and the fuel level in the test pan was held constant using a controlled fuel supply system.

The facility in which the experiments were conducted, namely the Fire Laboratory for Accreditation of Models and Experiments (FLAME) test cell in the Thermal Test Complex at Sandia National Laboratories is described in section 3.1.1. The facility was designed to replicate quiescent outdoor conditions in that no excess pressure or re-radiation from the walls impact the fire. Thus, it is considered acceptable to perform simulations without including the geometry of the FLAME facility. All experiments used a 2-m diameter test pan with a depth of 0.3 m to contain any spillage within the FLAME facility in the event of a boil over which is caused by rapidly vaporizing water entrained in the crude oil. The distance from the fuel surface to the top of the pan was 0.289 m.

Six narrow-angle radiometers and five wide-angle total heat flux gauges were used to measure the surface emissive power (SEP) and the incident heat flux. The narrow-angle radiometers had a view angle of 5.5^{o} and the wide-angle total heat flux gauge had a view angle of 150°. They were mounted near the FLAME wall at 9.1 m from the center of the fire. The narrow-view radiometers were mounted at heights of 0.5, 1, 1.5, 2, 3, and 4 m and had a spot diameter of about 0.8 m. The total heat flux gauges were mounted at heights of 1, 1.5, 2, 3, and 4 m. The line of sight for each instrument was horizontal, set to pass through the centerline of the fire, and were water-cooled. Table 4-9 provides the type of measurements taken and instruments used in the experiments. The fuel properties and mass flux for the Bakken crude oil test is provided in Table 4-10.

Table 4-9. Measurements and instrumentation for the Sandia indoor crude oil pool fire experiments

Measurement	Instrument
Total incident heat flux	Wide-angle heat flux gauge
Spot surface emissive power	Narrow-angle radiometers
Surface emissive power	Infrared cameras

Measurement	Instrument
Fire plume centerline temperature	Thermocouples
Flame length	Infrared cameras
Heat release rate	Gas analyzer
Derived total incident heat flux	Directional flame thermometer
Derived total heat flux to an engulfed object	Calorimeter

Table 4-10. Fuel properties and mass flux for the Sandia indoor pool fire experiment, Bakken 2.1

Test	Density (kg/m^3)	Carbon/Hydrogen mole ratio	Radiative Fraction	Heat of combustion (MJ/kg)	Mass flux (kg/m^2s)
Bakken 2.1	806	0.625	0.5	46.8	0.03

4.1.2.1. Sandia indoor crude oil pool fire tests: experimental comparisons and parameter variation

The experimental measurements for model comparison included in the MEP spreadsheet are provided in Table 4-11. If a model includes a sub-model for a narrow-view radiometer, then this can be used for comparison to spot surface emissive powers. The average surface emissive power was determined using infrared camera measurements by assuming a flame emissivity of one, transmissivity of 0.95, and including values greater than 16 kW/m^2. The flame height was determined using a surface emissive criterion of 30 kW/m^2 from the infrared camera measurements. To determine the propagated input uncertainty, the parameter to vary is provided in Table 4-12 which is the burn rate with a $\pm 7\%$ variation. This is based on the accuracy of the scale and the burn rate variation of repeat tests included in the test series.

Table 4-11. Sandia indoor pool fire experiment, Bakken test 2.1: measurements for validation

Parameter	Instrument	Measurement Uncertainty
Average radiative heat flux	Wide-angle radiometers	5%
Average spot surface emissive power	Narrow-angle radiometers	5%
Average surface emissive power	Infrared cameras	4.6%
Flame geometry	Infrared cameras	4.6%
Average fire plume temperature	Mineral-insulated, metal-sheath, 40 mil, Type K, thermocouples	5%

Table 4-12. Sandia indoor pool fire experiment, Bakken test 2.1: Experimental input parameter to vary

Tight 1 (Bakken)	
Parameter	**Variation**
fuel mass flux	0.028 kg/m^{2}s (low) 0.030 kg/m^{2}s (base) 0.032 kg/m^{2}s (high)

4.1.3. Sandia National Laboratories outdoor (SNL-Outdoor) crude oil pool fire experiments

A series of pool fire experiments involving crude oil with different compositions and vapor pressures were performed by Sandia National Laboratories [2]. The experiments were sponsored by the U.S. Department of Energy, U.S. Department of Transportation, and Transport Canada. The objective of the pool fire experiments was to compare measurements among the oils required for hazard evaluation which include burn rate, flame height, and surface emissive power. Two 2-m diameter pool fires were performed indoors, and four 5-m diameter pool fires were performed outdoors. All tests included a calorimeter placed within the fire to determine heat flux to an engulfed object. Only one of the tests is include in the MEP, namely the 5-m diameter Bakken crude oil test, herein identified as Tight 1 (Bakken), since it had the most accurate burn rate measurement among the outdoor tests. Note that this outdoor test involves the same crude oil as tested for the 2-m indoor tests described in section 3.1.2. The outdoor tests had a larger pool diameter, was subject to wind, and used a smaller calorimeter than the indoor tests. A general description of the Sandia crude oil pool fire experiments is provided in Table 4-13.

Table 4-13: General description of Sandia outdoor crude oil pool fire experiments

General description	
Test location	Sandia Thermal Test Complex, Albuquerque, NM, USA
Test performed by	Sandia National Laboratories
Pool diameter	5 m
Number of tests	1 (6 conducted in experimental series)
Fuel composition	crude oil (full composition provided in MEP spreadsheet)
Engulfed object	Yes
Data confidentiality	Publicly available
References	Luketa, et al. [2]

The measurements include flame length, flame tilt, incident radiative heat flux from wide- and narrow-angle radiometers, surface emissive power from infrared cameras, thermocouples attached to the calorimeter, and meteorological conditions. The flame length was identified by using a threshold surface emissive power of 30 kW/m^2 measured with infrared cameras. Average values for surface emissive power were determined by assessing values above 16 kW/m^2. The heat flux measurements include eight wide-angle radiometers with a view angle of 180^o and four narrow-angle radiometers with a view angle of 5.5^o. The wide-angle radiometers were placed at the north-east, north-west, south-

east, and south-west diagonals to the pool at approximately 5 m and 20 m from the center of the pool. The narrow-angle radiometers were placed approximately 20 m from the center of the pool. The radiometers were elevated 1-m from the bottom of the pan and aimed horizontally.

The calorimeter was constructed using a 1.5 mm thick stainless-steel tube filled with rolled high-temperature ceramic fiber blanket insulation. The diameter and length of the calorimeter was 0.27 m and 1 m, respectively, and was elevated 1-m from the bottom of the test pan to the calorimeter's centerline. Twelve thermocouples were attached to the inside surface of the stainless-steel tube, whose measurements were used to determine the surface heat flux using inverse heat conduction methods. The thermocouples were arranged in three rows in quarter increments along the length of the calorimeter. Four thermocouples were placed in each row at 90º intervals as shown in Figure 4-1.

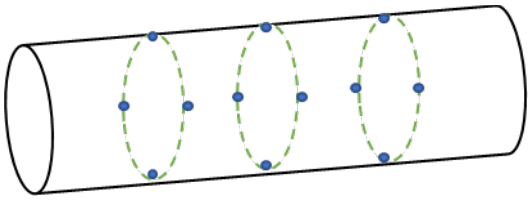

Figure 4-1: Positions of thermocouples placed on inner surface of calorimeter

Table 4-14 provides the type of measurements taken and instruments used in the experiments. The test conditions for the Tight 1 (Bakken) test are provided in Table 4-15. Wind speed and direction was measured at a station 215 m north-west from the center of the pool at an elevation of about 2 m.

Table 4-14. Measurements and instrumentation for the Sandia outdoor crude oil pool fire experiments

Measurement	Instrument
Incident radiative heat flux	Wide-angle radiometers
Spot surface emissive power	Narrow-angle radiometers
Surface emissive power	Infrared cameras
Flame length and tilt	Infrared cameras
Temperature inside surface of calorimeter	Thermocouples

Table 4-15. Test conditions for the Sandia outdoor pool fire experiment, Tight 1 (Bakken)

Test	Pool diameter (m)	Mass flux (kg/m^2s)	Air Temperature (ºC)	Relative humidity (%)	Wind Speed (m/s)	Wind direction (degrees from north clockwise)
Tight 1 (Bakken)	5	0.062	13.3	20	3.6	204

4.1.3.1. Sandia outdoor crude oil pool fire tests: experimental comparisons and parameter variation

The experimental measurements for model comparison included in the MEP spreadsheet are provided in Table 4-16. To determine the propagated input uncertainty, the parameter to vary is provided in Table 4-17 which is the mass flux with a ±10% variation based on flow meter and liquid level measurement uncertainty. If a model includes a sub-model for a narrow-view radiometer, then this can be used for comparison to spot surface emissive power.

Table 4-16. Sandia outdoor pool fire experiment, Tight 1 (Bakken): measurements for validation

Parameter	Instrument	Measurement Uncertainty
Average radiative heat flux	Wide-angle radiometers	5%
Spot surface emissive power	Narrow-angle radiometers	5%
Average surface emissive power	Infrared cameras	4.6%
Flame geometry	Infrared cameras	4.6%
Average heat flux to calorimeter	Thermocouples and inverse heat conduction methods	20% [33]

Table 4-17. Sandia outdoor pool fire experiment, Tight 1 (Bakken): Experimental input parameter to vary

Tight 1 (Bakken)	
Parameter	**Variation**
fuel mass flux	0.056 kg/m^{2}s (low) 0.062 kg/m^{2}s (base) 0.068 kg/m^{2}s (high)

4.1.4. Centre for Studies on Technological Risk (CERTEC) diesel pool fire experiments

A series of gasoline and diesel pool fire outdoor experiments were performed by the Centre for Studies on Technological Risk (CERTEC) at the Can Padro Safety Training Center near Barcelona, Spain [12] [13]. Of these experiments, the diesel pool fires are included in the MEP database. Pool diameters of 1.5, 3, 4, 5, and 6 m were created using circular concentric pools which were designed to prevent the inner smaller pools interfering with the larger pool by using different wall heights. For each test fuel was floated on a water layer and a small head space was left between the fuel surface and top of the containment pan to prevent spill over. The head space distance was not reported in the available references. A general description of the experiments is provided in Table 4-18.

Table 4-18: General description of CERTEC diesel pool fire experiments

General description	
Test location	Can Padro Safety Training Center, Barcelona, Spain
Test performed by	Centre for Studies on Technological Risk
Pool diameter	3 m, 4 m, 5 m, 6 m (1.5 m diameter performed; 1.5 m diameter test not included in MEP since complete data not provided)
Number of tests	5 (total number of tests performed for series not reported)
Fuel composition	Diesel oil
Engulfed object	No
Data confidentiality	Publicly available
References	Munoz, et al. [12], Rengel, et al. [13]

Table 4-19 provides the measurements and instrumentation used for the experiments. Measurements include the burn rate, flame height, flame tilt, flame centerline thermocouple temperatures, flame temperature from an infrared camera, and heat flux from a single radiometer placed external to the fire. The burn rate was measured using a small vessel connected to the pool by a flexible tube and a balance recorded the weight loss every 0.5 seconds. The flame length was determined from temperature contours from the IR camera where a temperature of 330°C was used to identify the flame boundary. Although the flame tilt was measured it was not reported in the available references. Five thermocouples at different elevations were mounted on a vertical rake placed in the center of the fire plume to measure temperature. The temperature measurements obtained from the infrared camera were used to calculate surface emissive power by assuming a flame emissivity of 0.98 for the 3-m diameter pool and a value of 1 for diameters greater than 4 m. Note that the surface emissive power is not included for comparison in the MEP database because there is a discrepancy between the values reported in references [12] and [13].

Weather conditions were measured at an elevation of 10 m above the ground. The wind speed and atmospheric temperature were provided, but not relative humidity and wind direction. Note that in reference [13] there is a discrepancy between the listed wind speeds provided in Table 1 versus those provided in Figures 6 and 7. The wind conditions for use in the MEP is taken from Table 1, however due to this discrepancy the wind speed is a parameter to determine the propagated uncertainty.

The wide-angle radiometer was placed in the opposite direction of the wind. Thus, it can be assumed that the radiometer was at the centerline of the fire on the downwind side. The view angle of the wide-angle radiometer was not provided, thus for purposes of the MEP an angle of 150° can be assumed. Note that in Figure 6(b) of reference [13] the heat flux at five pool diameters is plotted as a function of pool diameter. These heat flux values are not based on measurements from the radiometer but are based on a derived heat flux as presented in reference [12]. Thus, these values are not used in the MEP spreadsheet, rather those provided in Figure 8(c) in reference [13] are used. Table 4-20 provides the test conditions for the diesel pool fire experiments.

Table 4-19: Measurements and instrumentation for the CERTEC diesel pool fire experiments

Measurement	Instrument
Burn rate	Scale
Incident radiative heat flux	Wide-angle radiometer
Plume centerline temperature	Thermocouples
Surface emissive power	Infrared camera
Flame length and tilt	Infrared camera

Table 4-20: Test conditions for the CERTEC diesel pool fire experiments

Test	Pool diameter (m)	Mass flux (kg/m^2s)	Air Temperature (°C)	Wind Speed (m/s)
01_D3	3	0.054	12	2.39
04_D3	3	0.042	13	0.0
14_D4	4	0.058	20	0.43
10_D5	5	0.051	16	1.02
07_D6	6	0.051	19	1.1

4.1.4.1. CERTEC diesel pool fire tests: experimental comparisons and parameter variation

The experimental measurements for model comparison included in the MEP spreadsheet are provided in Table 4-21. To determine the propagated input uncertainty, the wind speed is chosen as a significant experimental parameter due to the discrepancy in reported values which differed between 0-74%. Test 14_D4 is chosen as the test to assess the propagated uncertainty since it had the largest discrepancy of the reported wind speeds. The relative humidity, which was not reported, is also included as a parameter due to its impact on atmospheric attenuation. The range for relative humidity was taken from historic weather records from the National Oceanic and Atmospheric Administration [34] for the months of April and October. These months were chosen based on the reported temperature for test 14_D4.

Table 4-21: CERTEC diesel pool fire experiments: measurements for validation

Parameter	Instrument	Measurement Uncertainty
Average radiative heat flux	Wide-angle radiometer	5% (Table 2-1)
Average temperature	Thermocouples placed vertically at pool centerline	5% (Table 2-1)
Average flame length	Infrared cameras	4.6% (Table 4-17)

Table 4-22: CERTEC diesel pool fire experiments: Experimental input parameter to vary

Test 14_D4	
Parameter	**Variation**
Mass flux (kg/m^{2}s)	0.056 kg/m^{2}s (low) 0.058 kg/m^{2}s (base) 0.060 kg/m^{2}s (high)
Wind speed (m/s)	0.11 m/s (low) 0.43 m/s (base) 0.75 m/s (high)
Relative humidity (%)	60 (low) 70 (base) 80 (high)

4.1.5. Sandia National Laboratories ethane, ethylene, propane, and isopentane pool fire experiments

Sandia National Laboratories conducted a series pool fire experiments at Sandia's Lurance Canyon Burn Site Facility [14]. The objective of the test series funded by the Pipeline and Hazardous Materials Administration (PHMSA) was to obtain data for model validation. Table 4-23 provides a general description of the experiments.

Four 5-m diameter pool fires were performed testing four different fuels that include ethane, ethylene, propane, and isopentane (Figure 4-2). The fuel delivery system involved using pressurized nitrogen to drive fuel out of a 20' International Organization for Standardization (ISO) container for each fuel through a 3" diameter, 100' long pipeline to a concrete pool. A diffuser was placed in the center of the pool and attached to the end of the fuel supply line to reduce splashing (Figure 4-3). The diffuser was approximately 1' in diameter, 3.5' in height, and 2" above the bottom of the pool. An open pipe at its top allowing vapor to escape was approximately 3" in diameter and 1' in length. Pool dimensions are provided in Figure 4-4.

Table 4-23: General description of Sandia ethane, ethylene, propane, and isopentane pool fires

General description	
Test location	Sandia Lurance Canyon Burn Site, Albuquerque, NM, USA
Test performed by	Sandia National Laboratories
Pool diameter	5 m
Number of tests	4
Composition of each fuel	Ethane (99%+), ethylene (99.5%+), propane (99%+), and isopentane (99%+)
Engulfed object	No
Data confidentiality	Publicly available
References	Luketa, et al.

(a) (b) (c)

(d)

Figure 4-2: Pool fire experiments: (a) ethane, (b) propane, (c) isopentane, and (d) ethylene

Figure 4-3: Diffuser attached to pipeline for Sandia pool fire experiments.

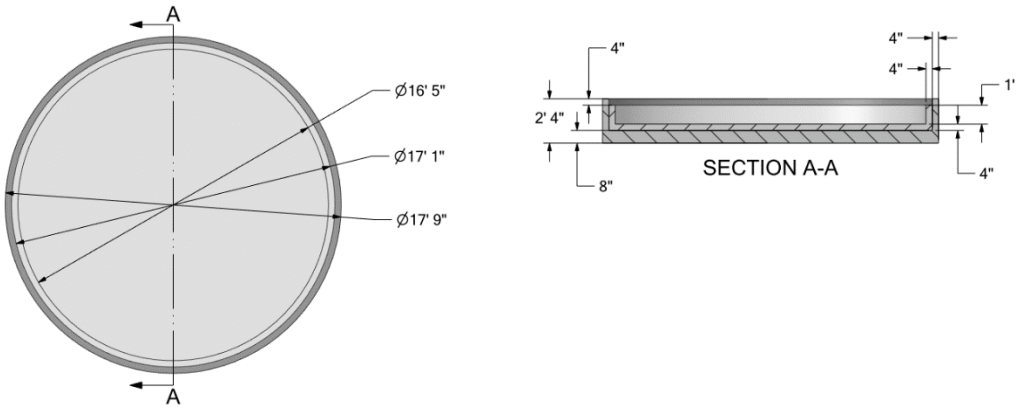

Figure 4-4: Concrete pool for Sandia pool fire experiments.

Measurements include flame length, flame tilt, heat flux, mass burn rate, and surface emissive power. Data was also collected from four weather towers, each measuring wind speed, wind direction, temperature, pressure, and relative humidity at three different elevations. Table 4-24 and Table 4-25 provides the type of measurements taken and instruments used in the experiments along with their uncertainty.

Table 4-24: Measurements and instrumentation for the SNL ethane, ethylene, propane, and isopentane pool fires

Measurement	Instrument	Measurement Uncertainty
Incident radiative heat flux	Wide-angle radiometers	±5.5 to ±5.8%
Surface emissive power	IR cameras	±6.3%
Flame length and tilt	Visible cameras	±10%
Mass flow rate	Diptube, orifice plate, vortex meter	±10%

Table 4-25: Wind speed and direction for SNL ethane, ethylene, propane, and isopentane pool fires

Measurement	Stations, Heights (m)	Uncertainty
Wind speed	All, 2, 5, 7.62	± 1% or 0.07 m/s, whichever is greater
Wind direction	All, 2, 5, 7.62	± 3°
Temperature	All, 2	± (0.226 - 0.0028T)°C at -80 to 20°C ± (0.055 + 0.0057T)°C at 20 to 60°C
Temperature	All, 5, 7.62	± 0.4 °C
Relative humidity	All, 2	± 1.4%
Pressure	East/South, 2	± 200 Pa at -40 to 60°C
Pressure	North/West, 2	± 600 Pa at -40 to 60°C

Infrared cameras were used to obtain flame length, flame tilt, and surface emissive power. The reported surface emissive power assumes a flame emissivity of 1 and is corrected for atmospheric attenuation. For all pool fire experiments the dimensions and surface emissive power are based on temperatures above 1123 K as measured from the IR camera. This temperature corresponds to an SEP value of 90 kW/m^2 assuming blackbody radiation. Inspection of real-time video provided confirmation that this temperature threshold is indicative of the visible flame. To measure incident radiation a total of 40 wide-angle total heat flux gauges were used with a field of view angle of 180°. All heat flux gauges were aimed horizontally. The flame length is measured from the center of the pool to the tip of the flame going through its middle and the tilt angle is with respect to the vertical axis. The flame length and tilt for all pool fires are determined from the visible cameras by masking the image to a black and white scheme where white indicates the luminous portion of the flame and black indicates either smoke or the surroundings.

Two methods were used to measure flow rate of the fuel supply, an orifice plate and vortex meter. The vortex meter proved unreliable for the ethane, ethylene, and propane experiments; thus, their reported flow rate is based on the orifice plate. Three diptubes were placed within the pool to measure the burn rate. For the ethane, ethylene, and propane pool fires the diptube instruments indicated that a liquid layer of at least ½" did not form within the pool for the given flow rates. The elevation of the diptubes were ½" from the bottom of the pool and thus can measure liquid depths greater than this distance. With sufficient flow rates a liquid layer is achievable for these fuels, but the rate was limited due to the maximum allowable working pressure of the ISO containers.

For each test the flame fully spread across the surface of the pool which indicated that a thin liquid layer did form. As the flow rate was increased the flame height increased which indicates that the burn rate was controlled by the fuel supply rate. Since the burn rate was controlled by the fuel supply rate, the configuration acted similar to a gas burner. The mass flow rate can thus be considered the burn rate of the fire. Experimentally, gas burners have been shown to preserve the gas phase dynamics of a liquid pool fire [35] [1]. This has also been confirmed through results from model validation of CFD codes in which the liquid pool is not modeled, rather gaseous fuel is supplied uniformly at the boundary of the pool's surface so only the gas phase is modeled [36].

For the isopentane pool fire a liquid layer of about 3" formed. Since the boiling point of isopentane is much higher than the other fuels, it did not rapidly vaporize upon contact with the concrete pool, thereby allowing for liquid accumulation. Thus, the burn rate was controlled by heat transferred from the flame to the surface of the pool. A loss coefficient due the diffuser was identified from data obtained from the isopentane experiment by comparing the flow rate measurements from the orifice plate to the three diptube measurements. This loss coefficient was used to correct the orifice plate flow rate measurements for the other experiments to determine a mass flow rate at the release point.

Table 4-26 provides the average wind speed among all stations for each experiment over periods in which the wind speed was relatively steady. The wind direction has been averaged among all stations and heights. Table 4-27 and Table 4-28 provides the atmospheric conditions and burn rate, respectively, over these same periods for each experiment.

Table 4-26: Wind conditions for SNL ethane, ethylene, propane, and isopentane pool fires

	Ethane		Ethylene		Propane	Isopentane
	Period 72-100 s	Period 129-156 s	Period 320-346 s	Period 433-462 s	Period 328-378 s	Period 356-383 s
Height (m)	Average wind speed (m/s)					
2	1.0 ± 0.04	1.2 ± 0.04	3.37 ± 0.13	4.16 ± 0.14	2.57 ± 0.10	1.40 ± 0.07
5	0.9 ± 0.03	1.3 ± 0.03	3.80 ± 0.15	4.88 ± 0.13	2.77 ± 0.12	1.45 ± 0.03
7.6	1.0 ± 0.04	1.2 ± 0.04	3.96 ± 0.15	5.11 ± 0.15	2.90 ± 0.10	1.44 ± 0.05
	Average wind direction (deg)					
all	276.7 ± 19.8	281.0 ± 13.3	223.2 ± 2.4	240.0 ± 1.4	278.3 ± 12.0	98.6 ± 1.9

Table 4-27: Atmospheric conditions for SNL ethane, ethylene, propane, and isopentane pool fires

Experiment	Ambient temperature (^{O}C)	Atmospheric Pressure (Pa)	Relative humidity (%)
Ethane	-1.2 ± 0.7	80,390 ± 0.2	46.4 ± 1.0
Ethylene	4.4 ± 0.2	81,250 ± 0.2	36.2 ± 1.1
Propane	-1.9 ± 0.2	81,186 ± 0.2	19.5 ± 0.7
Isopentane	-1.9 ± 0.6	81,020 ± 0.2	56.9 ± 1.4

Table 4-28: Average burn rate of SNL ethane, ethylene, propane, and isopentane pool fires

	Ethane		Ethylene		Propane	Isopentane
Period (s)	72-100	129-156	320-346	433-462	72-100	129-156
Mass burn rate (kg/m^{2}s)	0.163 ± 0.004	0.153 ± 0.004	0.117 ± 0.005	0.117 ± 0.005	0.112 ± 0.003	0.044 ± 0.001

4.1.5.1. SNL ethane, ethylene, propane, and isopentane pool fires: experimental comparisons and parameter variation

The experimental measurements for model comparison included in the MEP spreadsheet are provided in Table 4-29. Since surface emissive power was measured directly with infrared cameras these measurements are included to serve as an input into solid flame models or provide a comparison measurement for CFD-based models that have the capability to evaluate the SEP.

Table 4-29. SNL ethane, ethylene, propane, and isopentane tests: measurements for validation

Parameter	Instrument
Average incident radiative heat flux during steady state	Wide-angle radiometers
Average flame height during steady state	Cameras
Average flame tilt during steady state	Cameras

To determine the propagated input uncertainty, experimental parameter variations are provided in Table 4-30. The ethylene pool fire over the period of 433-462 seconds is chosen for the variational case. It had the highest average windspeed among the experiments and the greatest tilt. The fuel mass flux and wind direction are chosen as the parameters to vary.

Table 4-30: SNL ethylene pool fire: Experimental input parameters to vary

Ethylene pool fire	
Parameter	**Variation**
Mass flux	0.11 kg/m^{2}s (low) 0.12 kg/m^{2}s (base) 0.13 kg/m^{2}s (high)
Wind direction	235^o (low) 240^o (base) 245^o (high)

4.2. Jet fire experiments

4.2.1. Texas A&M University (TAMU) propane jet fire experiments

A series of propane jet fires were conducted at the Brayton Fire Training Field by Texas A&M University [15] [17]. A total of nineteen liquid and vapor jet fires were performed involving vertical releases from a 2.54 cm nozzle and horizontal releases from a 1.91 cm nozzle. The flow rates ranged from 0.015 – 0.11 kg/s. In reference [15] results were reported only for test series 3 involving horizontal releases which was comprised of five vapor jet fires and one liquid jet fire. In one of the vapor jet fire tests, the flow rate was ramped down to have a staircase pattern and held steady for 50 second for each flow rate. For the liquid releases the mass flow rates were not reported since accurate measurements could not be obtained. Thus, only vapor horizontal releases from test series 3 are included in the MEP. Table 4-31 provides a general description of the test series.

Table 4-31. General description of the TAMU propane jet fire experiments

General description	
Test location	Brayton Fire Training Field, College Station, Texas, USA
Test performed by	Texas A&M University (TAMU)
Mass release rates	0.015 – 0.11 kg/s
Number of tests	4 (21 conducted in experimental series)
Fuel composition	Propane (>90%)

General description	
Engulfed object	No
Data confidentiality	Open, publicly available only through journal publication thus complete dataset not available
References	Zhang, Laboureur, Gopalaswami [15] [17] [16]

Eleven radiometers placed 0.85 m above the ground were used to measure incident heat flux external to the jet, though measurements from only seven radiometers were reported for test series 3. The view angle of the radiometers was not provided; however, the magnitude of the measurements indicate that they were wide-angle radiometers. Thus, a view angle of 150° is assumed in the MEP. Real-time and infrared cameras were used to measure dimensions of flame liftoff, length, and width. Table 4-32 provides the type of measurements taken and instruments used in the experiments. The measurement uncertainties were not reported. Thus, uncertainties are based on values in Table 2-2 and information on the manufacturers of instrumentation provided in reference [17]. The accuracy of instrumentation was then obtained from the manufacturer's website. Table 4-33 provides the release conditions for the horizontal gas jet fires for test series 3.

Since the experiments were performed over the course of a day the atmospheric conditions provided in Table 4-34 is assumed to apply to all experiments included in the MEP database. The wind direction for the horizontal tests was reported as northwest, thus directing the jet fires towards the southeast in reference [16]. However, in reference [15] the wind direction is reported as NNE, N, NNW without providing explanation as to which test series these directions correspond to. Due to this discrepancy the wind direction is chosen as the parameter for variation. The elevation at which the atmospheric conditions were measured was not provided.

Table 4-32. Measurements and instrumentation for TAMU propane jet fire experiments

Measurement	Instrument	Measurement Uncertainty
Mass flow rate	Flow meter	±1.0%*
Incident radiative heat flux	Wide-angle radiometers (180° view angle)	±5%
Flame length and lift-off	Real time and infrared cameras	±10%**
Weather conditions	Wind speed and direction: Anemometers	±5%, ±3°

*Based on accuracy provided by manufacturer of flow meter.
**approximate value provided by subject matter experts at Sandia. Main contributing factor is error correction regarding the lens.

Table 4-33. Release conditions for TAMU LPG horizontal gas jet fire experiments

Test No.*	Release diameter** (mm)	Release pressure (MPa)	Release temperature (°C)	Mass flowrate (kg/s)	Exit velocity (m/s)
16	19.05	0.20	20	0.047	87.4
17	19.05	0.165	22	0.042	78.2
18	19.05	0.027	31	0.015	27.5

Test No.*	Release diameter** (mm)	Release pressure (MPa)	Release temperature (ºC)	Mass flowrate (kg/s)	Exit velocity (m/s)
19a	19.05	0.034	30	0.016	30.5
19b	19.05	0.076	30	0.025	46.5
19c	19.05	0.158	30	0.040	74.2
19d	19.05	-	-	0.054	101.0
19e	19.05	0.317	30	0.067	125.0
19f	19.05	0.586	30	0.11	205.8

*Test 19 ramped up in a staircase pattern and held steady for 50 second for each flow rate
** Elevation of nozzle 1.25 m from ground to centerline

Table 4-34. Atmospheric conditions for TAMU propane jet fire experiments

Temperature (ºC)	Relative humidity (%)	Wind direction (degrees)	Wind speed (m/s)
25.3 ± 1.7	50.9 ± 9.3	NNE, N, NNW [15] NNW [16]	2.2 ± 0.7

4.2.1.1. TAMU propane jet fires: experimental comparisons and parameter variation

The experimental measurements for model comparison are provided in Table 4-35. Flame length is defined as the distance from the release point to the furthest edge of the flame boundary which includes liftoff. Liftoff is defined as the distance from the release point to the closest point of the flame boundary. The flame length was determined using a real time camera. It was found that real-time images agreed with either 600 K or 700 K temperature contours measured with the IR camera. In the MEP, applicable models can use 650 K, an average of these temperatures, to determine the flame length. Note that positions for radiometers labeled R6 and R9 were switched because measurements from R9 were consistently higher for all tests and the reported R6 position was closest to the jet fire. The other positions were not candidates for modification because their measurements correlated with proximity to the fire. Regarding the propagated input uncertainty, a model should be assessed using the variation for wind direction due to the lack of information provided. Values to use for the variation are provided in Table 4-36. Test 19f with a mass flow rate of 0.11 kg/s was chosen for this purpose since it had the largest flame among the experiments.

Table 4-35. Measurements for validation for TAMU propane jet fires

Parameter	Instrument
Average incident radiation	Wide-angle radiometers
Average flame length	Real-time video

Table 4-36. TAMU propane jet fire Test 19f: Experimental input parameters to vary

Test 19f	
Parameter	**Variation**
Wind direction*	30° (low) 345° (base) 75° (high)

*Relative to the north or y-axis as shown in MEP spreadsheet. Base case will direct jet fire toward the SE direction.

4.2.2. Advantica and Shell (A-S) crude oil jet fire experiments

A series of six 'live' crude oil jet fire experiments involving fourteen horizontal releases were performed by Advantica and Shell Global Solutions at the Advantica Spadeadam Test Site as a Joint Industry Project, sponsored by seven oil and gas companies and the Health and Safety Executive [18]. The objective of the tests was to determine the effect of adding water to 'live' crude oil, either by mixing the oil with water prior to the release or by injecting additions immediately downstream of the release. The 'live' crude oil was simulated using a mixture of crude oil, propane, and natural gas producing two different gas-to-oil ratios of 253 m^3/m^3 and 257 m^3/m^3. The experiments included an engulfed pipe target, 0.91 m in diameter, 16 m long and 12.7 mm thick placed 15 m downstream of the release point to obtain measurements of heat flux. The two experiments involving no water addition are included for comparison in the MEP. Table 4-37 provides a general description of the test series.

Table 4-37: General description of the A-S crude oil jet fire experiments

General description	
Test location	Advantica Spadeadam Test Facility, England
Test performed by	Advantica and Shell
Mass release rates	5.0-5.4 kg/s
Number of tests	2 (14 conducted in experimental series)
Fuel composition	'Live' crude oil (mixture of crude oil, propane, and natural gas; mass fractions not reported)
Engulfed object	Yes
Data confidentiality	Open, publicly available only through journal publication thus complete dataset not available
References	Hankinson, et al. [18]

The engulfed pipe target was instrumented with forty circular foil calorimeters to measure total heat flux and two ellipsoidal radiometers to measure radiative heat flux. The calorimeters were blackened to provide a known emissivity ($\varepsilon \approx 1$) and were water-cooled to maintain a temperature of 60°C. Other measurements include six wide-angle radiometers to measure incident heat flux external to the jet fire. The view angle of the radiometers was not reported but can assumed to be 150° for the MEP. The wide-angle radiometers were placed 1-m above the ground and aimed at the vertical centerline of the pipe which was elevated 3-m above the ground, the same height as the release point. Thermal imaging was used to determine surface emissive power, while video cameras were used to determine flame size and shape. Table 4-38 provides the type of measurements taken and instruments used in the

experiments. The fuel was released through a circular hole cut in the center of a plate mounted at the end of the discharge pipeline (inner diameter of 38 mm) and ignited 1-m downstream using a propane pilot flame. Table 4-39 provides the release conditions for the two experiments included in the MEP database. Wind speed and direction were measured using a sonic anemometer mounted 20 m above the ground and 75 m upstream of the release point. The wind direction is relative to the release direction where zero degrees corresponds to a wind that is in the same direction as the release. The wind speed was measured at heights of 2.1 m, 5.3 m, 11.6 m, and 16.6 m above the ground. Atmospheric conditions such as pressure, temperature, and relative humidity were also measured. The atmospheric conditions during the experiments are provided in Table 4-40.

Table 4-38: Measurements and instrumentation for A-S crude oil jet fire experiments

Measurement	Instrument	Measurement Uncertainty
Mass flow rate	Mass flow meter	Not reported
Incident radiative heat flux	Wide-angle radiometers (150° view angle)	Not reported ±5% (Table 2-1)
Total heat flux to pipe	Calorimeters	Not reported ±20% (Table 2-2)
Radiative heat flux to pipe	Radiometers	Not reported ±23% (Table 2-2)
Surface emissive power	Infrared camera	Not reported ±10%*
Flame length and lift-off	Camera (crosswind)	Not reported ±10%*
Weather conditions	Wind speed and direction: Anemometers	Not reported

*Approximate value provided by subject matter experts at Sandia. Main contributing factor is error correction regarding the lens.

Table 4-39: Release conditions for A-S crude oil jet fire experiments

Test No.	Release diameter (mm)	Gauge pressure of release (bar) (psi)	Mass flowrate (kg/s)	Gas oil ratio (m^3/m^3)
1(a)	10.4	92.3 (1337)	5.3	253
2(a)	17.8	20.2 (293)	5.0	253

Table 4-40. Atmospheric conditions for A-S crude oil jet fire experiments

Test No.	Temperature (°C)	Relative humidity (%)	Wind direction (degrees)	Wind speed (m/s)
1(a)	6.2	91.1	-51	2.1
2(a)	4.1	89.6	-45	2.1

4.2.2.1. A-S crude oil jet fires: experimental comparisons and parameter variation

The experimental measurements for model comparison are provided in Table 4-41 . Flame length is defined as the horizontal distance from the release point to the furthest edge of the flame boundary. Liftoff was also measured and is defined as the horizontal distance from the release point to the closest point of the flame boundary. The fuel properties are used for parameter variation to determine the propagated uncertainty due to the lack of information provided. Values to use for the variation are provided in Table 4-42. Test 2(a) was chosen since all measurements were reported for this experiment.

Table 4-41. Measurements for validation for A-S crude oil jet fires

Parameter	Instrument
Average incident radiation	Wide-angle radiometers
Average flame length	Real-time video
Average Surface emissive power	Infrared camera
Average total heat load to pipe during steady state	Calorimeters
Average radiative load to pipe during steady state	Radiometers

Table 4-42. A-S crude oil jet fire Test 2a: Experimental input parameters to vary

Test 2a	
Parameter	**Variation**
Heat of combustion (MJ/kg)	42 (low) 45 (base) 48 (high)
C/H mole ratio	0.5 (low) 0.6 (base) 0.7 (high)

4.2.3. Sandia National Laboratories ethane, ethylene, and isopentane jet fire experiments

Sandia National Laboratories conducted a series jet fire experiments at Sandia's Lurance Canyon Burn Site Facility [14]. The objective of the test series funded by the Pipeline and Hazardous Materials Administration (PHMSA) was to obtain data for the MEP. Table 4-43 provides a general description of the experiments.

Three jet fires were performed testing three different fuels that include ethane, ethylene, and isopentane as shown in Figure 4-5. The fuel delivery system involved using pressurized nitrogen to drive fuel out of a 20' International Organization for Standardization (ISO) container for each fuel through a 3" diameter, 100' long pipeline. A plate was fitted at the end of the pipeline with a 5/8" diameter orifice. Measurements include flame length, heat flux, and surface emissive power. Data was also collected from four weather towers, each measuring wind speed, wind direction, temperature, pressure, and relative humidity at three different elevations. Table 4-44 and Table 4-45 provides the type of measurements taken and instruments used in the experiments along with their uncertainty.

Table 4-43: General description of Sandia ethane, ethylene, and isopentane jet fires

General description	
Test location	Sandia Lurance Canyon Burn Site, Albuquerque, NM, USA
Test performed by	Sandia National Laboratories
Mass release rates	1.7-2.3 kg/s
Number of tests	3
Composition of each fuel	Ethane (99%+), ethylene (99.5%+), and isopentane (99%+)
Engulfed object	No
Data confidentiality	Publicly available
References	Luketa, et al.

(a)

(b)

(c)

Figure 4-5: Jet fire experiments: (a) ethane, (b) ethylene, and (c) isopentane

Table 4-44: Measurements and instrumentation for the SNL ethane, ethylene, and isopentane jet fires

Measurement	Instrument	Measurement Uncertainty
Incident radiative heat flux	Wide-angle radiometers	±5.5 to ±5.8%
Surface emissive power	IR cameras	±6.3%
Flame length and tilt	Visible cameras	±10%
Mass flow rate	Orifice plate, vortex meter	±10%

Table 4-45: Wind speed and direction for SNL ethane, ethylene, and isopentane jet fires

Measurement	Stations, Heights (m)	Uncertainty
Wind speed	All, 2, 5, 7.62	± 1% or 0.07 m/s, whichever is greater
Wind direction	All, 2, 5, 7.62	± 3°
Temperature	All, 2	± (0.226 - 0.0028T) °C at -80 to 20°C ± (0.055 + 0.0057T) °C at 20 to 60°C
Temperature	All, 5, 7.62	± 0.4 °C
Relative humidity	All, 2	± 1.4%
Pressure	East/South, 2	± 200 Pa at -40 to 60°C
Pressure	North/West, 2	± 600 Pa at -40 to 60°C

Infrared cameras were used to obtain flame length, and surface emissive power. The reported surface emissive power assumes a flame emissivity of 1 and is corrected for atmospheric attenuation. For all pool fire experiments the dimensions and surface emissive power are based on temperatures above 1123 K as measured from the IR camera. This temperature corresponds to an SEP value of 90 kW/m^2 assuming blackbody radiation. Inspection of real-time video provided confirmation that this temperature threshold is indicative of the visible flame. To measure incident radiation a total of 40 wide-angle total heat flux gauges were used with a field of view angle of 180°. All heat flux gauges were aimed horizontally.

Since the flame angled horizontally from the release direction for all tests, the reported flame dimensions are distances projected onto the north-south axis or aligned with the release direction as viewed from the east cameras. Two methods were used to measure flow rate of the fuel supply, an orifice plate and vortex meter. For all tests the mass flow rate has been corrected for losses using a discharge coefficient of 0.6 for the sharp-edged orifice at the exit. There was agreement between the two methods of flow rate measurement for all tests.

Table 4-46 provide the average wind speed among all stations for each experiment. The wind direction has been averaged among all stations and heights. Table 4-47 and Table 4-48 provides the atmospheric conditions and fuel release rate for each experiment.

Table 4-46: Wind conditions for SNL ethane, ethylene, propane, and isopentane pool fires

	Ethane	Ethylene	Isopentane
Height (m)	Average wind speed (m/s)		
2	1.9 ± 0.2	2.2 ± 0.3	2.9 ± 0.6
5	2.2 ± 0.3	2.7 ± 0.4	3.5 ± 0.8
7.6	2.3 ± 0.2	3.1 ± 0.5	3.8 ± 0.8
	Average wind direction (deg)		
all	109.0 ± 3.9	110.6 ± 4.5	227.2 ± 9.0

Table 4-47: Atmospheric conditions for SNL ethane, ethylene, and isopentane jet fires

Experiment	Ambient temperature (^{O}C)	Atmospheric Pressure (Pa)	Relative humidity (%)
Ethane	3.3 ± 0.4	81,317 ± 0.2	33.4 ± 0.8
Ethylene	-1.0 ± 0.3	81,030 ± 0.2	39.4 ± 0.7
Isopentane	-0.2 ± 0.4	81,520 ± 0.2	28.8 ± 0.6

Table 4-48: Fuel release conditions of SNL ethane, ethylene, and isopentane jet fires

Release Condition	Ethane	Ethylene	Isopentane
Height of release (m)	1.0	1.0	1.0
Pressure (psig)	103.4 ± 1.9	78.0 ± 1.6	106.3 ± 6.1
Temperature (^{o}C)	-45.7 ± 3.5	-71.3 ± 2.6	-2.7 ± 0.4
Mass flow rate (kg/s)	3.1 ± 0.09	2.9 ± 0.08	3.9 ± 0.1
Mass flow rate at exit (kg/s)	1.9 ± 0.05	1.7 ± 0.05	2.3 ± 0.06

4.2.3.1. SNL ethane, ethylene, and isopentane jet fire tests: experimental comparisons and parameter variation

The experimental measurements for model comparison included in the MEP spreadsheet are provided in Table 4-49. Since surface emissive power was measured directly with infrared cameras these measurements are included to serve as an input into solid flame models or provide a comparison measurement for CFD-based models that have the capability to evaluate the SEP. The projected horizontal flame length and vertical flame height are distances projected onto the north-south axis or aligned with the release direction as viewed from the east cameras.

Table 4-49. SNL ethane, ethylene, and isopentane jet fire tests: measurements for validation

Parameter	Instrument
Average incident radiative heat flux during steady state	Wide-angle radiometers
Average projected horizontal flame length during steady state	Cameras
Average projected vertical flame height during steady state	Cameras

To determine the propagated input uncertainty, experimental parameter variations are provided in Table 4-50. The isopentane jet fire is chosen for the variational case since it had the highest fuel release rate among the experiments. The mass flow rate and wind direction are chosen as the parameters to vary. The mass flow rate range is based on the measurement uncertainty of 10%, while the wind direction range is based on the standard deviation of the measurements.

Table 4-50: SNL isopentane jet fire: Experimental input parameters to vary

Isopentane jet fire	
Parameter	**Variation**
Mass flow rate	2.5 kg/s (low) 2.3 kg/s (base) 2.1 kg/s (high)
Wind direction	218° (low) 227° (base) 236° (high)

4.3. Fireball experiments

4.3.1. Health and Safety Laboratory and BG Technology (HSL-BGT) propane fireball experiments

A series of four large-scale fireball experiments involving propane funded by the Council of the European Communities (CEC) were performed by the Health and Safety Laboratory and BG Technology [19]. For each test a vessel with capacity of 5.1 m^3 was used to release fuel masses ranging from 279 to 1708 kg. Table 4-51 provides a general description of the experiments and Table 4-52 provides the test matrix and release conditions. Note that the release temperature was not provided but was noted that the liquefied propane was at least 100°C higher than its boiling point of -42°C at atmospheric pressure.

Table 4-51. General description of the HSL-BGT propane fireball experiments

General description	
Test location	Not provided in publication
Test performed by	Health and Safety Laboratory and BG Technology
Mass released	Listed in Table 4-52
Number of tests	4
Fuel composition	propane (full composition not provided)
Engulfed object	No
Data confidentiality	Publicly available in journal publication
References	Roberts, Goss, and Hawksworth [19]

Table 4-52. Release conditions for HSL-BGT propane fireball experiments

Test No.	Vessel pressure (bar) (psi)	Fill ratio (%)	Released mass (kg)
1	16.5 (239)	20	279
2	21.3 (309)	41	710
3	18.6 (270)	60	1272
4	24.4 (354)	85	1708

The vessel for each test was ruptured by exposure to a jet fire which resulted in the pressure relief valve opening after 1 to 2 minutes and then failure in about 3 minutes after the PRV opened. For all experiments, the longitudinal axis of the vessel was aligned 15° clockwise with respect to the north-south axis. Instrumentation included video, infrared cameras, radiometers, thermocouples, pressure transducers, and anemometer. The incident thermal radiation was measured using slow- and fast-response, wide-angle radiometers. Note that the elevation and inclination of the wide-angle radiometers were not provided. The surface emissive power was determined using infrared cameras placed orthogonal to each other. Narrow-angle, fast response radiometers were used to measure spot surface emissive power.

Diameter, fireball rise height, and duration were measured using video and infrared cameras. The projected area of the fireball was determined in the crosswind direction using a temperature criterion of 670°C (45 kW/m^2 assuming blackbody) and in the upwind/downwind direction using a heat flux criterion of 40 kW/m^2. The fireball height at maximum area was reported but the definition of height was not provided in [19]. Thus, for the MEP, height can be assumed to be the distance from the ground to the center of the fireball which is a common definition. The fireball dimensions were generally greater in the east-west direction than in the north-south direction. The fireball duration was defined as the time between vessel rupture and the point when flame was no longer visible, however, it was noted that it was difficult to determine precisely due to the existence of small flame eddies just before extinction. The instrumentation used, and their uncertainty is provided in Table 4-53. The atmospheric conditions were measured and are provided in Table 4-54, however, the elevation at which the measurements were taken were not reported.

Table 4-53. Measurements and instrumentation for HSL-BGT propane fireball experiments

Measurement	Instrument	Measurement Uncertainty
Surface emissive power	Infrared cameras; Narrow-angle radiometers (1° view angle)	±15%
Incident radiative heat flux	Wide-angle radiometers (view angles not provided);	±5%*
Fireball diameter, height, rise time, and extinction	Video and infrared camera	±5%
Weather conditions	Wind speed and direction: Anemometers	Not reported

*Not reported; values taken from Table 2-2

Table 4-54. Atmospheric conditions for HSL-BGT propane fireball experiments

Test No.	Temperature (°C)	Relative humidity (%)	Approximate wind direction	Average wind speed (m/s)
1	19	80	westerly	3
2	20	60	westerly	4
3	17	95	south-easterly	5
4	18	90	westerly	2

4.3.1.1. HSL-BGT propane fireballs: experimental comparisons and parameter variation

The experimental measurements for model comparison are provided in Table 4-55. Note that radiometer heat flux measurements are reported only for Test 4. Since surface emissive power was measured directly with infrared cameras these measurements are included for comparison. Note that for Test 2 the infrared camera used in the crosswind direction is not included for comparison in the spreadsheet since the SEP values exceeded its set maximum range. The measurements from the other IR camera placed orthogonally exceeded the set range of 195 kW/m^2 while the crosswind IR camera peaked reached the set limit. For other tests the maximum range was set above 195 kW/m^2.

Table 4-55. Measurements for validation for HSL propane fireball experiments

Parameter	Instrument
Peak incident radiative flux	Wide-angle radiometers
Surface emissive power	Infrared cameras
Fireball geometry and duration	Infrared and video cameras

Fireball rise, dimensions, height, and duration consist of only four measurements, one for each test, thus no relative standard deviation or bias factor are calculated for these measurements for an individual test. To provide sufficient data to assess the model relative standard deviation and bias factor for these measurements, results from all fireball test series are automatically combined in a separate worksheet.

Table 4-56 provides the experimental input parameter to vary to determine the propagated input uncertainty, namely the wind direction since it has the greatest uncertainty where it was reported as westerly. In examining the radiometer measurements from Test 4, the results indicate that the wind direction was approximately 270° clockwise with respect to the north end of the tank. Thus, this direction is considered as the base case with a ±15% variation.

Table 4-56. HSL propane fireball Test 4: Experimental input parameters to vary

Test 4	
Parameter	**Variation**
Wind direction	255° (low) 270° (base) 285° (high)

4.3.2. British Gas (BG) propane and butane fireball experiments

A series of large-scale fireball experiments involving propane and butane were performed by British Gas for a Council of the European Communities (CEC) project co-funded by eight European organizations, U.K. Health and Safety Executive, Shell International Gas Ltd. and Calor Gas Ltd. [21]. Pressurized vessels with capacities of 5.66 m^3 and 10.80 m^3 were used to release fuel masses ranging from 1000 to 2000 kg. Table 4-57 provides a general description of the experiments and Table 4-58 provides the test matrix and release conditions.

Table 4-57. General description of the BG fireball experiments

General description	
Test location	British Gas Spadeadam Test Facility, Cumbria, England
Test performed by	British Gas
Mass released	Listed in Table 3-35
Number of tests	4 butane, 1 propane
Fuel composition	Approximately 97% propane and 65-94 mol% butane (full composition provided in spreadsheet for each test)
Engulfed object	No
Data confidentiality	Partial data available in conference publication. Permission granted by DNV to provide data for MEP from test report on condition of inclusion of disclaimer[2].
References	Johnson and Pritchard [20] (publicly available publication) Test report from British Gas

Table 4-58. Release conditions for BG fireball experiments

Test No.	Fuel	Vessel capacity (m^3)	Vessel pressure (bar) (psi)	Liquid temperature* (°C)	Fill ratio (%)	Released mass (kg)
1	Butane	5.659	15 (218)	94.2	77	2000
2	Butane	5.659	15 (218)	101.6	39	1000
3	Butane	5.659	7.5 (109)	49.2	68	2000
4	Butane	10.796	15 (218)	81.9	40	2000
5	Propane	5.659	15 (218)	35.4	80	2000

*Average between two thermocouples

[2] *The content of the reports is intended only to provide data and analysis of experimental studies and is not intended to be any substitute for professional advice. DNV Group of companies, including GL Industrial Services UK Ltd, and any other person or company concerned with furnishing information or data used therein, excludes to the maximum extent permissible by law any legal liability in contract and tort (including negligence) for the up-to-date nature, accuracy, completeness, quality, or usefulness of any information, apparatus, product, or process disclosed or demonstrated.*

For all experiments, the longitudinal axis of the vessel was aligned with the north-south direction and was fractured using linear shaped charges placed longitudinally at the top of the vessel. In most experiments the fracture propagated along the top of the vessel in both directions until reaching the dome ends. The fracture then propagated either through or around the dome ends. However, the fracture pattern for Tests 3 and 5 changed direction towards the south end by propagating circumferentially around the vessel prior to reaching the dome end. Several fragments from the heater, actuator, frame, and dome ends were thrown, indicating distances ranging from 10s to 100s of meters. Post-test recovery of the peeled open vessel wall was mostly intact except for the dome ends for some tests.

Instrumentation included video and cine cameras, radiometers, thermocouples, pressure transducers, anemometers and wind vanes. The incident thermal radiation was measured using slow response, wide-angle radiometers. The surface emissive power was determined using measurements from wide-angle, fast response radiometers in conjunction with a solid flame model and the shape derived from video cameras. Narrow-angle, fast response radiometers were used to measure spot surface emissive power. Diameter, fireball rise height, and duration were measured using video cameras placed at orthogonal locations to each other. The flame shape was converted to an equivalent spherical fireball with the height defined as the height of the center of the sphere above the ground. The equivalent spherical fireball diameter was generally greater in the east-west direction than in the north-south direction. The fireball duration was defined as the time between vessel rupture and the point when flame was no longer visible. The instrumentation used, and their uncertainty is provided in Table 4-59. The atmospheric conditions measured at a single location at an elevation of 15 m are provided in Table 4-60.

Table 4-59. Measurements and instrumentation for BG fireball experiments

Measurement	Instrument	Measurement Uncertainty
Surface emissive power	Wide-angle radiometers (55^{o} and 90^{o} view angle); Narrow-angle radiometers (1^{o} view angle)	±10%
Incident radiative heat flux	Wide-angle radiometers (90^{o} and 150^{o} view angle);	±3%
Fireball diameter, height, rise time, and extinction	Video camera	±10%
Weather conditions	Wind speed and direction: Anemometers	Not reported

Table 4-60. Atmospheric conditions for BG fireball experiments

Test No.	Temperature (^{o}C)	Ambient pressure (mbar)	Relative humidity (%)	Average wind direction (degrees)*	Average wind speed (m/s)
1	16.5	976 (14.2)	92.9	120	8.2
2	10	980 (14.2)	70	305	14.8
3	13	982 (14.2)	82	240	5.1
4	23	994 (14.4)	57	230	4.9

Test No.	Temperature (°C)	Ambient pressure (mbar)	Relative humidity (%)	Average wind direction (degrees)*	Average wind speed (m/s)
5	16	987 (14.3)	75	315	5.2

*From magnetic north

4.3.2.1. BG fireballs: experimental comparisons and parameter variation

The experimental measurements for model comparison are provided in Table 4-61. Although the surface emissive power is reported it was not directly measured, instead it was calculated using the radiometer measurements and video coverage. Thus, it is not considered to be a principal parameter for comparison since it is a derived quantity, as mentioned previously in Section 2.1.

Table 4-61. Measurements for validation for BG fireball experiments

Parameter	Instrument
Peak incident radiative flux	Wide-angle radiometers (90° and 150° view angle)
Fireball geometry and duration	Video camera

Fireball rise, dimensions, height, and duration consist of only five measurements, one for each test, thus no relative standard deviation or bias factor are calculated for these measurements for an individual test. To provide a sufficient amount of data to assess the model relative standard deviation and bias factor for these measurements, results from all fireball test series are automatically combined in a separate worksheet.

Table 4-62 provides the experimental input parameter to vary to determine the propagated input uncertainty, namely the mass of release whose range is based on the three tri-cock valves used to determine the liquid level. The measurements uncertainty wasn't provided, thus the same uncertainty for the fireball experiments in the MEP for LNG fires is used, namely, ±2% percent volume. The experiment chosen to perform the parameter variation is Test 1 for butane since it is the baseline test for the experimental series and is of similar configuration to Test 5 for propane.

Table 4-62. BG fireball Test 1: Experimental input parameters to vary

Test 1	
Parameter	**Variation**
Mass of release	1960 kg (low) 2000 kg (base) 2040 kg (high)

4.3.3. Sandia National Laboratories (SNL-Fireball) crude oil fireball experiments

A series of large-scale fireball experiments involving crude oil with different compositions and vapor pressures were performed by Sandia National Laboratories [4]. The experiments were sponsored by the U.S. Department of Energy, U.S. Department of Transportation, and Transport Canada. The

objective of the fireball experiments was to compare measurements required for hazard evaluation which include fireball maximum diameter, height at maximum diameter, duration, and surface emissive power for three types of crude oil with different vapor pressure. Table 4-63 provides a general description of the experiments and Table 4-64 provides the test matrix and release conditions.

Table 4-63. General description of the SNL crude oil fireball experiments

General description	
Test location	Sandia National Laboratories, Albuquerque, NM, USA
Test performed by	Sandia National Laboratories
Mass released	Listed in Table 4-64
Number of tests	3
Fuel composition	3 types of crude oil (full composition provide in MEP spreadsheet)
Engulfed object	No
Data confidentiality	Publicly available
References	Luketa, et al. [2]

Table 4-64. Release conditions for SNL crude oil fireball experiments

Test	Vessel pressure (psig)	Temperature (ºC)	Fill ratio (%)	Released mass (kg)
Tight 1 (Bakken)	250	275	40	1229
Tight 2 (Tx Shale)	250	300	40	1269
SPR	168	293	40	1303

The experiments released 1.5 m^3 (400 gallons) of heated oil from a re-usable pressurized 3.8 m^3 (1000-gallon) vessel for each test. The tank's top opening had an inner diameter of 0.18 m (45") and the wider portion a diameter 0.28 m (72"). The overall height from the ground to the top of the vessel was about 2.8 m (9.15'). For two of the experiments, SPR and Tight 2 (Tx Shale), the average velocity of the oil just above the release point was estimated using high-speed cameras and flow tracking software. The average release velocity for the SPR and Tight 2 (Tx Shale) was 62 m/s and 52 m/s, respectively. Note that for the Tight 1 (Bakken) experiment the average release velocity was not measured. In carrying out the MEP, a release velocity of 57 m/s can be used which is based on averaging the measured velocities between the others experiments.

The oil was released vertically from the vessel by failing a rupture disc that enclosed the top of the vessel. To control the timing of release and ignition of the oil, the disc was failed using linear-shaped charges and the oil was ignited using an explosive charge. The thermodynamic state was chosen to maximize the probability that the entire mass of the oil contributed to the fireball. Post-test examination indicated this condition was satisfied since no oil remained in the vessel and no residue was found on the ground. The measurements collected, instrumentation used, and their measurement uncertainty is provided in Table 4-65. The atmospherics conditions during the experiments are provided in Table 4-66.

Table 4-65. Measurements and instrumentation for SNL crude oil fireball experiments

Measurement	Instrument	Measurement Uncertainty
Surface emissive power	Infrared cameras (North, East)	±6%, ±8%
Incident radiative heat flux	Wide-angle radiometers (180° view angle)	±5%
Fireball diameter, height, rise time, and extinction	Infrared camera (North, East)	±6%, ±8%
Weather conditions	Wind speed and direction: Anemometers	±1%

Table 4-66. Atmospheric conditions for HSL propane fireball experiments

Test No.	Temperature (°C)	Relative humidity (%)	Approximate wind direction (degrees)	Average wind speed (m/s)
Tight 1 (Bakken)	18.3	65	Calm	<1.3
Tight 2 (Tx Shale)	6.0	51	119 (south-east)	2
SPR	5.6	64	Calm	<1.3

4.3.3.1. SNL crude oil fireballs: experimental comparisons and parameter variation

The experimental measurements for model comparison are provided in Table 4-67. Since surface emissive power was measured directly with infrared cameras these measurements are included to serve as an input into solid flame models or provide a comparison measurement for CFD-based models that have the capability to evaluate the SEP. The surface emissive power and geometry measurements are determined by using a heat flux criterion of 20 kW/m^2.

Table 4-67. Measurements for validation for SNL crude oil fireball experiments

Parameter	Instrument
Peak incident radiative flux	Wide-angle radiometers
Surface emissive power	Infrared cameras
Fireball geometry and duration	Infrared cameras

Fireball rise, dimensions, height, and duration consist of only three measurements, one for each test, thus no relative standard deviation or bias factor are calculated for these measurements for an individual test. To provide sufficient data to assess the model relative standard deviation and bias factor for these measurements, results from all fireball test series are automatically combined in a separate worksheet.

Table 4-68 provides the experimental input parameter to vary to determine the propagated input uncertainty, namely the average release velocity since this was estimated. A ±10% variation is assumed. The test involving Tight 2 (Tx shale) crude oil was chosen for variation since its vapor pressure was between the other two crude oils

Table 4-68. SNL crude oil fireball Tight 2 (Tx shale): Experimental input parameters to vary

Tight 2 (Tx shale)	
Parameter	**Variation**
Release velocity	47 m/s (low) 52 m/s (base) 57 m/s (high)

4.3.4. Sandia National Laboratories ethane, ethylene, and isopentane fireball experiments

Sandia National Laboratories conducted a series fireball experiments at Sandia's Lurance Canyon Burn Site Facility [14]. The objective of the test series funded by the Pipeline and Hazardous Materials Administration (PHMSA) was to obtain data for model validation. Table 4-69 provides a general description of the experiments.

Three fireball tests were performed using three different fuels that include ethane, ethylene, and isopentane (Figure 4-6). For the ethane and ethylene fireball experiments, 900-gallon capacity, double-walled vertical tanks, approximately 10' in height, were used to contain the fuel. The inner and outer tank diameters were 48" and 60", respectively. The tanks were vacuum sealed and insulated with loose-fill perlite to maintain a liquid state. The iso-pentane experiment used a single-walled 1150-gallon capacity vertical propane tank, 48" in diameter and approximately 11' in height. Linear shaped charges were used to release the fuel, and an explosive charge was used to ignite the fuel for each test. The fuel was released vertically from the tanks after simultaneous detonation of the and explosive charge.

Table 4-69: General description of Sandia ethane, ethylene, and isopentane fireball experiments

General description	
Test location	Sandia National Laboratories, Albuquerque, NM, USA
Test performed by	Sandia National Laboratories
Mass released	**Listed in**
Number of tests	3
Composition of each fuel	Ethane (99%+), ethylene (99.5%+), and isopentane (99%+)
Engulfed object	No
Data confidentiality	Publicly available
References	Luketa, et al.

(a) (b) (c)

Figure 4-6: Fireball experiments: (a) ethane, (b) ethylene, and (c) isopentane

Measurements include heat flux, surface emissive power, diameter, and rise height. Data was also collected from a weather tower, measuring wind speed, wind direction, temperature, pressure, and relative humidity at three different elevations. Table 4-70 provides the release condition and Table 4-71 provides the type of measurements taken and instruments used in the experiments along with their uncertainty. The wind and atmospheric conditions are provided in Table 4-72 and Table 4-73, respectively.

Table 4-70. Release conditions for Sandia ethane, ethylene, and isopentane fireball experiments

Test	Tank pressure (psig)	Temperature (°C)	Density (kg/m^3)	Released mass (kg)
ethane	181	-32.8	466	1157
ethylene	175	-59.4	497	1153
isopentane	164	114	509	1150

Table 4-71. Measurements and instrumentation for Sandia ethane, ethylene, and isopentane fireball experiments

Measurement	Instrument	Measurement Uncertainty
Surface emissive power	Infrared cameras (South, East)	±6.3%
Total heat flux	Wide-angle heat flux gauges (180° view angle)	±5.6%
Fireball diameter, height, rise time, and extinction	Infrared camera (South, East)	±6.3%

Measurement	Instrument	Measurement Uncertainty
Weather speed	Anemometer	± 1% or 0.07 m/s, whichever is greater
Wind direction	Anemometer	± 3°
Atmospheric temperature	Thermistor	± 0.4 °C
Relative humidity	Capacitive RH sensor	± 1.4%

Table 4-72: Wind conditions for Sandia ethane, ethylene, and isopentane fireball experiments

Height (m)	ethane	ethylene	isopentane
	Average wind speed (m/s)		
2	3.8 ± 0.4	0.88 ± 0.02	1.11 ± 0.1
5	4.2 ± 0.4	0.81 ± 0.03	0.81 ± 0.06
7.6	4.5 ± 0.4	0.75 ± 0.02	0.94 ± 0.1
	Average wind direction (deg)		
2	229.5 ± 7.5	56.9 ± 10.4	101.2 ± 11.2
5	237.1 ± 21.4	47.7 ± 13.4	107.8 ± 15.3
7.6	231.8 ± 13.2	60.0 ± 9.0	126.1 ± 17.1
Average among heights	232.8 ± 21.4	54.9 ± 10.9	111.8 ± 14.6

Table 4-73: Atmospheric conditions for Sandia ethane, ethylene, and isopentane fireball experiments

Condition	ethane	ethylene	isopentane
Atmospheric pressure (Pa)	80,188 ± 0.2	80,547 ± 0.2	81,260 ± 0.2
Atmospheric temperature (°C)	5.9 ± 0.02	2.1 ± 0.03	11.5 ± 0.05
Relative humidity (%)	36.5 ± 0.05	41.3 ± 0.06	26.4 ± 0.05

4.3.4.1. Sandia ethane, ethylene, and isopentane fireballs: experimental comparisons and parameter variation

The experimental measurements for model comparison are provided in Table 4-74. For all fireball experiments the dimensions and surface emissive power are based on temperatures above 1123 K as measured from the IR cameras. This temperature corresponds to an SEP value of 90 kW/m^2 assuming blackbody radiation.

Table 4-74Since surface emissive power was measured directly with infrared cameras these measurements are included to serve as an input into solid flame models or provide a comparison measurement for CFD-based models that have the capability to evaluate the SEP.

Table 4-74. Measurements for validation for Sandia ethane, ethylene, and isopentane fireball experiments

Parameter	Instrument
Peak total heat flux	Wide-angle radiometers
Surface emissive power	Infrared cameras
Fireball geometry and duration	Infrared cameras

Fireball diameter, rise height, and duration consist of only three measurements, one for each test, thus no relative standard deviation or bias factor are calculated for these measurements for an individual test. To provide sufficient data to assess the model relative standard deviation and bias factor for these measurements, results from all fireball test series are automatically combined in a separate worksheet.

The isopentane fireball was chosen for variation since it resulted in the maximum average SEP among the fuels tested. The wind direction provided in Table 4-75 is the experimental input parameter to vary to determine the propagated input uncertainty since it had the largest variance among the input parameters measured.

Table 4-75. Sandia isopentane fireball: Experimental input parameters to vary

Isopentane	
Parameter	**Variation**
Wind direction	97° (low) 112° (base) 126° (high)

4.4. Concrete wall experiments

4.4.1. SNL concrete and masonry wall experiments

A series of thermal experiments involving concrete walls were performed by Sandia National Laboratories at Sandia's Thermal Test Complex [14]. The experiments were funded by the Pipeline and Hazardous Materials Administration (PHMSA) to obtain data for the MEP. Two types of walls were tested which include a formed insulated concrete wall and an insulated concrete masonry wall. The walls were heated using ceramic heaters arranged in a half circle built up from twelve quarter-round ceramic heaters (Figure 4-7a). Combined the heaters have a maximum power output of 96 kW. The heaters heat a 1/8" thick stainless-steel shroud (5'4" x 5'4") placed 2" from the walls (Figure 4-7b). The purpose of the shroud is to provide a more uniform temperature and a well-characterized boundary condition for model validation. The formed concrete wall was tested at targeted shroud temperatures of 272°C, 375°C, and 444°C which corresponds to blackbody heat flux levels 5 kW/m^2, 10 kW/m^2, and 15 kW/m^2, while the masonry wall is tested at 470°C which corresponds to a blackbody heat flux of 17.3 kW/m^2. Of the three experiments involving the formed concrete wall, the targeted shroud temperature of 444°C is chosen for model validation since it had the most uniform shroud temperature among the tests.

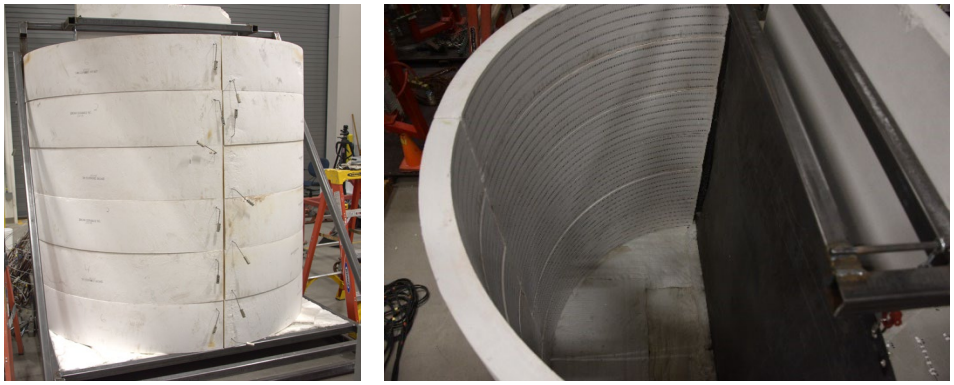

(a) (b)

Figure 4-7: Concrete wall experiments: (a) ceramic heaters, and (b) top view showing the stainless-steel shroud on the right

The formed (5'4" x 5'4") concrete wall had two layers of 3" thick standard concrete (3/8" aggregate) with 2" thick insulation board between them fitted with ties which provided shear strength and allowed the insulation to anchor to the concrete. The concrete layers also had mid-plane wire meshing reinforcement to prevent cracking. The dimensions of the formed concrete wall with the semi-circular heater are shown in Figure 4-8. This heater arrangement and placement are used for both walls. The concrete masonry wall, 4 blocks wide and 8 blocks high (5'4" x 5'4"), was comprised of hollow blocks (16" x 8" x 8") filled with loose-fill perlite. Figure 4-9 provides the dimensions of the masonry wall as well as the location of blocks with embedded thermocouples whose wires ran parallel to the front face of the wall.

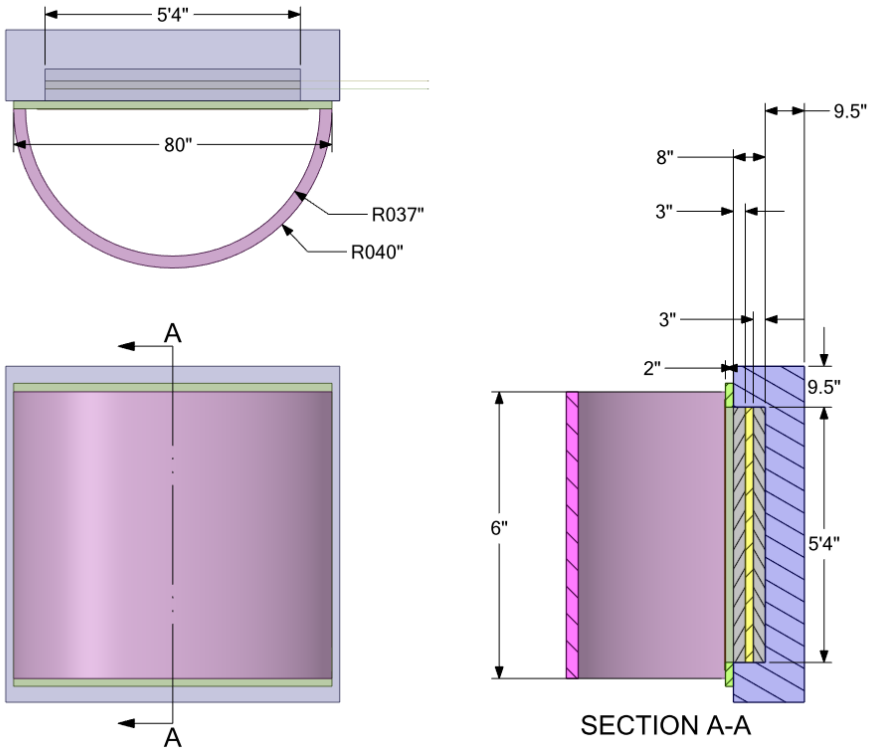

Figure 4-8: Formed concrete wall: Dimensions of heater and wall assembly.

Notes: 1. Thermocouples embedded in blue blocks
2. Cavities filled with loose-fill perlite

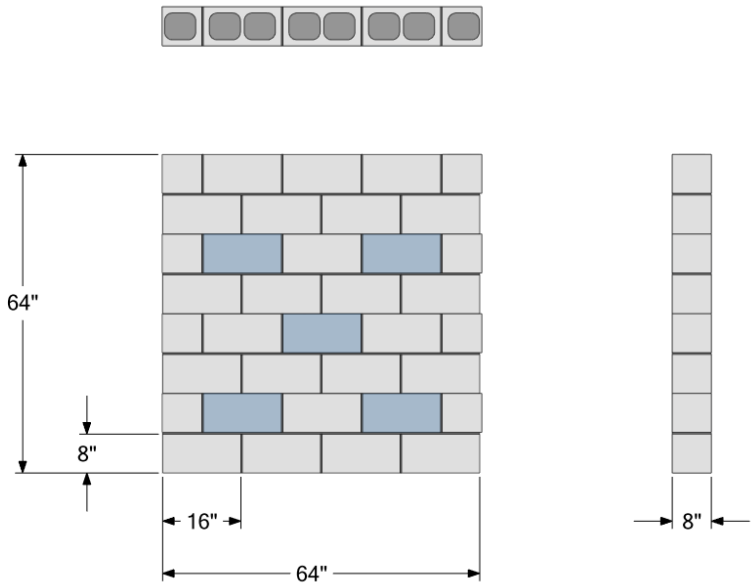

Figure 4-9: Masonry wall: Dimensions and blocks with surface and embedded thermocouples highlighted in blue.

For both walls tested, all sides except for the face exposed to the shroud were surrounded with 10" thick mineral-wool based insulation. Also, insulation extended from the shroud to the front face of the wall to prevent any gaps for both walls tested.

Both walls are instrumented with 0.062 gauge (1/16" dia.) ungrounded junction, mineral insulated metal sheathed, type K thermocouples (TCs) attached to the front and back faces as well as embedded. The uncertainty of the TCs is 1.1%. Figure 4-10 shows the embedded TCs in the formed concrete wall which are placed at heights of 1'6", 2'8", and 3'10". The middle height has only one station of embedded TCs while the other heights have two. At each height 3 TCs are placed ¾" apart in the concrete layers and one TC attached to each face of the insulation board. The TC wires extend parallel to the front face. Figure 4-11 shows the placement of TCs attached to the front and back face of the formed concrete wall which are in line with the embedded TCs. The labels of each TC station comprised of the surface and embedded TCs is also provided in Figure 4-11Figure 4-11 where the surface shown is facing the heated shroud.

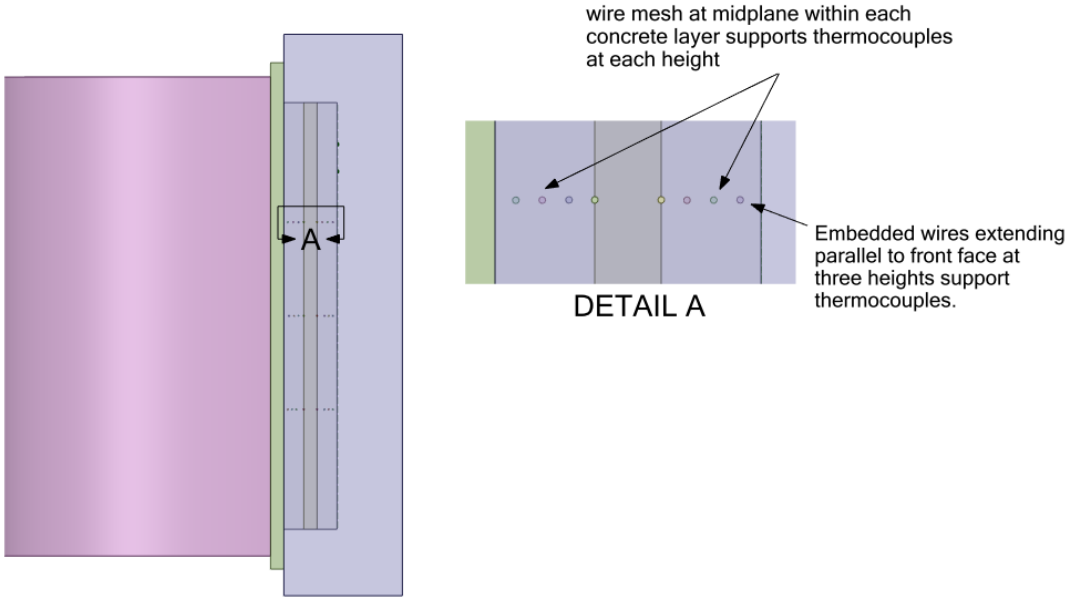

Figure 4-10: Formed concrete wall: Arrangement of embedded thermocouples.

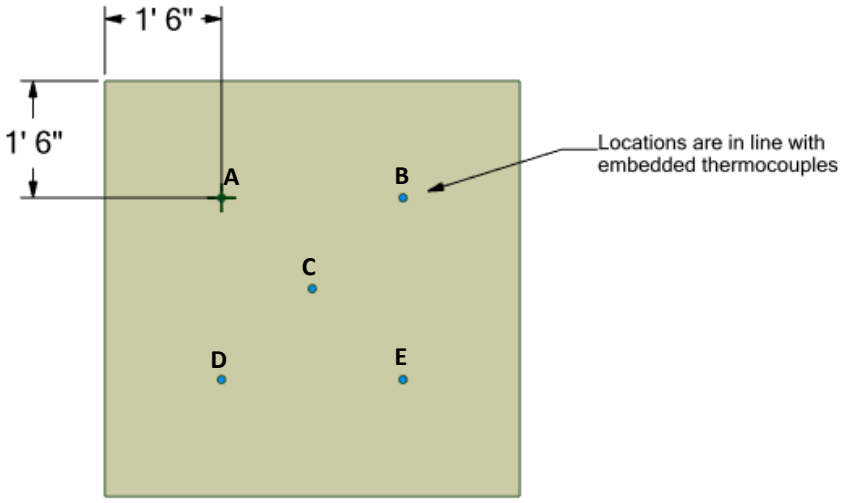

Figure 4-11: Formed concrete wall: Location of TC stations comprised of surface and embedded TCs. Surface shown is facing the heated shroud.

For the masonry wall, Figure 4-12 shows the placement of the TCs within the blocks highlighted in blue in Figure 4-9. The TCs are placed in 1" deep drilled holes within the block and their wires parallel to the front face of the wall. The TCs on the front and back faces of the wall are 1" from the top of a respective block and centered. The wires run between bricks within the mortar layer. The front and back faces of the masonry wall are instrumented with 5 TCs each and are shown as the red and blue dots in Figure 4-13. The identification of the TCs is provided in Figure 4-13 where the first letter in the identification refers to level, that is, 'L' refers to the lower level, 'M' the mid-level, and 'U' the upper level for blocks instrumented with TCs. The label 'through' in Figure 4-13 pertains to the sequential numbering of the thermocouples on the front and rear locations. For instance, the thermocouple to the right of the thermocouple labeled 'U-F1' is U-F2, with the incremental numbering continuing up to U-F10.

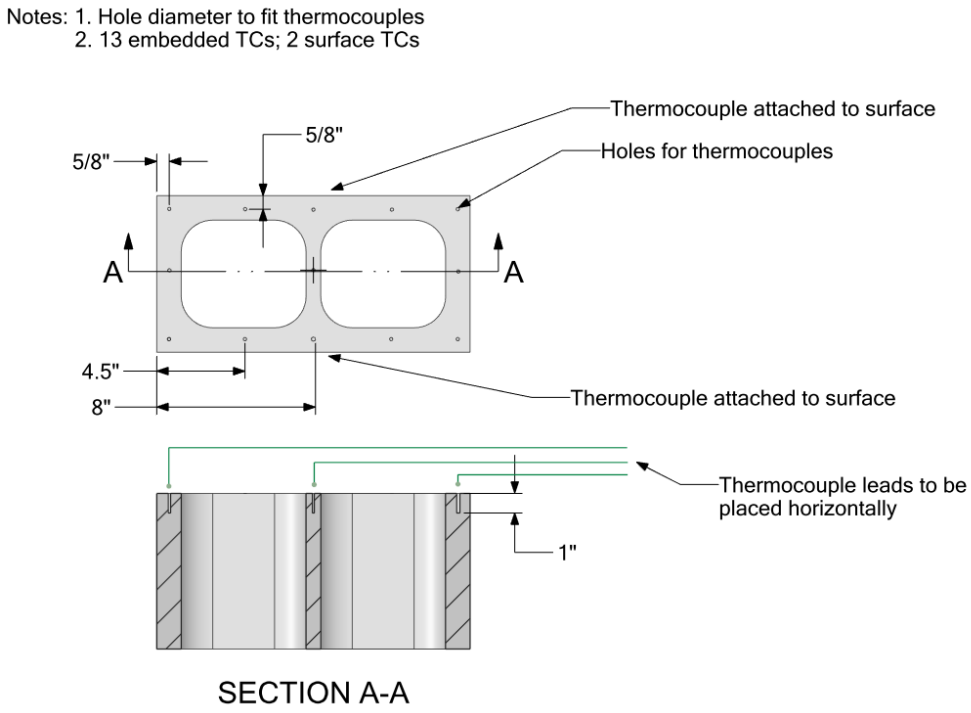

Figure 4-12: Masonry wall: Location of thermocouples for instrumented blocks

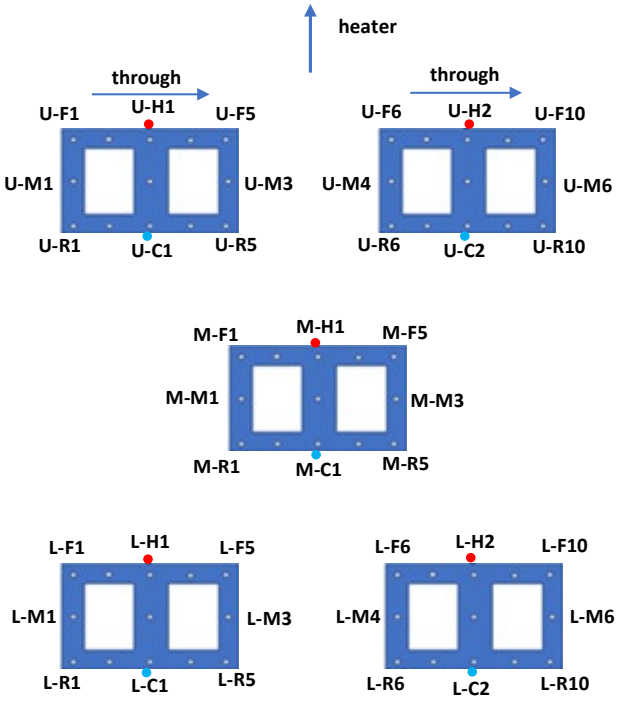

Figure 4-13: Masonry wall: Naming correspondence for thermocouples locations. 'L', 'M', and 'U' denote lower, middle, and upper level.

Figure 4-14 provides the number designation of the thermocouples attached to the surface of the shroud facing the wall. The temperature at these locations and at every 300 seconds is provided in the MEP database [27]. Since the shroud was not completely uniform in temperature, for modeling purposes the shroud could be divided into 9 equal areas, each corresponding to a TC location, and then each area is prescribed the temperature as measured by the TC over time. Although this is does not represent the actual spatial variation of temperature across the shroud, it is more accurate than using an average of all locations

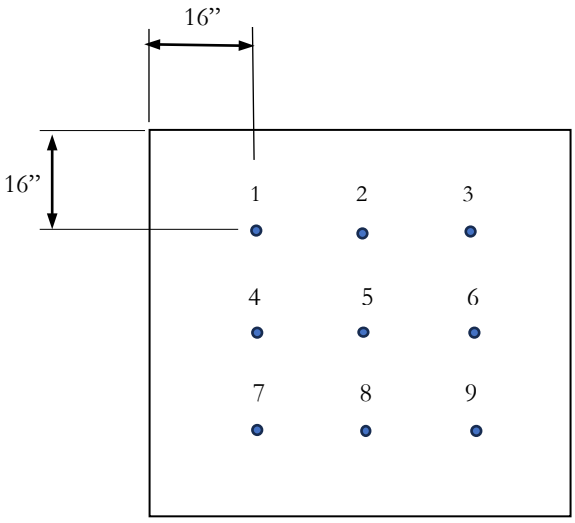

Figure 4-14: Number designation of the thermocouples attached to the shroud surface facing wall.

The thermal properties of the concrete, namely the thermal diffusivity, was determined by evaluating the temporal derivative and spatial second derivative of temperature using measurements from the experiments. The temporal derivative of temperature is determined by curve fitting a linear function to temperature measurements over time using the first embedded thermocouple. The linear function is fit to a range of ±10 seconds at each time evaluated. The derivative of the linear function with respect to time is then evaluated.

To evaluate the second derivative of temperature with respect to distance, a double exponential function is fit to temperature measurements as a function of distance. This is done for embedded thermocouples in the first layer of concrete for the formed concrete wall and at a block's web for the masonry wall. Measurements at the middle location for both walls are considered to more closely satisfy the one-dimensional assumption of the evaluation than other locations which are more impacted by lateral heat transfer despite the surrounding insulation. Thus, results from this analysis are provided using the center location of the wall of embedded thermocouples. Table 4-76 provides the thermal diffusivity using the above method for the concrete used in the wall experiments.

Table 4-76: Thermal diffusivity as a function of temperature for concrete used in wall experiments

	Formed (444°C)		Masonry (472°C)
Temp. (°C)	α (m^2/s)	Temp. (°C)	α (m^2/s)
25	4.47E-07	26	1.68E-07
31	3.07E-07	41	1.59E-07
41	2.61E-07	66	1.67E-07
51	2.48E-07	96	1.92E-07
61	2.45E-07	120	2.14E-07
72	2.62E-07	143	2.45E-07
82	2.75E-07	164	2.59E-07
92	2.9E-07	185	2.72E-07
102	3.01E-07	204	2.86E-07
112	3.11E-07	221	2.93E-07
122	3.24E-07	237	3.12E-07
132	3.41E-07	252	3.32E-07
142	3.48E-07	265	3.64E-07
152	3.51E-07	-	-
162	3.54E-07	-	-
172	3.52E-07	-	-
183	3.6E-07	-	-
193	3.65E-07	-	-
203	3.78E-07	-	-
212	3.83E-07	-	-
222	3.89E-07	-	-
232	3.88E-07	-	-
241	4.04E-07	-	-

The density of the concrete based on post-test measurements from several samples is 2133 kg/m^3 and 1616 kg/m^3 for the formed concrete wall and masonry wall, respectively. For the mineral wool

insulation, the thermal properties as provided by the manufacturer are listed in Table 4-77. The density of the insulation also provided by the manufacturer is 93 kg/m^3.

Table 4-78 provides the thermal properties of loose fill perlite [37] [38]. The density of the loose fill perlite based on post-test measurement from several samples is 93 kg/m^3. Measurement of emissivity on the surface of the shroud facing the wall is provided in Table 4-79.

Table 4-77: Thermal properties of mineral wool insulation

temperature (°C)	k (W/mK)	C_p (J/kgK)
20	0.0368	996.1
100	0.0462	1008.6
200	0.0612	1024.3
300	0.0807	1040
400	0.1058	1055.7
500	0.1375	1071.5

Table 4-78: Thermal conductivity and specific heat of loose fill perlite.

temperature (°C)	k (W/mK) [38]	temperature (°C)	C_p (J/kgK) [37]
0	0.043	2	761.0
93	0.059	25	802.0
149	0.076	127	919.5
204	0.090	177	965.6
260	0.105	227	1001.3
316	0.126	277	1030.3
371	0.141	327	1054.7
427	0.163	377	1075.8
538	0.214	-	-

Table 4-79: Shroud emissivity measurements.

Location*	emissivity
1	0.758 ± 0.002
2	0.748 ± 0.002
3	0.735 ± 0.007
4	0.747 ± 0.005
5	0.738 ± 0.0003
6	0.747 ± 0.004
7	0.763 ± 0.008
8	0.764 ± 0.001
9	0.739 ± 0.004
average	0.749 ± 0.004

*Locations correspond to those shown in Figure 4-14

4.4.1.1. Sandia concrete wall experiments: experimental comparisons and parameter variation

Although the experiments were performed until the back face indicated a rise in temperature which took almost 2 hours for both walls, for model comparison the duration is truncated to 0.5 hours to minimize simulation time. The experimental measurements for model comparison are provided in Table 4-80.

Table 4-80. Measurements for validation for Sandia concrete wall experiments

Parameter	Instrument
Temperature	Thermocouples

The thermal diffusivity of the concrete is chosen as the parameter to vary since it has the highest uncertainty. Based on the range of thermal properties of standard concrete provided in the review article by Kodur [39], the thermal diffusivity values in Table 4-76 for the formed concrete wall are to be reduced by 16% for the low variation case and increased by 16% for the high variation case.

Table 4-81. Sandia formed concrete wall: Experimental input parameter to vary

Formed concrete wall	
Parameter	**Variation**
Thermal diffusivity of concrete (m^2/s)	Table 4-76 - 16% (low) Table 4-76 (base) Table 4-76 + 16% (low)

5. REFERENCES

[1] R. Corlett, "Gas Fires with Pool-like Boundary Conditions: Further Results and Interpretations," *Combustion and Flame,* vol. 14, pp. 351-360, 1970.

[2] A. Luketa, B. Blanchat, D. Lord, J. Hogge, A. Cruz-Cabrera and R. Allen, "Pool Fire and Fireball Experiments in Support of the US DOE/DOT/TC Crude Oil Characterization Research Study," Sandia National Laboratories, Albuquerque, NM, SAND2019-9189, 2019.

[3] D. L. Brenchley, "Assessment of Research and Development (R&D) Needs in Ammonia Safety and Environmental Controls," Pacific Northwest Laboratory, sec. 5.4, September 1981.

[4] A. Luketa, A. Cruz-Cabrera, W. Gill, S. Adee and J. Hogge, "Experimental Results of 2-m Heptane, Bakken Crude Oil, and Dilbit Crude Oil Pool Fire Tests Performed for the National Research Council of Canada," Sandia National Laboratories, SAND2021-3206, 2021.

[5] T. Blanchat, P. Helmick, R. Jensen, A. Luketa, R. Deola, J. Suo-Anttila, J. Mercier, T. Miller, A. Ricks, R. Simpson, B. Demosthenous, S. Tieszen and M. Hightower, "The Pheonix Series Large Scale LNG Pool Fire Experiments," SAND2010-8676, (2011).

[6] D. Nedelka, J. Moorhouse and R. Tucker, "The Montoir 35 m diameter LNG pool fire experiments," in *Proc LNG IX, 9th Int Conf & Exp on LNG*, Nice, France, 1989.

[7] P. Croce, K. Mudan and J. Moorhouse, "Thermal Radiation from LNG (Liquefied Natural Gas) Trench Fires. Volume 1. Main Report," Arthur D. Little, Inc., Cambridge, MA, NTIS, PB85129096, 1984.

[8] P. Croce, K. Mudan and J. Moorhouse, "Thermal Radiation from LNG Trench Fires. Volume 2. Data," Arthur D. Little, Cambrdge, MA, NTIS, PBS85159465, 1984.

[9] B. Lowesmith and G. Hankinson, "Large scale high pressure jet fires involving natural gas and natural gas/hydrogen mixtures," vol. 90, 2012.

[10] S. Betteridge and L. Phillips, "Large scale pressurised LNG BLEVE experiments," *AIChemE Symp. Ser.,* no. 160, pp. 1-12, 2015.

[11] K. Mudan, "Hydrocarbon Pool and Vapor Fire Data Analysis," Arthur D. Little, Inc., October 1984.

[12] M. Munoz, E. Planas, F. Ferrero and J. Casal, "Predicting the emissive power of hydrocarbon pool fires," *J. Haz. Mat.,* vol. 144, pp. 725-729, 2007.

[13] B. Rengel, C. Mata, E. Pastor, J. Casal and P. E. , "A priori validation of CFD modelling of hydrocarbon pool fires," *J. of Loss Prevention in the Process Industries,* vol. 56, p. 18–31, 2018.

[14] A. Luketa, S. Adee, R. Allen and A. Cruz-Cabrerea, "Fire and Thermal Experiments in Support of the Model Evaluation Protocol for LNG Facility Fires," Sandia National Laboratories, Albuquerque, N.M., SAND2025-11078, 2025.

[15] B. Zhang, Y. Liu, D. Laboureur and S. Mannan, "Experimental Study on Propane Jet Fire Hazards: Thermal Radiation," *Ind. Eng. Chem. Res.,* vol. 54, no. 9251-9256, 2015.

[16] Gopalaswami, G., et al., "Experimental study on propane jet fire hazards: Comparison of main geometrical features with empirical models," *J. Loss Prev. Proc. Indus.,* vol. 41, pp. 365-375, 2016.

[17] Laboureur, D.M. et al, "Experimental study on propane jet fire hazards: Assessment of the main geometrical features of horizontal jet flames," *J. Loss Prev. Proc. Indus.,* vol. 41, pp. 355-364, 2014.

[18] G. Hankinson, B. Lowesmith, J. Evans and L. Shirvill, "Jet Fires Involving Releases of Crude Oil, Gas, and Water," *Trans IChemE, ParB,* vol. 85 (B3), pp. 221-229, May 2007.

[19] T. Roberts, A. Gosse and S. Hawksworth, "Thermal Radiation from Fireballs on Failure of Liquefied Petroleum Gas Storage Vessels," *Trans IChemE,* vol. 78, no. Part B, pp. 184-192, 2000.

[20] D. Johnson and M. Pritchard, "Large scale experimental study of Boiling Liquid Expanding Vapour Explosions (BLEVEs)," *GASTECH (1990): International LNG/LPG Conference and Exhibitiion Conference Papers,* vol. 1, no. 14, pp. session 3, paper 3.3, 1990.

[21] D. Johnson, M. Pritchard and M. Wickens, "A Large Scale Experimental Study of Bleves: Contract Report on CEC co-funded Research Project," Report No. 15367, January 1991.

[22] Brundage, A., et al., "Thermocouple Response in Fires, Part 2: Validation of Virtual Thermocouple Model for Fire Codes," *J. Fire Sciences,* vol. 29, pp. 213-226, 2011.

[23] K. McGrattan, S. Hostikka, R. McDermott, J. Floyd, C. Weinschenk and K. Overholt, "Fire Dynamics Simulator Technical Reference Guide volume 2: Verification," National Institute of Standards and Technology, Gaithersburg, Maryland, USA, and VTT Technical Research Centre of Finland, Espoo, Finland, January 2017, Sixth Edition.

[24] K. McGrattan, R. Peakcock and K. Overholt, "Fire Model Validation - Eight Lessons Learned," in *Fire Safety Science Proceedings of the eleventh International Symposium*, 958-968, 2014.

[25] B. Blanchat and V. Figueroa, "Large-scale Open Pool Experimental Data and Analysis for Fire Model Validation and Development," Sandia National Laboratories, SAND2008-1204C, Albuquerque, NM, 2008.

[26] J. Nakos, "Uncertainty Analysis of Steady State Incident Heat Flux Measurements in Hydrocarbon Fuel Fires," SAND2005-7144, Albuquerque, NM, 2005.

[27] A. Luketa, "Model Evaluation Protocol for Fire Models Involving Fuels at Liquefied Natural Gas Facilities (Version 2)," Sandia National Laboratories, SANDXXXX-2026, 2026.

[28] A. Rohatgi, "WebPlotDigitizer," July 2020. [Online]. Available: https://automeris.io/WebPlotDigitizer.

[29] A. Luketa, "Recommendations on the Prediction of Thermal Hazard Distances from Large Liquefied Natural Gas Pool Fires on Water for Solid Flame Models," Sandia National Laboratories, SAND2011-9415, 2011.

[30] J. Nakos and J. Engerer, "Data Reduction Tools and Uncertainty Analysis of Incident Heat Flux Measurement Tools from Directional Flame Thermometers Used in Hydrocarbon Fuel Pool and Furnace Fires," Sandia National Laboratories, SAND2018-10332, Albuquerque, NM, 2018.

[31] I. Bradley, "A Review of the Applicability of the Jet Fire Resistance Test Method to Severe Release Scenarios," Health and Safety Executive Report, RR1120, 2017.

[32] D. L. Lord, J. W. Hogge and R. G. Allen, "Fuels Characterization for National Research Council Canada 2-m Pool Fire Test Series," Sandia National Laboratories, SAND2021-3389, 2021.

[33] V. Figueroa, J. Nakos and J. Murphy, "Uncertainty Analysis of Heat Flux Measurements Estimated Using a One-Dimensional, Inverse Heat-Conduction Program," Sandia National Laboratories, SAND2005-0339, 2005.

[34] NOAA, "National Centers for Environmental Information," [Online]. Available: https://www.ncei.noaa.gov/data/world-weather-records/series-11/access/data/WWR_Region06_2011-2016_tables.txt.

[35] R. Corlett, "Gas fires with pool-like boundary conditions," *Combustion and Flame,* vol. 12, no. 1, pp. 19-32, Feb. 1968.

[36] K. McGrattan, et al., "Fire Dynamics Simulator Techical Reference Guide Volume 3: Validation," NIST Special Publication 1018-3, Sixth Edition, April 4, 2025.

[37] E. King, S. Todd and K. Kelley, "Perlite: Thermal Data and Energy Required for Expansion. Report of Investigation," Bureau of Mines, Washington, D.C., 1948.

[38] ASTM 549-23, *Standard Specification for Perlite Loose Fill Insulation,* 2023.

[39] V. Kodur, "Properties of Concrete at Elevated Temperatures," *ISRN Civil Engineering,* vol. 2014, pp. 1-15, 2014.

[40] J. Nakos, J. Pantuso and J. Bentz, "Final Report - Summary of Thermal Testing of the Furnace Characterization Unit (FCU) for the Coast Guard," Sandia National Laboratories, SAND2000-1534, Albuquerque, NM, 2000.

This page left blank

APPENDIX A. MONTOIR POOL FIRE TEST DATA

The following Sections A.1 through A.4 provide data from the Montoir pool fire tests. Measurements include average heat from wide-angle radiometers (A.1), average surface emissive power (A.2), average spot surface emissive power from narrow-angle radiometers (A.3), and total incident heat flux to calorimeters above pool surface (A.4).

A.1. Average surface emissive power

Table A-1. Average surface emissive power Montoir Test 1

Instrument (position) (view angle)	Calculated Transmissivity values	Average values of Surface Emissive Power (kW/m2) with standard deviations (value in parenthesis corrected for atmospheric attenuation using the calculated transmissivity value)		
		Period 1 60-100 sec	Period 2 130-170 sec	Over period 1 and 2 60-170 sec
Barnes 3 (47) (40°x70°)	0.69	206±21 (298±31)	177±18 (256±26)	195±19 (282±18)
Barnes 4 (75) (40°x70°)	0.73	201±15 (276±21)	205±19 (281±26)	204±17 (279±23)
Barnes 5 (15) (40°x70°)	0.71	180±23 (254±32)	167±11 (235±16)	171±18 (241±25)
IRD 1 (17) (55°)	0.70	173±15 (247±22)	168±14 (240±20)	170±14 (243±14)
IRD 2 (76) (55°)	0.71	163±15 (230±21)	164±18 (231±25)	163±16 (230±23)
Land 1 (13) (90°)	0.73	209±24 (286±24)	216±15 (269±21)	219±20 (300±27)

Table A-2. Average surface emissive power Montoir Test 2: Periods 1, 2, and 3

Instrument (position) (view angle)	Calculated Transmissivity values	Average values of Surface Emissive Power (kW/m^2) with standard deviations (value in parenthesis corrected for atmospheric attenuation using the calculated transmissivity value)		
		Period 1 30-50 sec	Period 2 65-80 sec	Period 3 108-130 sec
Barnes 3 (47) (40°x70°)	0.69		195±21 (282±30)	213±22 (309±32)
Barnes 4 (75) (40°x70°)	0.71	183±16 (258±23)	193±19 (272±27)	183±20 (258±28)
Barnes 5 (15) (40°x70°)	0.71	203±19 (286±27)	202±17 (285±24)	197±18 (277±26)
IRD 2 (74) (55°)	0.73	183±20 (250±28)	191±18 (261±24)	179±16 (245±22)
Land 1 (13) (90°)	073	191±18 (262±25)	193±19 (265±26)	174±18 (238±24)

Table A-3. Average surface emissive power Montoir Test 2: Period 4 and spanning all periods

Instrument (position) (view angle)	Calculated Transmissivity values	Average values of Surface Emissive Power (kW/m^2) with standard deviations (value in parenthesis corrected for atmospheric attenuation using the calculated transmissivity value)	
		Period 4 165-185 sec	Over periods 1 through 4 35-185 sec
Barnes 3 (47) (40°x70°)	0.69	195±19 (283±27)	196±18 (284±26)
Barnes 4 (75) (40°x70°)	0.71	189±19 (266±27)	187±18 (264±26)
Barnes 5 (15) (40°x70°)	0.71	187±17 (263±24)	197±18 (277±25)
IRD 2 (74) (55°)	0.73	165±16 (226±22)	179±15 (245±20)
Land 1 (13) (90°)	073	182±18 (249±25)	285±18 (254±24)

Table A-4. Average surface emissive power Montoir Test 3: Periods 1, 2, and 3

Instrument (position) (view angle)	Calculated Transmissivity values	Average values of Surface Emissive Power (kW/m^2) with standard deviations (value in parenthesis corrected for atmospheric attenuation using the calculated transmissivity value)		
		Period 1 57-70 sec	Period2 90-120 sec	Period 3 130-160 sec
Barnes 3 (47) (40°x70°)	0.69	195±20 (283±30)	168±17 (243±25)	173±19 (251±28)
Barnes 4 (75) (40°x70°)	0.71	189±18 (266±25)	211±22 (297±31)	204±16 (288±22)
Barnes 5 (15) (40°x70°)	0.71	173±21 (244±29)	183±21 (258±30)	185±18 (261±26)
IRD 1 (17) (55°)	0.70	179±16 (255±23)	181±16 (258±23)	193±17 (276±24)
IRD 2 (76) (55°)	0.71	174±17 (239±23)	189±19 (259±26)	192±18 (263±24)
Land 1 (13) (90°)	073	198±18 (279±25)	170±17 (240±21)	172±18 (242±26)

Table A-5 . Average surface emissive power Montoir Test 3: Spanning all periods

Instrument (position)* (view angle)	Calculated Transmissivity values	Average values of Surface Emissive Power (kW/m^2) with standard deviations (value in parenthesis corrected for atmospheric attenuation using the calculated transmissivity value)
		Over period 1 through 3 57-160 sec
Barnes 3 (47) (40°x70°)	0.69	183±18 (265±26)
Barnes 4 (75) (40°x70°)	0.71	205±20 (289±28)
Barnes 5 (15) (40°x70°)	0.71	206±20 (290±28)
IRD 1 (17) (55°)	0.70	184±17 (263±24)
Land 1 (13) (90°)	0.73	188±17 (257±23)
Land 5 (45) (90°)	071	174±16 (245±23)

A.2. Average heat flux from wide -angle radiometers measurements

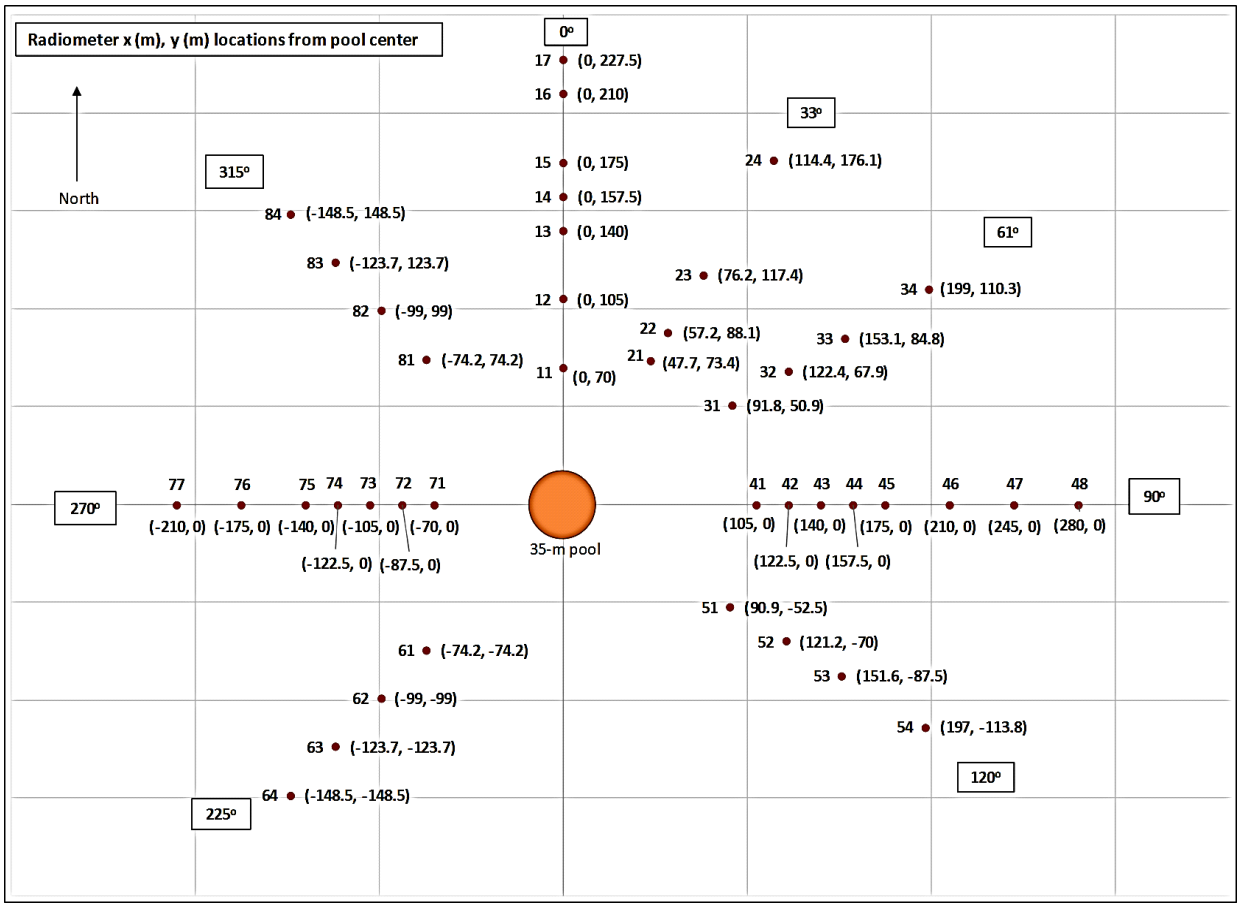

Figure A-1: Wide-angle radiometer locations for Montoir Test 1.

Table A-6. Averaged wide-angle radiometer measurements Montoir Test 1

Incident heat flux (kW/m^2)						
	Period 1 60-100 sec		Period 2 130-170 sec		Over periods 1 and 2 60-170 sec	
Position	Ave.	Std. dev.	Ave,	Std. dev.	Ave.	Std. dev.
11	10.6	1.0	6	6.0	10.7	0.9
12	5.8	0.4	5.7	5.7	5.8	0.5
13	3.3	0.2	3.3	3.3	3.3	0.3
14	2.2	0.1	2.2	2.2	2.2	0.1
15	1.6	0.3	1.3	1.3	1.5	0.3

Incident heat flux (kW/m^2)						
16	1.6	0.1	1.6	1.6	1.6	0.1
17	1.3	0.2	1.3	1.3	1.3	0.2
21	6.7	0.6	5.7	5.7	6.2	0.7
22	4.9	0.4	4.0	4.0	4.4	0.5
23	3.0	0.3	2.5	2.5	2.8	0.3
24	1.3	0.1	1.1	1.1	1.2	0.1
31	5.0	0.4	3.6	3.6	4.3	0.7
32	3.0	0.3	2.3	2.3	2.6	0.4
33	2.1	0.2	1.6	1.6	1.8	0.3
34	1.0	0.1	0.8	0.8	0.9	0.1
41	5.2	0.4	3.5	3.5	4.3	0.9
42	4.0	0.3	2.6	2.6	3.3	0.6
43	3.2	0.3	2.2	2.2	2.7	0.5
44	2.6	0.2	1.8	1.8	2.2	0.4
45	2.1	0.2	1.5	1.5	1.8	0.3
46	1.6	0.2	1.1	1.1	1.3	0.3
47	1.2	0.2	0.9	0.9	1.1	0.2
48	0.6	0.1	0.4	0.4	0.5	0.1
51	5.5	0.5	3.7	3.7	4.5	0.9
52	4.1	0.4	2.9	2.9	3.5	0.6
53	2.2	0.2	1.6	1.6	1.9	0.3
54	1.0	0.1	0.8	0.8	0.9	0.1
62	7.1	1.1	6.5	6.5	6.7	0.9
63	3.2	0.5	3	3.0	3.1	0.4
64	0.6	0.3	0.2	0.2	0.4	0.2
71	20.3	3.4	39.9	39.9	30.1	9.3
72	14.8	2.3	26.3	26.3	20.6	5.6
74	6.3	0.8	-	-	-	-
75	4.8	0.9	6.3	6.3	5.6	1.5
76	2.8	0.4	3.3	3.3	3.1	0.7
77	0.9	0.2	1.1	1.1	1.0	0.3
81	6.0	0.8	-	-	-	-
82	4.1	0.5	4.7	4.7	4.5	0.6
83	2.5	0.3	2.8	2.8	2.7	0.4
84	0.9	0.2	1	1.0	1.0	0.2

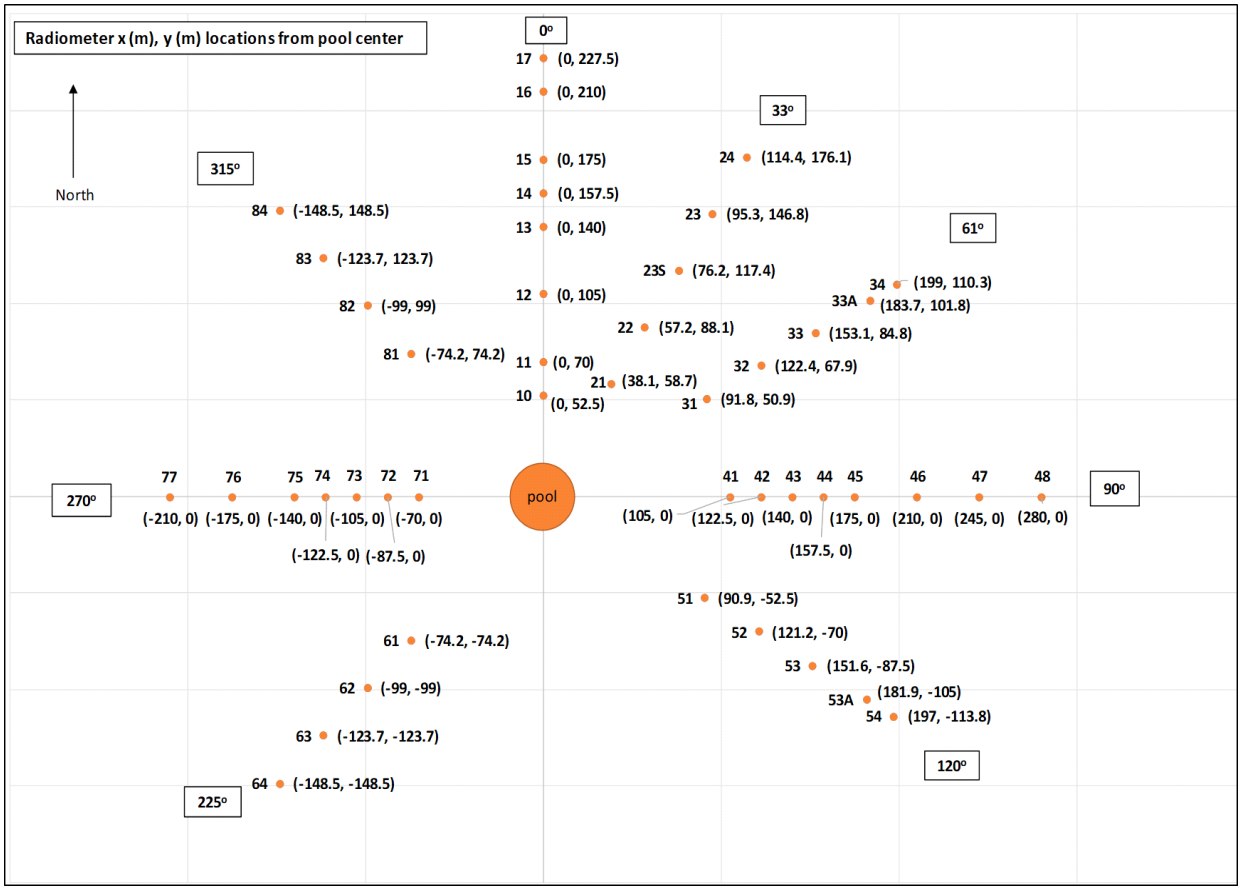

Figure A-2: Wide-angle radiometer locations for Montoir tests 2 and 3.

Table A-7. Average wide-angle radiometer measurements Montoir Test 2

Incident heat flux (kW/m^2)										
	Period 1 35-50 s		Period 2 65-85 s		Period 3 100-130 s		Period 4 165-185 s		Over periods 1 through 4 35-185 s	
Position	Ave.	Std. Dev.	Ave.	Std. Dev.	Ave.	Std. Dev.	Ave.	Std. Dev.	Ave.	Std. Dev.
10	17.3	1.1	16.0	1.1	18.1	1.3	18.9	2.5	18.2	1.2
11	12.5	0.6	11.3	0.6	12.7	0.8	13.1	1.7	12.7	1.2
12	6.7	0.4	6.1	0.3	7.0	0.6	7.1	1.0	6.9	0.7
13	3.8	0.3	3.5	0.2	3.9	0.3	4.0	0.6	3.9	0.4
14	3.0	0.2	2.8	0.2	3.2	0.3	3.0	0.4	3.1	0.3
15	1.8	0.3	1.7	0.2	1.9	0.3	1.8	0.2	1.8	0.3
16	2.1	0.1	1.9	0.1	2.1	0.2	2.2	0.3	2.1	0.2
17	1.2	0.3	1.1	0.2	1.2	0.3	1.2	0.3	1.2	0.3
21	17.5	1.4	16.7	1.7	18.4	1.7	18.4	1.9	18.6	1.1
22	8.4	0.6	7.8	0.5	8.5	0.9	8.3	0.7	8.5	0.9

Incident heat flux (kW/m^2)										
23S	4.7	0.4	4.4	0.4	4.9	0.5	4.6	0.4	4.8	0.5
23	2.8	0.2	2.5	0.2	2.8	0.2	2.9	0.3	2.8	0.3
24	1.6	0.2	1.4	0.2	1.5	0.2	1.5	0.2	1.5	0.2
31	12.6	1.2	11.5	1.2	13.5	1.8	13.9	1.2	13.2	1.8
32	5.2	0.5	4.5	0.3	5.2	0.6	5.4	0.4	5.0	0.6
33	3.3	0.4	2.9	0.3	3.3	0.4	3.4	0.3	3.1	0.4
33A	2.1	0.3	1.8	0.2	2.0		2.1	0.2	1.9	0.3
34	1.4	0.2	1.2	0.2	1.3	0.2	1.4	0.2	1.3	0.2
41	15.1	2.5	14.8	1.9	15.3	0.2	14.7	1.6	14.5	2.3
42	10.3	1.3	9.6	1.2	10.3	1.9	10.1	0.9	9.6	1.4
43	7.5	0.9	6.6	0.8	7.4	0.9	7.4	0.6	6.8	1.1
44	-	-	-	-	-	-	-	-	-	-
45	3.2	0.4	2.7	0.3	3.1	0.6	3.3	0.3	2.9	0.5
46	2.1	0.3	1.7	0.2	2.1	0.2	2.1	0.3	1.9	0.4
47	-	-	0.9	0.3	1.2	0.2	1.5	0.3	-	-
48	0.6	0.1	0.4	0.1	0.6	0.3	0.6	0.1	0.5	0.1
51	11.5	1.1	10.4	1.9	10.2	0.1	10.0	1.0	10.0	1.6
52	5.3	0.8	4.8	1.0	4.9	1.7	5.0	0.7	4.8	0.9
53	3.0	0.3	2.6	0.3	2.8	0.9	3.1	0.4	2.8	0.4
53A	1.6	0.2	1.4	0.2	1.5	0.3	1.7	0.2	1.5	0.3
54	1.2	0.2	1.0	0.2	1.1	0.2	1.3	0.2	1.1	0.2
61	3.7	0.3	3.1	0.3	3.1	0.2	3	0.2	3.1	0.4
62	2.8	0.3	2.2	0.3	2.3	0.3	2.2	0.2	2.3	0.3
63	1.8	0.2	1.5	0.2	1.4	0.2	1.4	0.1	1.5	0.2
64	0.5	0.1	0.3	0.1	0.3	0.1	0.3	0.1	0.3	0.1
71	5.9	0.3	5.1	0.3	5.5	0.4	5.6	0.5	5.6	0.4
72	4.2	0.2	3.6	0.3	3.9	0.3	4	0.3	3.9	0.3
73	2.8	0.1	2.5	0.2	2.7	0.2	2.7	0.3	2.7	0.2
74	2.4	0.3	2.2	0.3	2.3	0.3	2.3	0.3	2.3	0.3
75	1.8	0.3	1.2	0.2	1.6	0.3	2.1	0.3	1.7	0.4
76	1.3	0.1	1.1	0.1	1.2	0.1	1.2	0.1	1.2	0.1
77	0.3	0.0	0.2	0.0	0.3	0.0	0.3	0.1	0.3	0.1
81	3.6	0.2	3.2	0.2	3.7	0.3	3.9	0.6	3.6	0.4
82	2.5	0.1	2.2	0.1	2.6	0.2	2.8	0.4	2.6	0.3
83	1.6	0.1	1.5	0.1	1.7	0.2	1.8	0.3	1.7	0.2

Incident heat flux (kW/m^2)										
84	0.8	0.1	0.7	0.1	0.9	0.1	0.9	0.2	0.8	0.1

Table A-8. Averaged wide-angle radiometer measurements Montoir Test 3

Incident heat flux (kW/m^2)								
	Period 1 57-70 s		Period 2 90-120 s		Period 3 130-160 s		Over periods 1 through 3 57-160 s	
Position	Ave.	Std. Dev.	Ave.	Std. Dev.	Ave.	Std. Dev.	Ave.	Std. Dev.
10	14.6	1.1	14.8	1.1	14.7	1.2	14.9	1.2
11	10.2	1.0	10.1	1.0	10.1	1.1	10.3	1.2
12	5.2	0.5	5.3	0.4	5.3	0.4	5.3	0.4
13	3.1	0.3	3.1	0.2	3.2	0.3	3.2	0.3
14	2.4	0.2	2.5	0.3	2.5	0.3	2.5	0.2
15	2.5	0.3	2.4	0.4	2.4	0.4	2.5	0.4
16	1.4	0.1	1.2	0.1	1.2	0.1	1.2	0.1
17	1.3	0.3	1.3	0.3	1.3	0.4	1.3	0.3
21	8.4	0.7	8.0	0.6	7.8	0.7	8.1	0.7
22	4.9	0.4	4.6	0.4	4.5	0.5	4.5	0.5
23S	2.9	0.2	2.8	0.2	2.7	0.2	2.8	0.2
23	2.1	0.2	1.9	0.1	1.9	0.2	2.0	0.2
24	1.2	0.1	1.2	0.1	1.2	0.1	1.2	0.1
31	4.6	0.5	4.1	0.4	4.0	0.4	4.1	0.5
32	-	-	-	-	-	-	-	-
33	2.0	0.2	1.8	0.1	1.7	0.1	1.8	0.2
33A	1.1	0.1	1.0	0.1	1.0	0.1	1.0	0.1
34	1.0	0.1	0.9	0.1	0.9	0.1	0.9	0.1
41	9.1	0.9	8.0	0.9	7.8	0.8	8.2	1.0
42	4.8	0.5	4.2	0.4	4.1	0.4	4.3	0.4
43	3.1	0.3	2.7	0.3	2.7	0.3	2.8	0.4
44	2.7	0.3	2.4	0.2	2.3	0.2	2.3	0.3
45	2.1	0.3	1.9	0.2	1.8	0.2	1.8	0.2
46	1.5	0.2	1.3	0.1	1.3	0.1	1.3	0.1
47	1.3	0.3	1.2	0.2	1.1	0.2	1.2	0.3

Incident heat flux (kW/m^2)								
48	0.6	0.1	0.5	0.0	0.5	0.1	0.5	0.1
51	5.0	0.5	4.5	0.5	4.5	0.4	4.6	0.5
52	3.1	0.3	2.8	0.3	2.7	0.3	2.7	0.4
53	2.1	0.2	1.9	0.1	1.9	0.2	2.0	0.2
53A	1.3	0.1	1.2	0.1	1.2	0.2	1.2	0.1
54	1.0	0.1	0.9	0.1	0.9	0.1	0.9	0.1
61	10.0	1.1	10.2	1.2	10.6	0.1	10.3	1.2
62	5.0	0.5	5.0	0.5	5.1	0.4	5.0	0.5
63	1.2	0.3	3.1	0.3	3.2	0.3	3.1	0.3
64	1.0	0.1	0.9	0.1	0.9	0.1	0.9	0.1
71	26.7	2.4	29.3	2.9	30.5	2.7	30.1	3.0
72	16.7	1.8	17.8	1.9	28.4	1.9	18.3	1.9
73	-	-	-	-	-	-	-	-
74	-	-	7.0	0.9	7.0	0.9	-	-
75	5.8	0.8	5.9	0.9	6.4	0.9	6.1	1.0
76	3.3	0.3	3.4	0.3	3.5	0.3	3.5	0.3
77	1.2	0.1	1.3	0.1	1.3	0.1	1.3	0.2
81	6.2	0.6	6.4	0.5	6.6	0.6	6.5	0.6
82	4.2	0.4	4.1	0.3	4.1	0.4	4.0	0.4
83	2.4	0.2	2.5	0.2	2.6	0.3	2.5	0.3
84	1.0	0.1	1.1	0.1	1.1	0.1	1.1	0.1

A.3. Average spot surface emissive power from narrow -angle radiometers

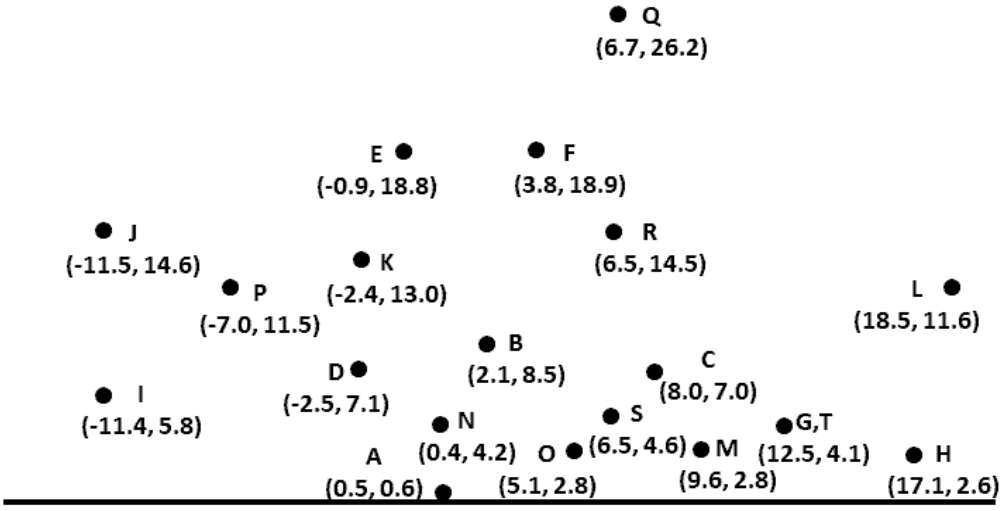

Figure A-3: Narrow-angle radiometer spot locations with respect to pool center, (in meters) Montoir Test 1.

Table A-9. Average spot surface emissive power Montoir Test 1

Position	Time After Ignition (Seconds)	Mean Emissive Power* (kW/m^2)	Maximum value observed** (kW/m^2)	Minimum value observed (kW/m^2)
A	5.0-33.0	59 (81)	N.R.	N.R.
B	46.4-47.0	212 (289)	247 (337)	N.R.
C	47.4-55.0	206 (279)	249 (340)	109 (147)
D	58.0-59.0	170 (232)	221 (303)	N.R.
E	65.0-69.0	224 (306)	292 (394)	N.R.
F	77.0-78.3	326 (445)	373 (509)	261 (358)
G	146.2-152.6	143 (196)	216 (295)	80 (110)
H	153.7-162.9	133 (182)	214 (294)	N.R.
I	165.0-173.1	130 (178)	163 (299)	N.R.
J	173.9-183.7	174 (237)	227 (312)	N.R.
K	185.2-195.0	241 (330)	364 (499)	N.R.
L	196.3-205.1	196 (267)	256 (350)	N.R.
M	232.1-242.2	155 (213)	230 (315)	N.R.
N	243.2-250.8	174 (239)	241 (330)	N.R.

Position	Time After Ignition (Seconds)	Mean Emissive Power* (kW/m^2)	Maximum value observed** (kW/m^2)	Minimum value observed (kW/m^2)
O	251.8-257.4	122 (166)	188 (256)	N.R.
P	260.7-272.8	171 (236)	201 (275)	N.R.
Q	274.3-278.0	169 (232)	248 (375)	N.R.
R	279.2-290.6	233 (318)	303 (414)	N.R.
S	304.0-310.5	253 (346)	323 (442)	N.R.
T	311.5-320.8	61 (83)	110 (150)	N.R.

*Values quoted in brackets were obtained by dividing by a value of 0.73 to allow for attenuation by the atmosphere.
**N.R. – not recorded

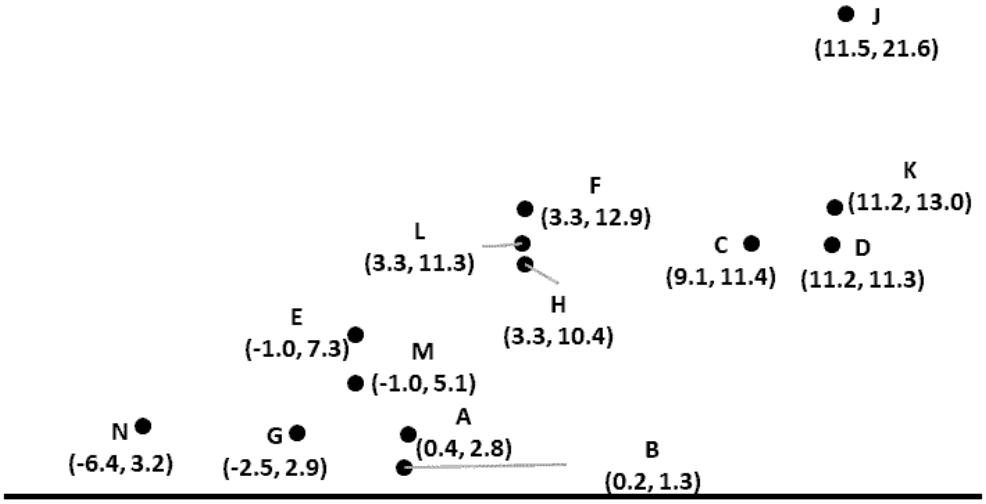

Figure A-4. Narrow-angle radiometer spot locations with respect to pool center (in meters), Montoir Test 2, position 46.

Table A-10. Average spot surface emissive power Montoir Test 2 (Position 46)

Position	Time After Ignition (Seconds)	Mean Emissive Power* (kW/m^2)	Standard Deviation (kW/m^2)	Maximum** (kW/m^2)	Minimum (kW/m^2)
A	10-14	119 (170)	16 (23)	146 (208)	88 (125)
B	14-19	104 (148)	21 (30)	155 (221)	80 (114)
C	117-125	198 (282)	32 (46)	271 (386)	121 (172)
D	129-134	135 (192)	28 (40)	181 (258)	43 (61)
E	141-148	120 (171)	27 (38)	181 (258)	82 (117)
F	160-169	122 (174)	31 (44)	201 (286)	90 (128)
G	174-182	134 (191)	33 (47)	170 (242)	90 (128)

Position	Time After Ignition (Seconds)	Mean Emissive Power* (kW/m^2)	Standard Deviation (kW/m^2)	Maximum** (kW/m^2)	Minimum (kW/m^2)
H	187-190	151 (215)	40 (57)	190 (271)	71 (101)
I	206-215	168 (239)	70 (100)	303 (435)	65 (93)
J	216-223	162 (231)	38 (54)	229 (326)	60 (85)
K	226-233	191 (272)	30 (43)	230 (328)	120 (171)
L	239-244	153 (218)	20 (28)	194 (276)	117 (167)
M	248-255	164 (234)	24 (34)	205 (292)	111 (158)

*Values quoted in brackets were obtained by dividing by a value of 0.702 to allow for attenuation by the atmosphere.
**N.R. – not recorded

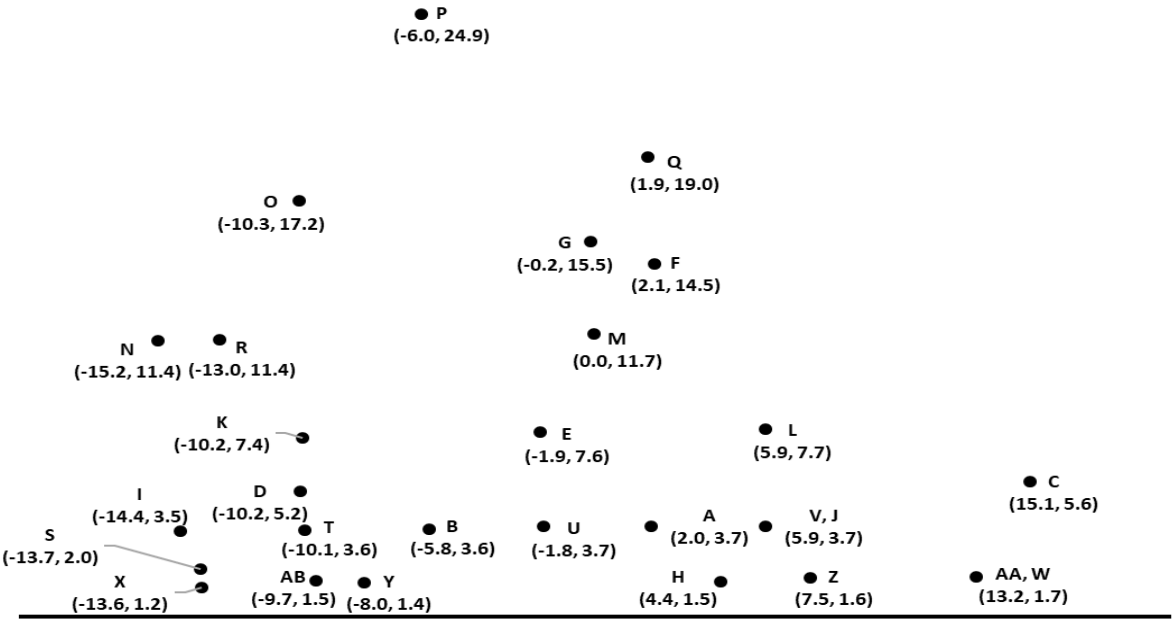

Figure A-5: Narrow-angle radiometer spot locations with respect to pool center (in meters), Montoir Test 2, position 75.

Table A-11. Average spot surface emissive power Montoir Test 2 (Position 75)

Position	Time After Ignition (Seconds)	Mean Emissive Power* (kW/m^2)	Standard Deviation (kW/m^2)	Maximum** (kW/m^2)	Minimum (kW/m^2)
A	8-17	204 (280)	9 (12)	222 (305)	186 (255)
B	26-36	197 (271)	38 (52)	246 (338)	95 (130)
C	37-40	114 (157)	56 (77)	239 (328)	68 (93)
D	43-49	220 (302)	14 (19)	236 (324)	197 (271)
E	53-60	218 (299)	25 (34)	290 (399)	190 (261)

Position	Time After Ignition (Seconds)	Mean Emissive Power* (kW/m^2)	Standard Deviation (kW/m^2)	Maximum** (kW/m^2)	Minimum (kW/m^2)
F	63-70	140 (192)	38 (52)	220 (302)	72 (99)
G	71-80	77 (106)	57 (77)	222 (305)	16 (22)
H	96-101	226 (310)	12 (16)	238 (327)	2024 (280)
I	107-112	173 (238)	24 (33)	219 (301)	94 (129)
J	117-121	210(288)	16 (22)	239 (328)	186 (255)
K	124-132	228 (313)	31 (43)	299 (411)	188 (258)
L	135-141	183 (251)	39 (54)	246 (338)	110 (152)
M	144-152	154 (211)	51 (70)	246 (338)	46 (63)
N	153-161	142 (195)	43 (59)	246 (338)	71 (98)
O	163-173	98 (135)	37 (51)	220 (302)	35 (48)
P	174-186	107 (147)	36 (50)	154 (211)	31 (43)
Q	186-193	54 *74)	30 (41)	115 (158)	11 (15)
R	194-201	107 (147)	46 (63)	191 (262)	44 (60)
S	202-208	209 (287)	16 (22)	244 (335)	185 (254)
T	209-218	179 (246)	17 (23)	210 (288)	169 (232)
U	219-226	158 (217)	19 (26)	201 (276)	121 (166)
V	226-231	189 (260)	23 (32)	205 (282)	130 (179)
W	233-240	133 (183)	29 (40)	197 (271)	79 (108)
X	243-248	169 (232)	14 (19)	202 (277)	157 (216)
Y	249-254	126 (173)	15 (21)	-	-
Z	254-259	153 (210)	38 (52)	222 (305)	105 (144)
AA	259-269	174 (239)	17 (23)	204 (280)	97 (133)
BB	287-294	161 (221)	14 (19)	187 (257)	105 (144)

*Values quoted in brackets were obtained by dividing by a value of 0.728 to allow for attenuation by the atmosphere.
**N.R. – not recorded

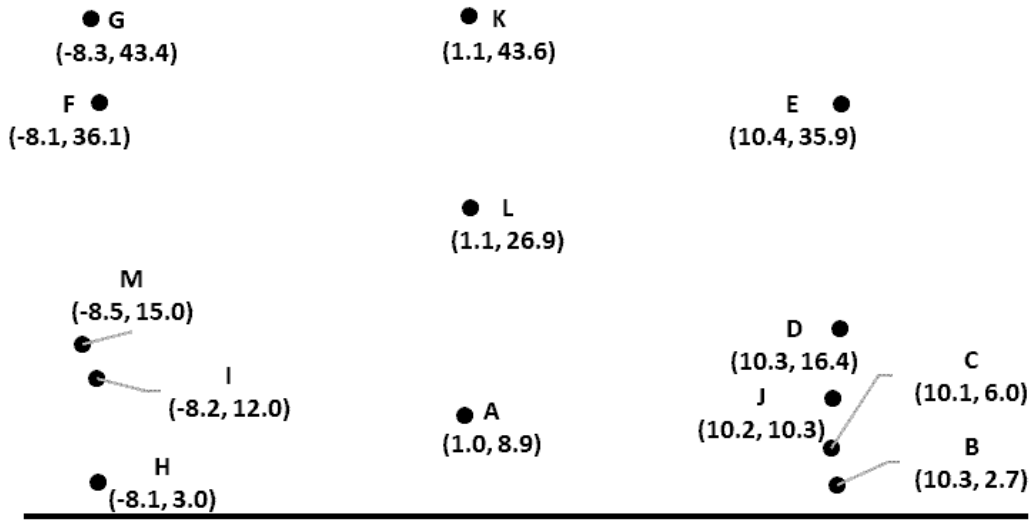

Figure A-6: Narrow-angle radiometer spot locations with respect to pool center (in meters), Montoir Test 3, position 46.

Table A-12. Average spot surface emissive power Montoir Test 3 (Position 46)

Position	Time After Ignition (Seconds)	Mean Emissive Power* (kW/m^2)	Standard Deviation (kW/m^2)	Maximum** (kW/m^2)	Minimum (kW/m^2)
A	45.4-54.2	216 (308)	11 (16)	239 (341)	198 (282)
B	55.0-55.7	139 (198)	5 (7)	-	-
C	57.5-63.0	219 (312)	8 (11)	234 (334)	-
D	63.5-68.7	193 (275)	21 (30)	243 (347)	157 (224)
E	70.0-74.9	98 (140)	79 (113)	271 (387)	11 (16)
F	74.6-77.1	127 (181)	55 (78)	196 (280)	41 (58)
G	77.6-83.3	122 (174)	54 (77)	229 (327)	18 (26)
H	85.1-107.8	219 (312)	9 (13)	241 (344)	199 (284)
I	109.9-120.2	195 (278)	27 (39)	246 (351)	137 (195)
J	120.7-124.7	186 (265)	24 (34)	234 (334)	128 (183)
K	133.8-145.5	100 (143)	50 (71)	197 (281)	22 (31)
L	147.1-156.1	187 (227)	23 (33)	230 (328)	127 (181)
M	169.1-174.2	206 (294)	34 (49)	255 (364)	146 (208

*Values quoted in brackets were obtained by dividing by a value of 0.701 to allow for attenuation by the atmosphere.
**N.R. – not recorded

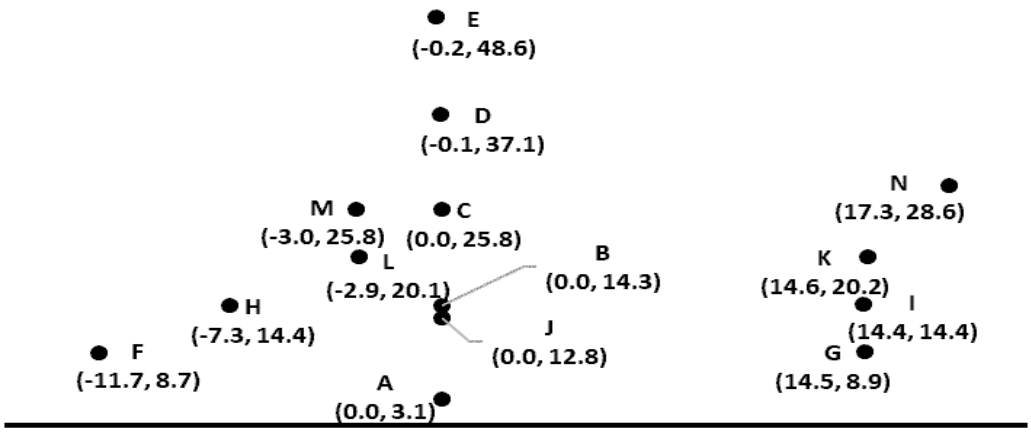

Figure A-7: Narrow-angle radiometer spot locations with respect to pool center (in meters), Montoir Test 3, position 75.

Table A-13. Average spot surface emissive power Montoir Test 3 (Position 75)

Position	Time After Ignition (Seconds)	Mean Emissive Power* (kW/m^2)	Standard Deviation (kW/m^2)	Maximum** (kW/m^2)	Minimum (kW/m^2)
A	35.1-41.9	143 (197)	27 (37)	186 (256)	88 (121)
B	42.8-51.0	235 (323)	28 (39)	289 (398)	175 (241)
C	51.8-60.9	219 (301)	36 (50)	312(429)	150 (206)
D	62.0-70.5	247 (340)	43 (59)	326 (448)	136 (187)
E	72.0-80.0	166 (228)	82 (113)	340 (468)	16 (22)
F	101.5-108.8	208 (286)	15 (21)	231 (318)	169 (232)
G	111.2-119.0	141 (194)	39 (54)	232 (319)	81 (111)
H	122.0-128.9	192 (264)	32 (44)	243 (334)	91 (125)
I	132.7-137.8	157 (216)	61 (84)	245 (337)	22 (30)
J	138.8-146.9	148 (204)	39 (54)	283 (389)	76 (105)
K	148.6-157.1	245 (337)	41 (56)	350 (481)	152 (209)
L	158.3-166.0	211 (290)	-	295 (406)	67 (92)
M	167.2-175.8	198 (272)	45 (62)	255 (351)	5 (7)
N	177.2-186.8	250 (344)	67 (92)	366 (503)	36 (50)

*Values quoted in brackets were obtained by dividing by a value of 0.727 to allow for attenuation by the atmosphere.
**N.R. – not recorded

A.4. Total incident heat flux to calorimeters above pool surface

The test reports note that since the calorimeters were water cooled for protection, soot deposited onto the surface of the calorimeters despite the large flow rate of purge nitrogen being used. The deposition layer causes a reduction in radiative heat transfer to the sensor and an increase in conduction through the sensor window. Uncertainties from engulfed water-cooled heat flux gauges can range from about 20%-40% as discussed in [26].

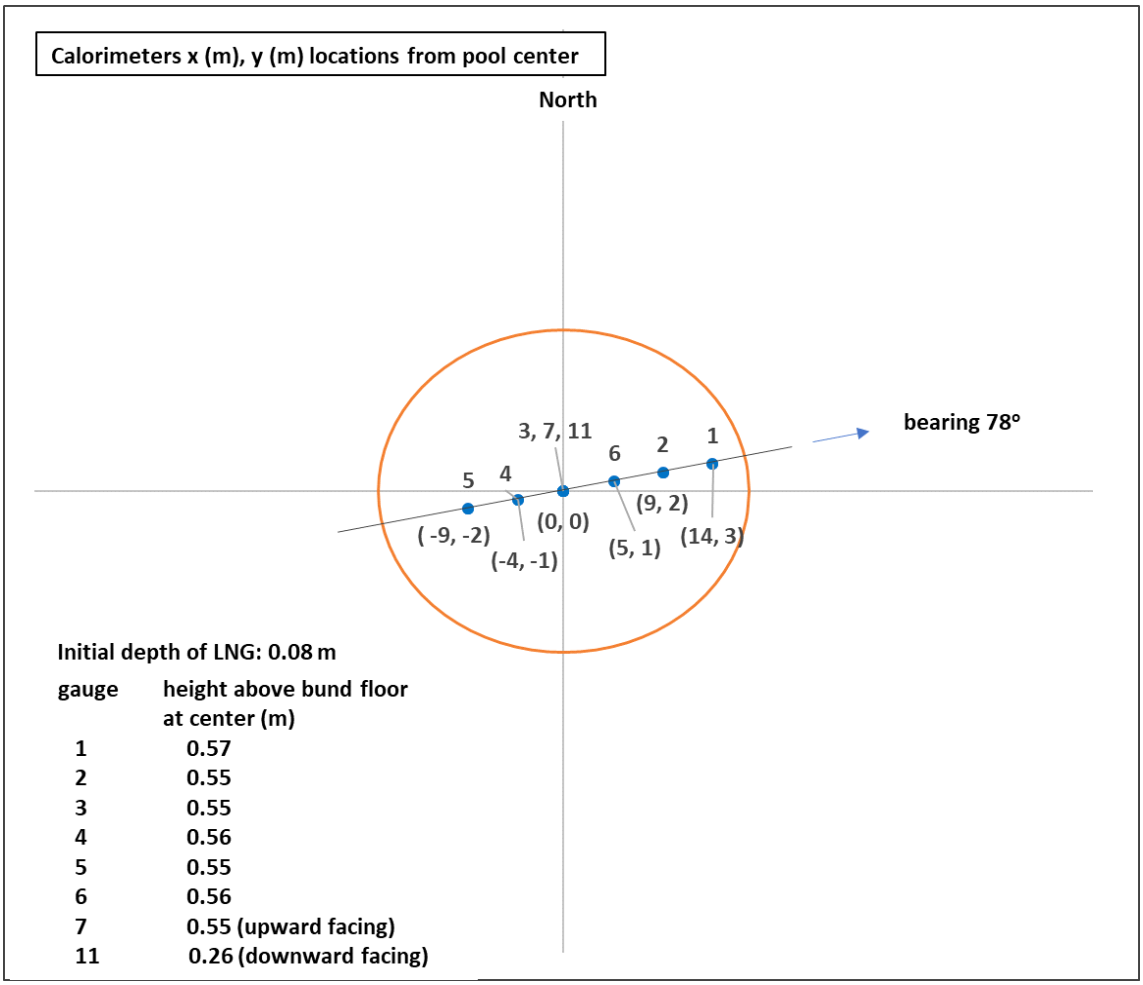

Figure A-8 : Calorimeter placement within pool

Table A-14 . Montoir Test 1: Average total incident heat flux from calorimeters*

Average total incident heat flux (kW/m^2)			
Position	**averaging period: 60-100 sec**	**averaging period: 130-170 sec**	**averaging period: 60-170 sec**
1**	115.9 ±21.7	111.3 ±29.6	107.6 ±25.4
2	211.6 ±30.5	198.4 ±29.7	203.6 ±29.6
3	149.9 ±51.3	236.4 ±44.9	193.9 ±59.9

Average total incident heat flux (kW/m^2)			
4	131.0 ±58.5	208.3 ±47.9	172.9 ±63.7
5	193.8 ±70.0	210.4 ±63.6	187.2 ±66.7
6	203.9 ±40.2	221.2 ±27.9	212.8 ±34.5
7	100.1 ±10.4	101.5 ±6.2	100.9 ±8.1

*Calorimeter 11 not used in test

**Reported has having inconsistent results compared to other measurements for t<200s and thus may not be reliable

Table A-15. Montoir Test 2: Average total incident heat flux from calorimeters*

Average total incident heat flux (kW/m^2)					
Position	**Ave. period: 35-50 sec**	**Ave. period: 65-80 sec**	**Ave. period: 108-130 sec**	**Ave. period: 165-185 sec**	**Ave. period: 35-185 sec**
1**	140.2 ±24.8	213.0 ±31.5	146.0 ±46.0	123.5 ±34.4	157.0 ±48.1
2	215.2 ±78.9	248.8 ±56.2	223.3 ±58.7	164.9 ±46.1	221.7 ±66.0
3	217.9 ±51.7	234.7 ±41.9	236.7 ±41.1	217.3 ±44.5	232.0 ±44.6
4	212.7 ±38.4	221.4 ±35.0	215.0 ±37.0	241.4 ±39.0	222.9 ±36.9
5	210.2 ±27.3	194.1 ±26.8	185.0 ±28.9	210.8 ±28.9	194.2 ±31.2
6	203.0 ±65.0	231.1 ±54.3	225.1 ±52.4	178.7 ±47.6	215.6 ±56.6
7	101.8 ±35.5	95.3 ±17.8	65.4 ±8.4	54.2 ±6.7	76.8 ±26.0

*Average for calorimeter 11 not reported

**reported has having inconsistent results compared to other measurements for t<200s and thus may not be reliable

Table A-16. Montoir Test 3: Average total incident heat flux from calorimeters*

Average total incident heat flux (kW/m^2)				
Position	**Ave. period: 57-70 sec**	**Ave. period: 90-120 sec**	**Ave. period: 130-160 sec**	**Ave. period: 57-160 sec**
1**	-0.5 ±4.2	81.9 ±103.4	198.0 ±44.1	102.7 ±106.1
2	199.2 ±21.8	196.9 ±23.8	206.8 ±27.8	203.7 ±25.6
3	206.8 ±59.7	193.0 ±46.6	197.2 ±47.5	198.8 ±49.0
4	121.9 ±38.3	160.4 ±49.2	173.6 ±48.6	159.3 ±49.0
5	143.2 ±78.3	119.1 ±41.8	135.8 ±48.9	128.4 ±51.8
6	212.3 ±23.7	214.7 ±36.6	218.6 ±42.1	211.3 ±36.5

*Average for calorimeter 7 and 11 not reported

**low measurement due to a portion of the bund cover falling onto the detector. A small piece of charred plastic was found on the surface of the calorimeter after the test

DISTRIBUTION

Email—Internal

Name	Org.	Sandia Email Address
Michael Starr	08533	mjstarr@sandia.gov
Carlos Lopez	01532	carlope@sandia.gov
Technical Library	01977	sanddocs@sandia.gov

Email—External

Name	Company Email Address	Company Name
Scott Davis	Scott.G.Davis@gexcon.com	Gexcon
Bjorn Erling	Bjorn.Erling.Vembe@dnv.com	DNV
Jason Floyd	Jason.Floyd@ul.org	Underwriters Laboratory Fire Safety Research Institute
Filippo Gavelli	fgavelli@blueeandc.com	BLUE Engineering and Consulting
Bryant Hendrickson	bryant.hendrickson@jensenhughes.com	Jensen Hughes
Andrew Kohout	Andrew.Kohout@ferc.gov	Federal Energy Regulatory Commission
Kevin McGrattan	kevin.mcgrattan@nist.gov	National Institute of Standards and Technology
Thach Nguyen	thach.d.nguyen@dot.gov	Pipeline and Hazardous Materials Safety Administration
James Stewart	James.Stewart@hse.gov.uk	Health and Safety Executive

This page left blank

This page left blank

Sandia National Laboratories

Sandia National Laboratories is a multimission laboratory managed and operated by National Technology & Engineering Solutions of Sandia LLC, a wholly owned subsidiary of Honeywell International Inc. for the U.S. Department of Energy's National Nuclear Security Administration under contract DE-NA0003525.